NASA TECHNICAL NOTE

NASA TN D-6160

EXPERIMENTAL INVESTIGATION OF HEAT-TRANSFER CHARACTERISTICS OF A FILM-COOLED PLUG NOZZLE WITH TRANSLATING SHROUD

by Francis C. Chenoweth and Arthur Lieberman

Lewis Research Center
Cleveland, Ohio 44135

NATIONAL AERONAUTICS AND SPACE ADMINISTRATION • WASHINGTON, D. C. • FEBRUARY 1971

1. Report No.	2. Government Accession No.	3. Recipient's Catalog No.
NASA TN D-6160		

4. Title and Subtitle	5. Report Date
EXPERIMENTAL INVESTIGATION OF HEAT-TRANSFER CHARACTERISTICS OF A FILM-COOLED PLUG NOZZLE WITH TRANSLATING SHROUD	February 1971
	6. Performing Organization Code
7. Author(s)	8. Performing Organization Report No.
Francis C. Chenoweth and Arthur Lieberman	E-5551
	10. Work Unit No.
9. Performing Organization Name and Address	720-03
Lewis Research Center National Aeronautics and Space Administration Cleveland, Ohio 44135	11. Contract or Grant No.
	13. Type of Report and Period Covered
12. Sponsoring Agency Name and Address	Technical Note
National Aeronautics and Space Administration Washington, D.C. 20546	14. Sponsoring Agency Code

15. Supplementary Notes

16. Abstract

An experimental study of the application of gaseous film cooling to the surface of a plug nozzle was conducted. The nozzle model was 8.5 in. (21.6 cm) in diameter, and the maximum gas temperature was limited to 1000° R (555 K). The Hatch-Papell film cooling correlation was used to predict plug and shroud surface temperatures. Application of the correlation used local conditions for the primary stream and slot conditions for the coolant stream. The agreement between predicted and measured surface temperatures under varying conditions of nozzle pressure ratio, coolant-weight-flow ratio, coolant slot geometry, and nozzle geometry are discussed.

17. Key Words (Suggested by Author(s))

Coolant slots
Cylindrical ejector
Ejector
Ejector shroud
Film cooling
Heat transfer
Plug nozzle

18. Distribution Statement

Unclassified - unlimited

19. Security Classif. (of this report)	20. Security Classif. (of this page)	21. No. of Pages	22. Price*
Unclassified	Unclassified	83	$3.00

*For sale by the National Technical Information Service, Springfield, Virginia 22151

EXPERIMENTAL INVESTIGATION OF HEAT-TRANSFER CHARACTERISTICS OF A FILM-COOLED PLUG NOZZLE WITH TRANSLATING SHROUD

by Francis C. Chenoweth and Arthur Lieberman

Lewis Research Center

SUMMARY

The application of gaseous film cooling to the surface of a plug nozzle was studied in the Lewis static test facility. The model, a low-angle conical plug, was 8.5 inches (21.6 cm) in diameter, had a simulated iris primary throat, an overall design pressure ratio of 26.3, and a translating cylindrical shroud. The maximum gas temperature was limited to 1000° R (555 K). The coolant was injected at three locations along the plug for plug cooling and between the primary nozzle and external shroud for shroud cooling. The data are compared with the Hatch-Papell film-cooling correlation developed for a flat plate with no pressure gradient in a subsonic stream. The correlation (modified for the plug geometry) used local conditions for the primary stream and slot conditions for the coolant. The data generally agreed with the modified Hatch-Papell correlation. The maximum deviation in cooling efficiency from the correlation was about 0.42, but generally the agreement was significantly better over the range of test variables.

For all shroud positions, the deviations in the data from the correlation for plug surface cooling could generally be associated with gradients in the plug pressure distributions. In general, it appears that in regions of favorable pressure gradients immediately downstream of a coolant slot, cooling efficiencies were significantly higher than the correlation values. In regions of adverse pressure gradients immediately downstream of a coolant slot, cooling efficiencies were less than the correlation values. Also in regions of adverse pressure gradients downstream of an initially favorable pressure gradient, losses in cooling efficiency were particularly abrupt.

Increases in coolant-weight-flow ratio at the upstream slot result in small increases in cooling efficiency as compared to the same coolant-weight-flow change at the downstream slot under the same conditions of nozzle flow. The wakes from the plug support struts caused a large drop in cooling efficiency with the coolant slot located upstream of the throat, but had less effect with the slots further aft.

The correlation predicts external shroud surface temperatures very well, except toward the shroud exit where the cooling efficiency levels off or increases due to nozzle pressure ratios which caused the primary stream to separate from the shroud.

INTRODUCTION

In a continuing program in airbreathing propulsion, the Lewis Research Center is evaluating various nozzle geometries which are applicable for supersonic cruise aircraft. Plug nozzles are receiving considerable emphasis because they have demonstrated the ability to provide good aerodynamic performance over a wide range of flight conditions (ref. 1). However, the cooling of a plug nozzle is a significant problem because of the immersion of the plug surface in the hot gas stream. The external shroud, which is required to contain the internal expansion at high nozzle pressure ratios, also requires cooling.

Numerous cooling schemes applicable to this configuration have been proposed and are discussed in reference 2. Among those suggested were regenerative cooling, transpiration cooling, liquid and gaseous film cooling, as well as various combinations of these methods. Gaseous film cooling has generally been used for aircraft exhaust nozzles.

Various investigations have been made of the film-cooling problem. The results of these investigations generally are published in the form of an empirical or semiempirical correlation of film-cooling data. The results of several of these investigations are presented in references 3 to 9. A modification of the correlation presented in references 6 and 7 was applied with some success by Lucas and Golladay (refs. 10 and 11) to correlate experimental data for film cooling a convergent-divergent rocket nozzle. The revised correlation presented in reference 11 was found to be applicable in predicting the cooling performance of a cylindrical ejector for a small afterburning turbojet engine. These results are presented in reference 12. Reference 13 uses the Hatch-Papell correlation (ref. 6) in a procedure somewhat similar to reference 12 in predicting the cooling characteristics for another cylindrical ejector operating over a larger range of flow conditions.

This report documents an experimental study of the application of gaseous film cooling to a plug nozzle. The aerodynamic performance of this nozzle without cooling flow is presented in reference 1, and with cooling flow in reference 14. The nozzle used a 10° half-angle conical plug with a translating external cylindrical shroud. Three plug configurations, each containing a different slot location, were used. The coolant was injected tangentially along the plug surface. The tests were conducted in the Lewis Research Center's static test facility. Dry air at room temperature was burned with "white gasoline" (72 octane) to provide the primary flow with a maximum temperature of 1000° R (555 K) at the nozzle. The cooling flow was dry air at ambient temperature. The nozzle pressure ratio was varied from 2 to 30, and the corrected coolant-weight-flow ratio was varied from 0 to 0.06.

APPARATUS AND PROCEDURE

Facility

A schematic of the static test facility is shown in figure 1. The primary air is obtained from the main air supply line. Part of the air is diverted through the burner and then remixed with the main stream to supply the required temperature to the model. By maintaining a temperature of 1650° R (918 K) in the burner cans, the temperature of the mixed gases at the model was approximately 1000° R (555 K). The fuel used was "white gasoline" (72 octane). The secondary air was tapped off the main supply line upstream of the burner can and routed to the model to be dumped either through a coolant slot in the plug or between the primary nozzle and the external shroud for shroud cooling.

Pressures and temperatures were measured at the various locations indicated in figure 1. The nozzle primary airflow was calculated from pressure and temperature measurements in the bellmouth section of the mounting pipe, which was calibrated using an ASME calibration nozzle. The secondary airflow was measured by means of a standard ASME flow-metering orifice in the external supply line. The model installed in the test facility is shown in figure 2.

Nozzle Configurations

The full-length plug nozzle was tested with a single primary nozzle simulating an iris-type primary operating in the maximum afterburning position with a throat- to nacelle-area ratio of 0.36. Basic nozzle dimensions are shown in figure 3(a). Three external shrouds (fig. 3(b)) of different lengths were tested to simulate translation. The internal expansion pressure ratio and internal area ratio for each of these shrouds are listed in table I.

Various coolant slot configurations were tested at each of three locations along the plug, as shown in figure 4. The slots were either open or partially blocked with spacing tabs. The geometry of the slot with spacing tabs is shown in figure 5, with detailed dimensions given in table II. All film-cooled surfaces were made of 304 stainless steel 0.050 inch (0.127 cm) thick to decrease axial conduction.

For the shroud-cooling tests, the 1/4-inch (0.635-cm) thick shrouds were replaced with a thin-walled cylinder which extended to the tip of the plug. This shroud was run with and without insulation on the outer surface (high-temperature-resistant polyurethane foam-in-place resin) to determine the effect of radiation and ambient convection on the film-cooling efficiency of the ejector.

Nozzle Instrumentation

Plug surface temperatures were measured by two rows of thermocouples, located at 0° and 270° looking upstream, shown on figure 6. A row of static-pressure orifices was located at an angle of 180°. The instrumentation for the shroud-cooling tests is shown in figure 7.

The total pressure of the primary stream was obtained from pressure probes on the rake shown in figure 8. The two shielded thermocouples located on the rakes were used to determine the total temperature of the primary stream.

The total pressure P_s (fig. 8) and fluid temperature T_s (fig. 7) of the shroud secondary flow were measured between the primary nozzle and the shroud. The total pressure of the plug coolant flow P_c was measured as the flow exited the center sting and entered the plug (fig. 6). The plug coolant flow temperatures T_c were measured using unshielded thermocouples in a cavity just upstream of the coolant slot. These are also shown in figure 6.

Procedure

Pressure ratios were set by maintaining a constant nozzle-inlet pressure and varying the exhaust pressure. Each configuration was tested over a range of pressure ratios which were applicable for the particular shroud extension ratio. Cooling efficiencies were obtained for a primary temperature of 1000° R (555 K) and a coolant temperature of 520° R (288 K). At each nozzle pressure ratio the coolant-weight-flow ratio was varied from 0 to the maximum available for the particular cooling configuration being tested. Data were then recorded once the monitored surface thermocouples indicated a steady-state condition had been reached.

Data Reduction

The film-cooling efficiency, defined in reference 6, was determined from the recovery temperature of the primary stream $T_{r,p}$, the static temperature of the coolant at the coolant slot t_c, the local wall temperature T_w, and was defined as

$$\eta = \frac{T_{r,p} - T_w}{T_{r,p} - t_c} \tag{1}$$

These data have been compared with the Hatch-Papell film-cooling correlation which is presented in reference 6 as

$$\ln \eta = - \left[\frac{(\pi h D_{pl})_0^x}{(w C_p)_c} - 0.04 \right] \left(\frac{S V_p}{\alpha_c} \right)^{0.125} f\left(\frac{V_p}{V_c} \right) \qquad (2)$$

where

$$f\left(\frac{V_p}{V_c} \right) = 1 + 0.4 \tan^{-1}\left(\frac{V_p}{V_c} - 1 \right) \qquad \text{for} \quad \frac{V_p}{V_c} \geq 1.0$$

and

$$f\left(\frac{V_p}{V_c} \right) = \left(\frac{V_c}{V_p} \right)^{1.5[(V_c/V_p) - 1]} \qquad \text{for} \quad \frac{V_p}{V_c} \leq 1.0$$

The coolant flow rate w_c was measured directly in the secondary flow line. The specific heat at constant pressure $(C_p)_c$, thermal diffusivity α_c, and coolant velocity used in equation (2) were evaluated for the static pressure p_c and temperature t_c at the coolant slot exit. These static values were computed using one-dimensional compressible flow, continuity, total pressure P_c, total temperature T_c, and the area of the coolant slot. The slot height S was the measured value at the coolant slot exit.

The Hatch-Papell correlation was developed for a film-cooled flat plate with subsonic flow and no pressure gradient. Thus when applied to a plug nozzle, some of the parameters must be selected differently than suggested by the original authors. Local values of all parameters for the primary stream were used, except the heat-transfer coefficient parameter $\pi h D_{pl}$. These values were obtained using the axial static-pressure distribution, the primary total pressure P_p, and isentropic flow equations. A method suggested by Lucas and Golladay in reference 11 was used to obtain an average value of the heat-transfer coefficient parameter $(\pi h D_{pl})_0^x$ from the point of injection to the point of interest. The local values of $\pi h D_{pl}$ were integrated over the distance x using the trapezoidal rule for integration. The local values of the heat-transfer coefficient were obtained from

$$h = 0.0265 \frac{k_c}{D_{pl,x}} (Re)_f^{0.8} (Pr)_f^{0.3}$$

The Reynolds number, Prandtl number, and thermal conductivity were evaluated at a film temperature which is defined as the arithmetic average of the local static temperature of the primary stream and the static temperature of the coolant stream at the slot.

In determining the cooling characteristics for the shroud, the same approach as outlined above was used except that the shroud inside diameter D_{sh} was used instead of D_{pl}, and the coolant slot conditions were evaluated in the secondary flow exiting between the primary flap trailing edge and the shroud.

RESULTS AND DISCUSSION

Fifty-Percent Coolant Slot Location

The first configuration to be discussed is a full-length plug with the coolant slot located midway between the primary nozzle and the tip of the conical section (fig. 4(a)).

The pumping characteristics for this coolant slot location are presented in figure 9. The effective coolant-flow-area ratio $(A_c/A_p)_{eff}$ was calculated by using the equation for choked flow at both the coolant and primary throats. The equation reduces to

$$\left(\frac{A_c}{A_p}\right)_{eff} = \omega\sqrt{\tau}\left(\frac{K_p}{K_c}\right) \quad \text{for} \quad \frac{P_c}{P_7} = 1$$

where

$$K = \frac{\sqrt{\frac{\gamma g}{R}}}{\left(\frac{\gamma + 1}{2}\right)^{\frac{\gamma + 1}{2(\gamma - 1)}}}$$

By utilizing the choke line (straight portion of the curve) of figure 9, the effective flow-area ratio is read directly from the abscissa at $P_c/P_7 = 1$. The correction factors due to differences in gas properties are then applied. The corrected effective flow-area ratios for the various slot configurations are 0.0117, 0.0168, and 0.028 for the two partially blocked slots and the full-open slot, respectively.

Typical plug pressure distributions are shown in figure 10 at selected nozzle pressure ratios for each of the shroud positions. Also included on figure 10(c) is a pressure distribution for a plug with no coolant slot (ref. 1). As can be seen, the plug pressure distributions are not significantly affected by coolant injection. The high-pressure

values indicated at an x/L of 0.50 are located just inside the coolant slot and thus are a function of coolant flow rate.

All the cooling efficiency data taken with the large coolant area ($(A_c/A_p)_{eff} = 0.028$) and the retracted shroud (x/d = -0.235) are shown on figure 11. The line in this and future figures represents the predicted values from the Hatch-Papell correlation (eq. (2)). Considerable deviation was obtained under certain conditions of nozzle pressure ratio and coolant weight flow, as will be discussed. Leaders are shown for the various nozzle pressure ratios and corrected coolant-weight-flow ratios and identify the point nearest the plug tip.

Part of the data from figure 11 are presented in figure 12 to show the effect of nozzle pressure ratio at three corrected coolant-weight-flow ratios. From figure 12 we see very good agreement between the experimental data and the Hatch-Papell correlation, for nozzle pressure ratios less than or equal to 4. At a pressure ratio of 7, the experimental data show a maximum divergence from the correlation of 0.42 in cooling efficiency near the tip of the plug for the 0.02 corrected weight-flow ratio (fig. 12(a)). At a corrected weight-flow ratio of 0.03 and 0.04, the divergence decreases to 0.35 (fig. 12(b)) and 0.31 (fig. 12(c)), respectively. At the nozzle pressure ratio of 11, the divergence from the correlation is a maximum of 0.24. Thus the correlation predicts lower temperatures than were actually measured at the higher pressure ratios. It is quite obvious there is a disturbance of the film which affects the cooling efficiencies at these higher nozzle pressure ratios.

Variations in corrected coolant-weight-flow ratio at nozzle pressure ratios greater or less than 7 have little effect on the deviation of cooling efficiency from the correlation, as is evident from figure 13. As previously noted, the main disagreement is associated with higher nozzle pressure ratios. For a nozzle pressure ratio of 11 (fig. 13(a)), there is very little scatter although the data are shifted away from the correlation. For the low pressure ratios (figs. 13(b) and (c)), the data agree very well with the correlation.

The plug pressure distribution for the retracted shroud (fig. 10(a)) shows that the plug pressures vary considerably with nozzle pressure ratio but not with coolant corrected weight flow. For a nozzle pressure ratio of 3, the plug static pressure reaches values below free-stream static pressure p_0 near the throat, and then oscillates about p_0 for the length of the plug. Figures 12, 13(b), and 13(c) show very good agreement between the correlation and the data at this pressure ratio, which provides a static-pressure distribution with a near-constant mean value. For a nozzle pressure ratio of 7, figure 10(a) shows a steep favorable pressure gradient ending in a large overexpansion followed by a long recompression that extends out to near the end of the plug. This long recompression region (adverse pressure gradient) may be responsible for the large drop in cooling efficiency and the large deviation of the data from the correlation for this pressure ratio, as shown in

figure 12. For the nozzle pressure ratio of 11, figure 10(a) shows a steep favorable pressure gradient extending further downstream than for the pressure ratio of 7, followed by a shorter and milder adverse pressure gradient. This gradient is followed by a constant-pressure region. Figure 12 indicates closer agreement of the data with the correlation for a pressure ratio of 11 than for a pressure ratio of 7. Thus it appears that the cooling efficiency will be higher for the pressure distributions having an initially longer favorable pressure gradient on the plug upstream of the slot (and thus a shorter adverse pressure gradient), as occurred for the nozzle pressure ratio of 11.

Figure 14 is a comparison of experimental data for a large coolant area with the shroud extended to the intermediate location. The nozzle pressure ratio effect seen with the retracted shroud (in fig. 11) is again evident. Specific comparisons for constant nozzle pressure ratios and corrected coolant-weight-flow ratios are not made because of this similarity to the previous results. Here again, as for the retracted shroud, the cooling efficiency shows a significant reduction from the correlation at a nozzle pressure ratio in the range of 8.6; whereas for the higher nozzle pressure ratios, the cooling efficiency is more nearly as predicted by the correlation. A review of the plug pressure distribution for the intermediate length shroud location (fig. 10(b)) shows a large, favorable pressure gradient followed by a long, large recompression region for a pressure ratio of 8.6. For the higher pressure ratios, the favorable pressure gradient extends further down the plug, followed by a relatively flat pressure profile which approaches the zero pressure gradient for which the Hatch-Papell correlation was developed.

The data for a fully extended shroud and large coolant area are shown in figure 15. A nozzle with this shroud extension would normally be operated at nozzle pressure ratios greater than 10.0. For these pressure ratios the data agree satisfactorily with the correlation.

The effect of the coolant slot area on the cooling efficiency is shown in figure 16 with the shroud retracted. All three cases show similar trends.

The effect of the coolant slot area on the cooling efficiency when the shroud is fully extended is seen in figure 17. The correlation agrees very well with the data for the open coolant slot. However, when the spacing tabs are put in the coolant slot, the correlation would predict wall temperatures higher than those obtained experimentally. For these cases the total pressure of the cooling flow is considerably higher than the primary total pressure, as indicated in figure 9.

The effect of the plug support struts on the surface temperature is shown in figure 18 for a full-open coolant slot. For the low flow conditions the cooling efficiencies downstream of a support strut (flagged data at 270^{o}) vary up to 0.04 higher than efficiency measured between struts at 0^{o}. As would be expected, the difference decreases at positions further downstream. The higher flow rates tend to minimize this difference for both nozzle pressure ratios. Additionally, in a temperature gradient region, a tendency

appears for the flagged values to lag behind the unflagged values.

Compounded with this support strut effect is the effect of the small spacer tabs (fig. 5) shown in figure 19. An open area in the coolant slot was at 0° and the tab blockage at 270°. Thus any effect would be added to the difference caused by the support strut. Again there is a cooling efficiency difference of as much as 0.04. It is concluded that the presence of tabs in the slot in line with the thermocouples has negligible effect on the coolant efficiency. This conclusion is found to be true for both ranges of nozzle pressure ratio considered.

Ten-Percent Coolant Slot Location

By using the same procedure as described for the 50-percent coolant slot location, the effective flow-area ratios were obtained for the 10-percent coolant slot location from figure 20. These values are 0.0260, 0.0178, and 0.0146. Again very little effect of shroud location is seen. To obtain a corrected coolant-weight-flow ratio of 2 percent, a coolant total-pressure ratio P_c/P_7 of 1.4 is required for the slot with the small area, and a P_c/P_7 of 0.75 for the slot with the large effective area. These pumping requirements become quite important when considering the effect on the performance of the engine cycle.

The plug pressure distributions with the large coolant slot located at $x/L = 0.10$ at various nozzle pressure ratios for the three shroud length positions are shown in figure 21. These plug pressure distributions are very similar to those for the 50-percent coolant slot location (fig. 10). Therefore it is concluded that the pressure distributions are not significantly influenced by moving the coolant injection point from the 50-percent location upstream to the 10-percent location. This is also apparent by comparing data from reference 1 without coolant flow with the present data (fig. 21(c)).

All the data taken for the large coolant flow area, $(A_c/A_p)_{eff} = 0.026$, with the retracted shroud are shown in figure 22. In general, the data agree well with the correlation. Cooling efficiencies vary from a maximum of 0.15 below the correlation to 0.3 above. Again, as for the large deviation which occurred with the 50-percent slot location at pressure ratios near 7, a significant deviation, but of much smaller magnitude, can be seen at the pressure ratio of 6. Also there seems to be a trend showing a sudden decrease in nozzle cooling efficiency near a value of the correlation parameter of 0.50.

When the data are plotted at constant values of coolant corrected weight flow (fig. 23), we see that the greatest deviation of the correlation from the data occurs at the low corrected weight-flow ratio and near the midpoint of the plug. The deviation is such that the correlation would predict plug temperatures higher than those obtained experimentally.

An effect of corrected coolant-weight-flow ratio is seen in figure 24 by comparing the data at constant nozzle pressure ratio. At the higher pressure ratios a sharp drop

in cooling efficiency is apparent, which is then followed by a nearly constant value. As the pressure ratio is lowered, the steepness of the dropoff decreases. This trend is more apparent on figure 25, which shows plots of cooling efficiency variation with plug position for varying corrected weight-flow ratio at a constant nozzle pressure ratio. At pressure ratios of 13 and 9 (figs. 25(a) and (b)), respectively), the sharp drop in efficiency begins at a plug position of about $x/L = 0.37$ and levels off at position $x/L = 0.63$. Referring to figure 21(a) at the pressure ratio of 13, the plug position $x/L = 0.37$ occurs at the end of a steep favorable pressure gradient, and the plug position $x/L = 0.63$ at about the end of a mild recompression.

For a nozzle pressure ratio of 6 (fig. 25(c)), the sudden drop in cooling efficiency is not as pronounced as in the previous cases, but originates at a similar location of about $x/L = 0.28$. Again referring to figure 21(a) at this pressure ratio, it is noted that this position represents the end of the initial favorable gradient. Here again, as for the 50-percent slot location, the long recompression region is apparently responsible for the low cooling efficiencies at this pressure ratio as compared to other higher and lower pressure ratios for a particular weight flow (see fig. 23). For a pressure ratio of 3 (fig. 24(d)), the correlation agrees very well with all data as it did for the 50-percent slot data. The corresponding pressure distribution oscillates about the ambient static pressure p_0.

It is again observed that as the initial favorable pressure gradient extends down the plug (increasing pressure ratio above 6) the cooling efficiencies increase. Also the cooling efficiencies are considerably reduced in the region with a long adverse pressure gradient.

A comparison of cooling efficiency data for the retracted shroud (10-percent coolant slot (fig. 22) and the 50-percent coolant slot (fig. 11)) provides some interesting observations on overall cooling capability. In both cases minimum cooling efficiencies occur near the plug tip. At a corrected weight flow of 0.02, the cooling efficiency near the plug tip is no better with coolant injection at the 50-percent slot than with injection at the 10-percent slot for nozzle pressure ratios of 6 to 7. At higher nozzle pressure ratios, the 50-percent slot is slightly more efficient in cooling the tip, as would be expected since the slot is closer to the point being cooled. At the lower pressure ratios, as would be predicted from the Hatch-Papell parameter, the 50-percent slot cooling efficiencies are significantly higher than those of the 10-percent slot. These trends are also observed at the higher corrected weight flows.

Figures 26 and 27 show comparisons of the experimental data with the Hatch-Papell film-cooling correlation for the large slot with the shroud in the intermediate and fully extended positions, respectively. These longer shroud lengths are normally required at the higher nozzle pressure ratios and are plotted accordingly. There is more scatter for the intermediate shroud than for the longer shroud, primarily due to the data at the lower

pressure ratio of 8. For the extended shroud, the data show little sensitivity to nozzle pressure ratio when the corrected weight flow is kept constant.

Figure 28 shows the apparent effect of corrected coolant-weight-flow ratio at specific nozzle pressure ratios on cooling efficiency for the intermediate shroud. Figure 29 shows the variation in cooling efficiency with plug surface position for the weight flows and pressure ratios shown in figure 28. Here again, as for the retracted shroud, the start of the drop in cooling efficiency occurs at the end of the initial favorable gradient (see fig. 21(b)) for the pressure ratio of 8. As the pressure ratio increases, data (not presented here) show that the point of sudden decrease in efficiency moves downstream. The plug pressure distribution for a pressure ratio of 18.7 (fig. 21(b)) indicates there is a long, steep, favorable pressure gradient extending to about $x/L = 0.54$. Figure 29(b) shows only a small drop in efficiency at this position.

Figures 30 and 31 show data for the fully extended shroud for weight flows and pressure ratios similar to those shown on figures 28 and 29. Here again, the start of the steep drop in cooling efficiency coincides with the end of the initial favorable pressure gradient (see fig. 21(c)).

When the plug surface pressure profiles for the intermediate shroud and the extended shroud are compared at the nozzle pressure ratio of 19, the initial favorable pressure gradient is seen to extend much further downstream for the intermediate shroud. Again it appears that, with a longer initial favorable pressure gradient along the plug surface, higher cooling efficiencies can be expected.

The effect of coolant slot area on the cooling efficiency of the plug surface with the retracted shroud is shown in figure 32. There is a general trend of decreasing efficiencies with decreasing area. Maximum deviations in cooling efficiencies from the correlation are from +0.30 to -0.15 for the large coolant slot, +0.10 to -0.20 for the intermediate slot, and +0.10 to -0.30 for the small slot. In general, the data correlate fairly well with the Hatch-Papell film-cooling correlation. Similar data for an extended shroud condition are shown in figure 33. As seen in previous figures, the large coolant slots tend to produce higher cooling efficiencies than the correlation. Very good agreement is obtained for the two smaller coolant slot areas, $(A_c/A_p)_{eff} = 0.0178$ and 0.0146.

The effect of the plug support struts on the cooling characteristics of the plug surface is shown in figure 34 for the extended shroud and the large coolant flow area. The maximum difference in coolant efficiency is approximately 0.04 near the point of injection of the coolant flow and is higher behind the strut. This difference decreases to practically zero downstream of the coolant slot, a distance $x/L = 0.4$.

Typical results showing the effect of the coolant slot spacer tabs on the cooling characteristics for the plug surface are shown in figure 35. These results include the almost negligible effect of the plug support struts. For corrected weight-flow ratios of approximately 0.02, there are higher cooling efficiencies downstream of the slot tab, of

the order of 0.1 near the point of injection of the coolant slot. These differences are decreased by increasing the amount of coolant flow and thus building a thicker, more efficient layer of coolant air. As would be expected, this difference disappears at greater distances downstream from the coolant slot.

The previous discussion of the slot spacer tab effect on the cooling efficiency for the 50-percent coolant slot location indicated negligible effect. The 10-percent slot location shows an appreciable effect due to the spacer tabs on the temperature measured downstream in line with the tabs. Doubling of the tab width due to the slot geometry (table II) probably caused this increase in cooling efficiency.

Minus Ten-Percent Coolant Slot Location

The effective flow areas for this configuration were obtained from the pumping characteristics shown on figure 36. The values of effective flow-area ratio obtained were 0.0433 and 0.0295. As in the cases of the two previous coolant slot locations, the shrouds have no significant effect on the pumping characteristics. A coolant total-pressure ratio of approximately 1.0 and 0.8 would be required to obtain 2 percent corrected coolant flow for the smaller and larger slots, respectively.

The plug pressure distributions for the small slot are shown in figure 37. These plug pressure distributions are quite similar to those for the 50- and 10-percent coolant slot location. As observed previously, the pressure distributions are not significantly influenced by the coolant slot locations along the surface, or by the corrected coolant flow ratio. The small adverse pressure gradient which is seen just upstream of the slot is caused by a combination of local geometry and, to a lesser, extent, by the high slot inlet pressure.

Since neither of the two coolant slot configurations for this location is blocked with tabs, most of the discussion will be for the small effective flow-area ratio which is approximately equal to the large values at the two downstream coolant slot locations. These results for the retracted shroud are shown on figure 38. The maximum deviation of cooling efficiency from the correlation is from +0.25 to -0.25, as compared to +0.30 to -0.15 for the 10-percent slot location, retracted shroud. The maximum deviation for the 50-percent slot was from +0.42 to -0.10 for the same weight-flow range and retracted shroud. Except for the nozzle pressure ratios of about 7 with the latter configuration, the deviations are less than 0.25.

The effect of the nozzle pressure ratio on the cooling characteristics is shown in figure 39. As can be seen, the scatter is decreased considerably when a comparison is made based on a constant corrected coolant-weight-flow ratio.

The effects of coolant flow rate at constant nozzle pressure ratio are shown in figure 40. The data shift from above the correlation to below the correlation with increasing corrected coolant-weight-flow ratio. The data agree with the correlation at about a weight-flow ratio of 0.03, which from the pumping characteristics (fig. 31) occurs at a coolant total-pressure ratio P_c/P_7 of about 1.25. It is apparent that the effect of the corrected coolant-weight-flow ratio causes more significant deviations from the correlation for this slot location than for those downstream of the primary nozzle. The actual variation in cooling efficiencies with corrected weight flow is small; however, variations in the Hatch-Papell parameter in the range shown are almost inversely proportional to the coolant weight flow. At a nozzle pressure ratio of 9 (fig. 40(a)), a deviation from the correlation of as much as +0.15 and -0.22 in cooling efficiency is obtained by varying the corrected coolant-weight-flow ratio from 0.022 to 0.052. This is also true at a nozzle pressure ratio of 3 (fig. 40(b)). Figure 41 shows cooling efficiency plotted against axial distance along the plug surface. A steep drop in cooling efficiency occurs upstream of the throat, followed by a leveling off. From figure 4(c) we see the flow is initially injected tangent to the surface. A short distance downstream, the surface turns away from the tangential coolant flow. This turning could cause lower cooling efficiencies in the throat region. For the pressure ratio of 9 (fig. 41(a)), a second significant drop in cooling efficiency occurs at about $x/L = 0.63$. This location coincides with a recompression region on the plug surface (fig. 37(a)). For the pressure ratio of 3 (fig. 41(b)), the drop is more gradual over the length of the plug.

As with the +10-percent slot, a longer favorable pressure gradient (fig. 37(a)) generally yields higher cooling efficiency, as shown when figure 41(a) is compared to figure 41(b). Also at the +10-percent slot location, it was generally found that the data fell above the correlation for a long initial favorable pressure gradient. At the -10-percent slot, this is only true for the 0.02 coolant weight flow (fig. 40). This difference can be attributed to the very sharp drop in cooling efficiency at the point of injection and the negligible effect of additional flow on that cooling efficiency (fig. 41). The coolant pressure at 0.02 coolant weight flow is about equal to the primary total pressure; and at higher coolant flows, the pressure is higher than the primary value. The lack of increased cooling efficiency with increased coolant flow may be due to this higher coolant pressure.

The effect of the shroud length position is shown by comparing figure 38 (retracted shroud) with figure 42 (intermediate shroud) and figure 43 (extended shroud). The maximum deviation is approximately the same for the retracted, the intermediate, and the extended shrouds, although for the extended shroud there is a significant decrease in the range of deviation for any particular nozzle pressure ratio. Again, as for the retracted shroud, the data agree best with the correlation at a corrected coolant-weight-flow ratio of 0.03 for the intermediate and extended shroud configurations.

Figures 44 and 45 show cooling efficiency plotted against axial distance along the plug for the intermediate and extended shrouds. Here again, as with the retracted shroud, the intermediate and extended shrouds show an initially steep drop in cooling efficiency leveling off at a point near the throat. In addition, it shows the relative ineffectiveness of additional flow. In figure 44(b) the second drop in cooling efficiency appears to coincide with the recompression region starting at $x/L = 0.45$ shown in figure 37(b). On the other hand, for the nozzle pressure ratio of 18 (fig. 37(b)), the pressure profile is relatively flat beyond $x/L = 0.50$ and the cooling efficiencies (fig. 44(a)) also remain constant. When figure 45(b) is compared with figure 37(c), we again see that the start of the second drop in cooling efficiency is at $x/L = 0.36$, which is a little beyond the start of a long recompression region. Figure 45(a), on the other hand, when compared to figure 37(c) shows a drop in cooling efficiency with a favorable pressure gradient following a short adverse pressure gradient. The initial favorable gradient barely drops p_x below ambient pressure.

The effect of the coolant slot area is shown in figure 46 for the retracted shroud and in figure 47 for the extended shroud. In both cases, the lower coolant weight flow shifts further above the correlation and the higher weight flow approaches the correlation. For the larger slot, higher values of cooling efficiency were obtained just downstream of the slot. It can again be seen that weight flows requiring pressures higher than the primary pressure (fig. 36) did not significantly improve the cooling efficiency over lower coolant flows. This further confirms that for the slot geometry investigated, coolant flows requiring pressures greater than the primary pressure were not as effective as they should be. In both cases, at the corrected coolant-weight-flow ratio of about 0.05, the data are most nearly predicted by the correlation. From figure 36 the pumping characteristics show this flow rate to correspond to a coolant total-pressure ratio of $P_c/P_7 = 1.25$, which is the same value obtained for the smaller slot.

The effect of the plug support struts, as shown in figure 48, is quite large. The maximum loss of cooling efficiency behind the strut (relative to the undisturbed flow) was 0.5 near the point of injection. This difference diminishes further downstream to a value of 0.15 near $x/L = 0.10$. At this station a sudden reversing effect occurs to provide a higher cooling efficiency behind the strut, with a maximum difference of 0.08. This difference in cooling efficiency continues downstream but at smaller values.

Shroud Cooling

The shroud flow pumping characteristics for the plug nozzle operating with a full-length shroud are shown in figure 49. The effective choking area obtained, as previously described, was $(A_s/A_p)_{eff} = 0.230$, as compared to the geometric area of 0.24 between

the shroud and the maximum diameter of the primary nozzle. This shroud was actually longer than required for acceptable aerodynamic performance; however, to obtain adequate heat-transfer results, a full-length shroud was tested.

The pressure distributions along the shroud are shown in figure 50. At low secondary flows (fig. 50(a)), the primary flow stream impinges on the shroud a short distance downstream from the point of injection of shroud secondary cooling air. The secondary flow is due to entrainment by the primary stream. The increase in pressure near the exit at low nozzle pressure ratios is due to separation and recompression of the overexpanded primary stream. At the higher pressure ratios, it is believed that the primary stream remains attached to the shroud and that the moderate increase in pressure is caused by a coalescence of compression waves from the plug.

The flow field shown by the pressure distribution in figure 50(b) is for a smoothly attached flow condition. This attached flow is obtained at high nozzle pressure ratios and high corrected secondary-weight-flow ratios. The primary flow becomes smoothly attached to the shroud, and then shows an expansion and compression profile similar to figure 50(a).

The effect of insulation on the cooling characteristics of the shroud is shown in figure 51. Leaders are shown for the various nozzle pressure ratios and corrected coolant weight-flow ratios and identify the point nearest the shroud tip. For the insulated case (fig. 51(a)), the experimental data fit the correlation for higher values of correlation parameter than for the uninsulated shroud (fig. 51(b)). The insulated case also provides somewhat lower efficiencies, as would be expected since the insulation reduced radiation and convection effects of the external shroud surface. The sudden increase in cooling efficiency near the exit corresponds to the pressure rise due to the separation of the primary stream.

The effects of nozzle pressure ratio and corrected secondary-weight-flow ratio seem to be adequately corrected for by the Hatch-Papell film-cooling correlation in the region of practical interest. These data are presented in figures 52 and 53, respectively. The point at which separation appears to affect the cooling characteristics is a function of the corrected secondary-weight-flow ratio, as seen in figure 53.

SUMMARY OF RESULTS

The heat-transfer characteristics for a film-cooled plug nozzle were investigated experimentally in the Lewis Research Center's static test facility. The model was 8.5 inches (21.6 cm) in diameter, and the maximum gas temperature was limited to 1000° R (555 K). A low-angle conical plug with a small boattail angle was chosen as the nozzle design to be tested. The nozzle had a simulated iris primary throat, an overall design

pressure ratio of 26.3, and a translating cylindrical outer shroud to adjust the internal expansion of the nozzle. The coolant was injected at either one of three locations along the plug for plug cooling or between the primary nozzle and the external shroud to provide shroud cooling. Different coolant slot geometries were tested.

The data were compared with the Hatch-Papell film-cooling correlation. This correlation was developed for a flat plate with no pressure gradient. For application to a plug nozzle, certain modifications were necessary. The local properties of the primary stream were used. The coolant stream properties were taken at the coolant slot. The following results were obtained:

1. The pressure distributions along the plug surface with coolant injection are very similar, for all configurations, to those presented by previous investigators who studied the aerodynamic performance of a plug nozzle.

2. For all shroud positions, the deviations in the data from the correlation could generally be associated with plug pressure distributions.

3. Coolant slots (without spacers) located downstream of the throat:

(a) For the 50-percent slot, the correlation accurately predicts cooling efficiencies for low nozzle pressure ratios (3 and 4) where the pressure distribution along the plug shows a series of rapid pressure fluctuations about the nozzle exit pressure. For the 10-percent slot, the cooling efficiencies were slightly above the correlation values.

(b) In regions of favorable pressure gradient immediately downstream of a coolant slot, cooling efficiencies were always significantly higher than the correlation values.

(c) In regions of adverse pressure gradients immediately downstream of the slot, cooling efficiencies were significantly less than the correlation.

(d) Adverse pressure gradients tend to accelerate a decrease in cooling efficiency when following a favorable pressure gradient.

4. Coolant slots (with spacers; smaller area) located downstream of throat:

(a) For the 50-percent slot location, cooling efficiencies equal to or higher than the correlation were obtained at a nozzle pressure ratio of 3, where the pressure distribution along the plug shows a series of rapid pressure fluctuations about the nozzle exit pressure. For the 10-percent slot, cooling efficiencies were on or below the correlation for the same nozzle pressure ratio.

(b) In regions of favorable pressure gradients immediately downstream of a coolant slot, cooling efficiencies matched the correlation for low weight flow or were lower than correlation values for the higher weight flows.

(c) Adverse pressure gradients tend to accelerate a decrease in cooling efficiency when following a favorable pressure gradient.

5. Coolant slots (without spacers) located upstream of throat:

(a) For low corrected coolant-weight-flow ratios at coolant total pressures

equal to or less than primary total pressure, cooling efficiencies were significantly better than predicted by the correlation. These slots are naturally followed by a favorable pressure gradient and, as noted for the downstream slots, provide cooling efficiencies higher than the correlation.

(b) Higher corrected coolant-weight-flow ratios require total coolant pressure greater than primary total pressure. These larger flow rates give little or no improvement in cooling efficiency over the lower flow rates. It is possible that these higher pressures cause the cooling flow to overexpand and recompress on the plug shoulder, which reduces their effectiveness.

(c) The correlation matched the data best at a coolant-total-pressure-to-primary-total-pressure ratio of 1.25 which, for the retracted and extended shrouds, occurs at 0.03 and 0.05 corrected coolant-weight-flow ratio, respectively.

6. Plug support strut effects:

(a) For the coolant slot located upstream of the primary throat, plug support-strut blockage caused a very large drop in cooling efficiency just downstream of the slot. A little distance downstream of the throat the plug support strut effect reversed and caused a slight increase in cooling efficiency.

(b) Plug support strut effects on cooling efficiency for the slots located downstream of the primary throat were small, varying to as much as 0.04 higher cooling efficiency.

7. The coolant flow slot spacer tabs had no visible effect on cooling efficiency downstream of the tab when the coolant flow was injected midway between the primary throat and the tip of the plug. At the 10-percent downstream coolant injection point where the spacer tabs were approximately twice as wide, the spacer tabs caused variations in cooling efficiencies as much as 0.1 higher than without spacer tabs. The slot spacer tab effect diminishes with downstream distance and also as the coolant weight flow is increased.

8. Shroud cooling efficiencies measured on the shroud, in general, agreed with the correlation values. Deviations from the correlation were observed at low cooling efficiencies with an uninsulated shroud and in regions where the primary stream separated from the shroud.

Lewis Research Center,
National Aeronautics and Space Administration,
Cleveland, Ohio, September 14, 1970,
720-03.

APPENDIX - SYMBOLS

A	area
A_c/A_p	ratio of minimum coolant flow area to primary throat area (coolant flow area ratio)
A_s/A_p	ratio of minimum secondary flow area to primary throat area (secondary flow area ratio)
B	slot width
C	half tab width
C_p	specific heat at constant pressure
D	diameter
d	model diameter
g	gravitational constant
h	heat-transfer coefficient
K	constant
k	thermal conductivity
L	length of uncooled plug measured from nozzle throat
P	total pressure
Pr	Prandtl number
p	static pressure
R	gas constant
Re	Reynolds number
r	radius
S	slot height
T	total temperature
T_r	recovery temperature
T_w	wall temperature
t	static temperature
V	velocity
w	weight-flow rate
x	axial distance measured from nozzle throat
α	thermal diffusivity
γ	ratio of specific heats
η	cooling efficiency, equation (1)
τ	ratio of total temperatures, T_c/T_p or T_s/T_p
ω	ratio of weight-flow rates, w_c/w_p or w_s/w_p

Subscripts:

c	plug coolant
eff	effective
f	film, arithmetic average of coolant and hot gas
p	primary
pl	plug
r	recovery
s	secondary
sh	shroud
sl	slot
w	wall or surface
x	condition at distance x
7	nozzle inlet
8	nozzle throat
9	nozzle exit
0	ambient

REFERENCES

1. Breshahan, Donald L.: Experimental Investigation of a 10^{o} Conical Turbojet Plug Nozzle with Iris Primary and Translating Shroud at Mach Numbers from 0 to 2.0. NASA TM X-1709, 1968.

2. Eckert, E. R. G.; and Livingood, John N. B.: Comparison of Effectiveness of Convection-, Transpiration-, and Film-Cooling Methods with Air as Coolant. NACA Rep. 1182, 1954.

3. Wieghardt, K.: Hot-Air Discharge for De-Icing. Translation F-TS-919-RE, Air Material Command, Dec. 1946.

4. Chin, J. H.; Shirven, S. C.; Hayes, L. E.; and Silver, A. H.; Adiabatic Wall Temperature Downstream of a Single Tangential Injection Slot. Paper 58-A-107, ASME, 1958.

5. Papell, S. Stephen; and Trout, Arthur M.: Experimental Investigation of Air Film Cooling Applied to an Adiabatic Wall by Means of an Axially Discharging Slot. NASA TN D-9, 1959.

6. Hatch, James E.; and Papell, S. Stephen: Use of a Theoretical Flow Model to Correlate Data for Film Cooling or Heating an Adiabatic Wall by Tangential Injection of Gases of Different Fluid Properties. NASA TN D-130, 1959.

7. Papell, S. Stephen: Effect of Gaseous Film Cooling of Coolant Injection Through Angled Slots and Normal Holes. NASA TN D-299, 1960.

8. Seban, R. A.: Heat Transfer and Effectiveness for a Turbulent Boundary Layer with Tangential Fluid Injection. J. Heat Transfer, vol. 82, no. 4, Nov. 1960, pp. 303-312.

9. Goldstein, R. J.; Eckert, E. R. G.; Tsou, F. K.; and Haji-Sheikh, A.: Film Cooling with Air and Helium Injection Through a Rearward-Facing Slot into a Supersonic Air Flow. Rep. HTL-TR No. 60, Univ. of Minnesota, Feb. 1965.

10. Lucas, James G.; and Golladay, Richard L.: An Experimental Investigation of Gaseous-Film Cooling of a Rocket Motor. NASA TN D-1988, 1963.

11. Lucas, James G.; and Golladay, Richard L.: Gaseous-Film Cooling of a Rocket Motor with Injection Near The Throat. NASA TN D-3836, 1967.

12. Chenoweth, Francis C.; and Steffen, Fred W.: Comparison of Experimental and Predicted Heat Transfer Characteristics for a Cylindrical Ejector. NASA TM X-1641, 1968.

13. Chenoweth, Francis C.; and Lieberman, Arthur: Prediction of Heat-Transfer Characteristics for Ejector Exhaust Nozzles. Analytic Methods in Aircraft Aerodynamics. NASA SP-228, 1970, pp. 623-638.

14. Jeracki, Robert J.; and Chenoweth, Francis C.: Coolant Flow Effects on the Performance of a Conical Plug Nozzle at Mach Numbers From 0 to 2.0. NASA TM X-2076, 1970.

TABLE I. - SHROUD VARIABLES

Shroud axial-length-to-diameter ratio, x/d	Internal expansion pressure ratio, P_7/P_9	Internal area ratio, A_9/A_8
-0.235	1.89	1.00
.215	8.87	1.81
.618	11.93	2.13

TABLE II. - COOLANT SLOT VARIABLES

Axial distance from primary nozzle, x/L	Number of tabs	Slot diameter, D_{sl}		Slot width, B		Half tab width, C		Slot inside diameter, ID		Slot outside diameter, OD		Slot height, S		Flow area	
		in.	cm	in.	cm	in.	cm	in.	cm	in.	cm	in.	cm	$in.^2$	cm^2
0.50	0	2.375	6.04	-----	-----	-----	-----	2.205	5.60	2.376	6.04	0.085	2.158	0.598	3.86
	90	2.365	6.01	0.056	0.142	0.012	0.0305							.403	2.60
	90	2.365	6.01	.042	.107	.019	.0483							.302	1.95
0.10	0	4.260	10.81	-----	-----	-----	-----	4.166	10.56	4.278	10.87	0.056	0.1422	0.621	4.01
	90	4.256	10.80	0.096	0.244	0.020	0.0508							.389	2.51
	90	4.256	10.80	.074	.188	.037	.094							.300	1.93
-0.10	0	-----	-----	-----	-----	-----	-----	4.40	11.18	4.58	11.64	0.091	0.231	1.342	8.66
	0									4.48	11.38	.042	.107	.599	3.87

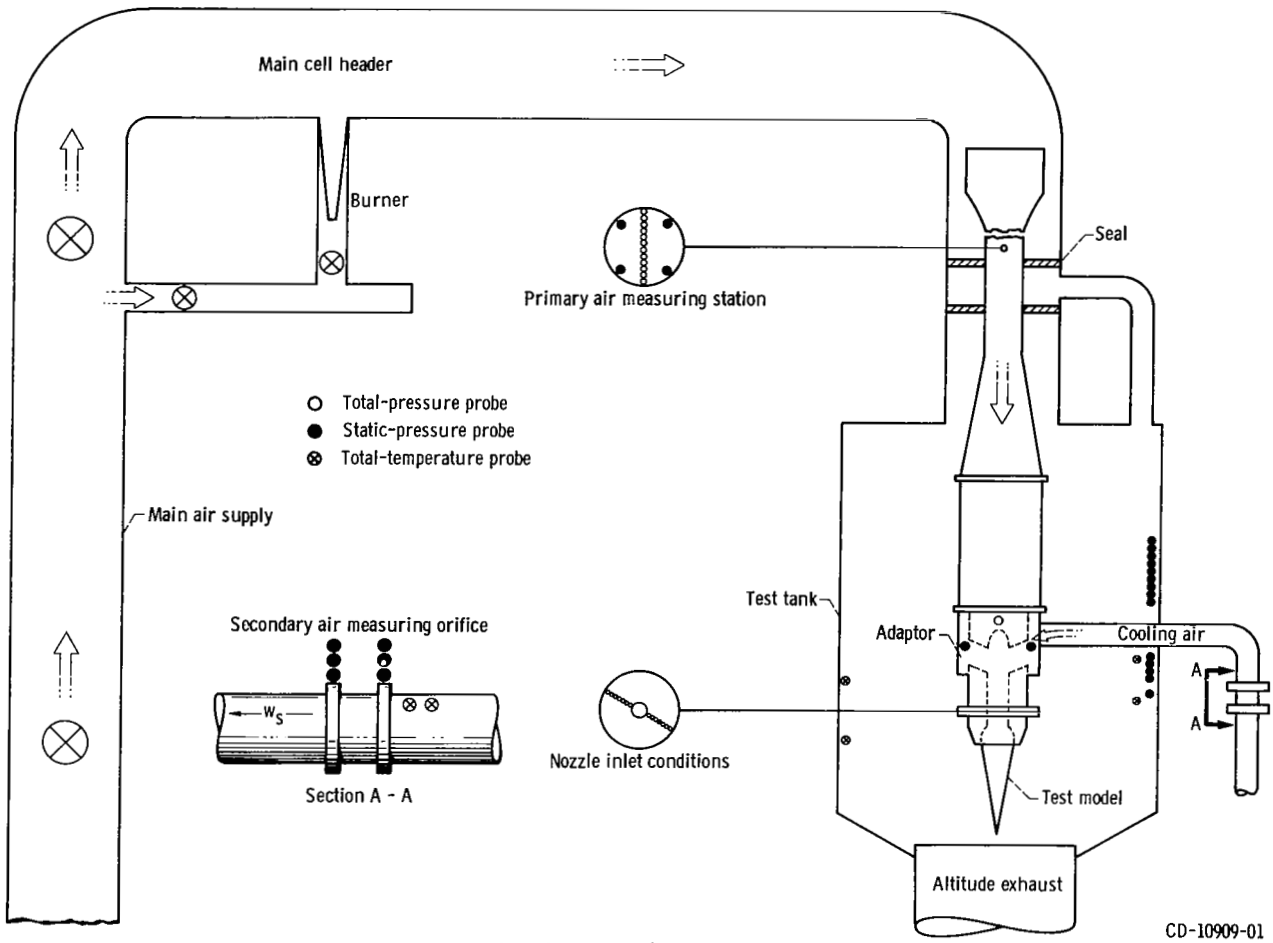

Figure 1. - Schematic of test facility.

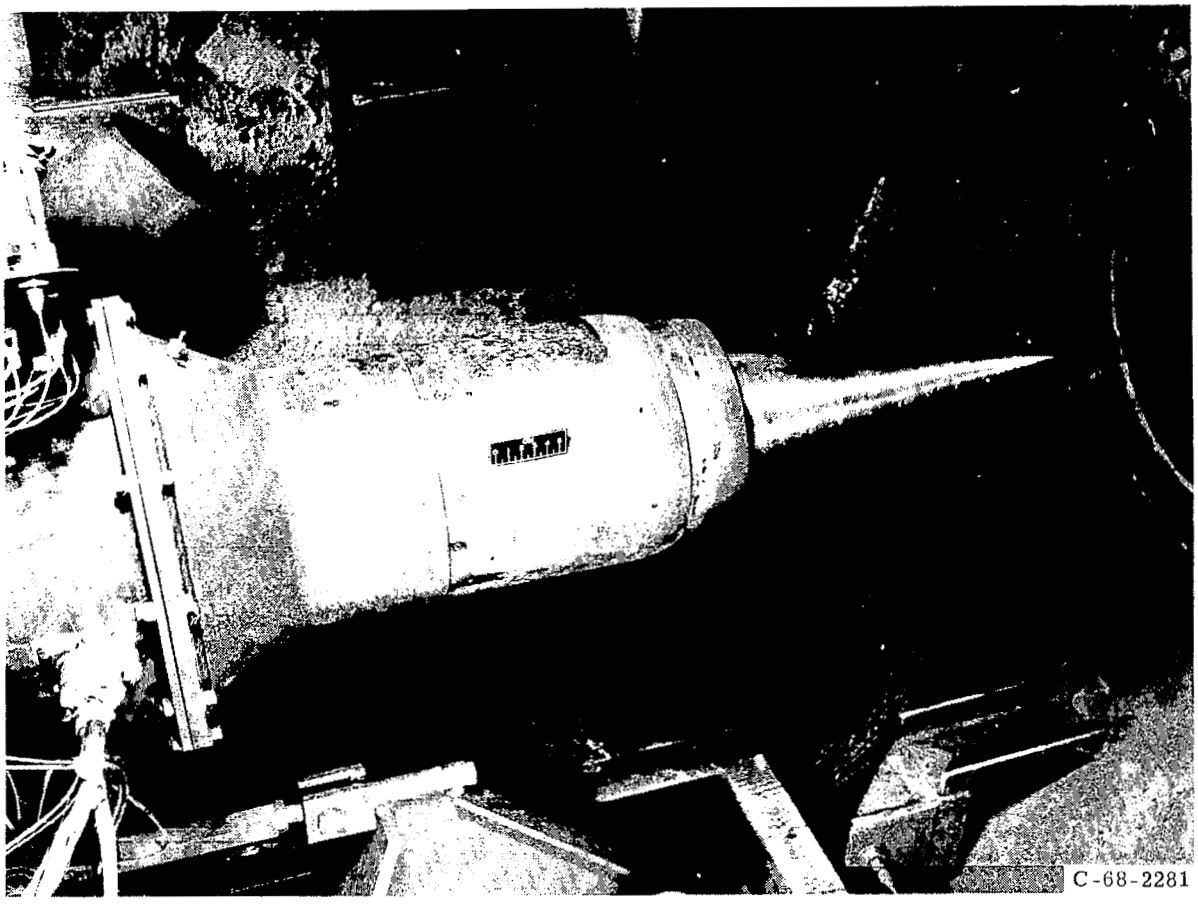

Figure 2. - Installation of model in test facility.

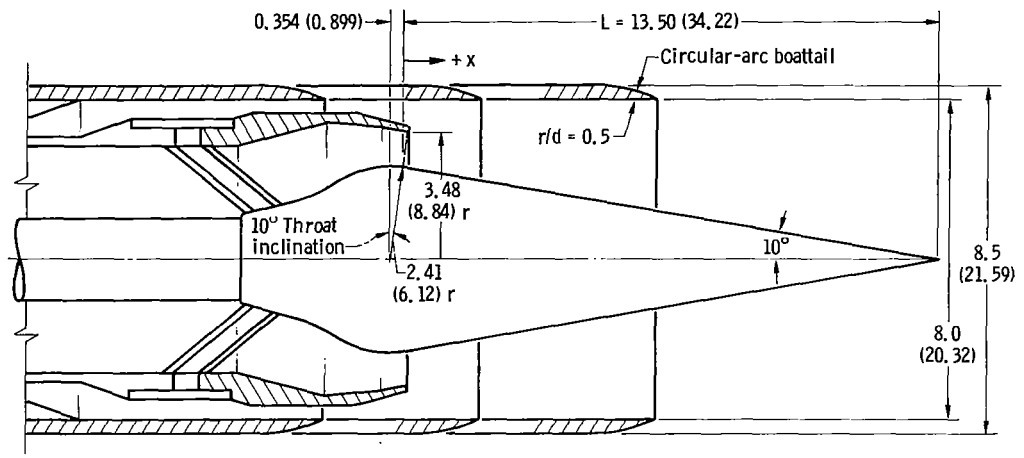

(a) Plug nozzle model dimensions.

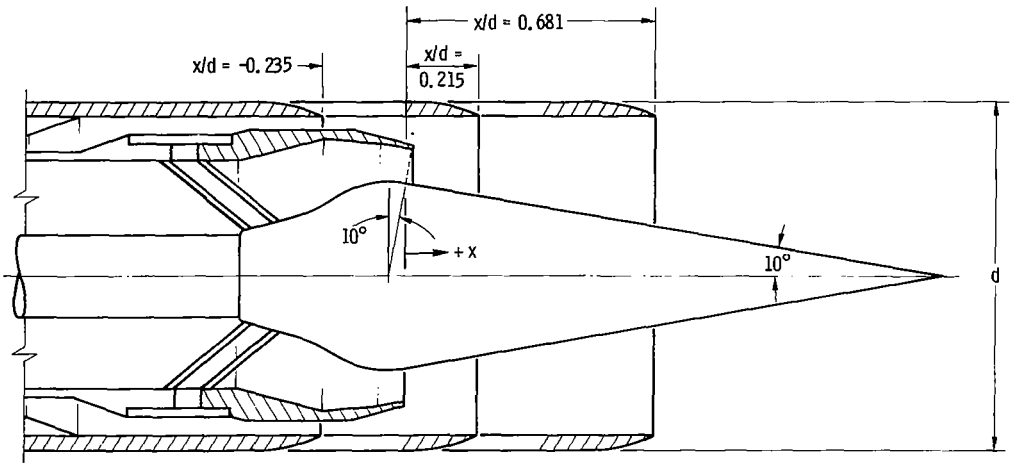

(b) Plug nozzle shroud locations.

CD-10910-01

Figure 3. - Model dimensions and geometric variables. (All dimensions are in inches (cm) unless otherwise noted.)

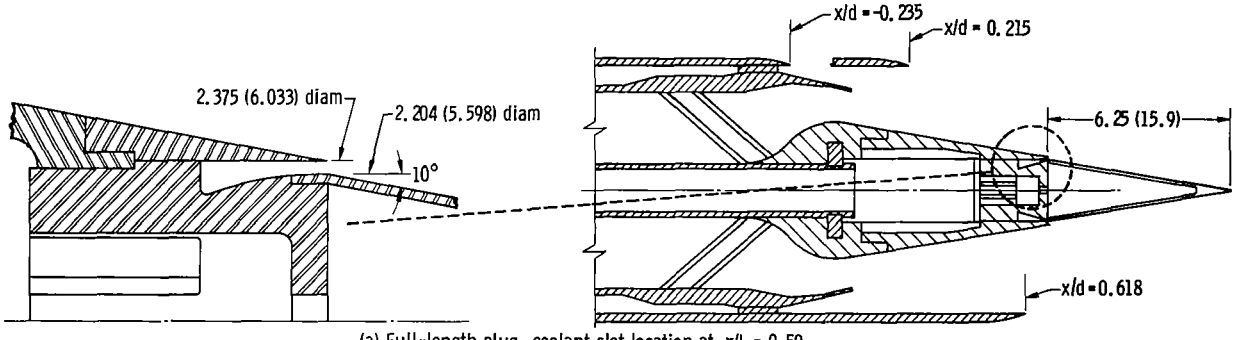

(a) Full-length plug, coolant slot location at x/L = 0.50.

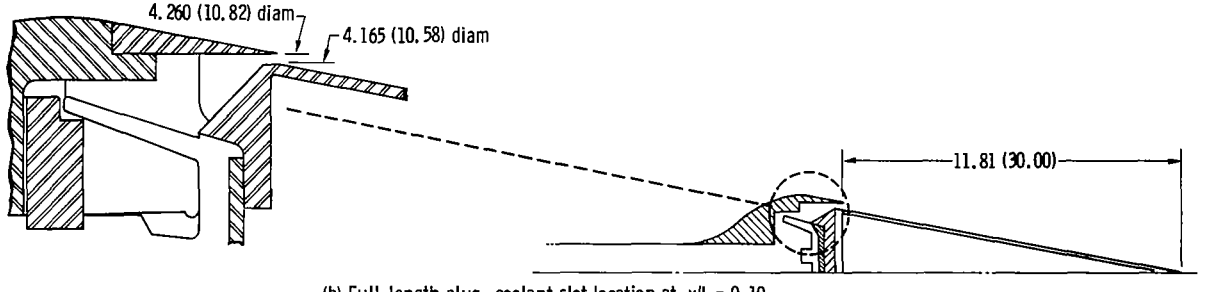

(b) Full-length plug, coolant slot location at x/L = 0.10.

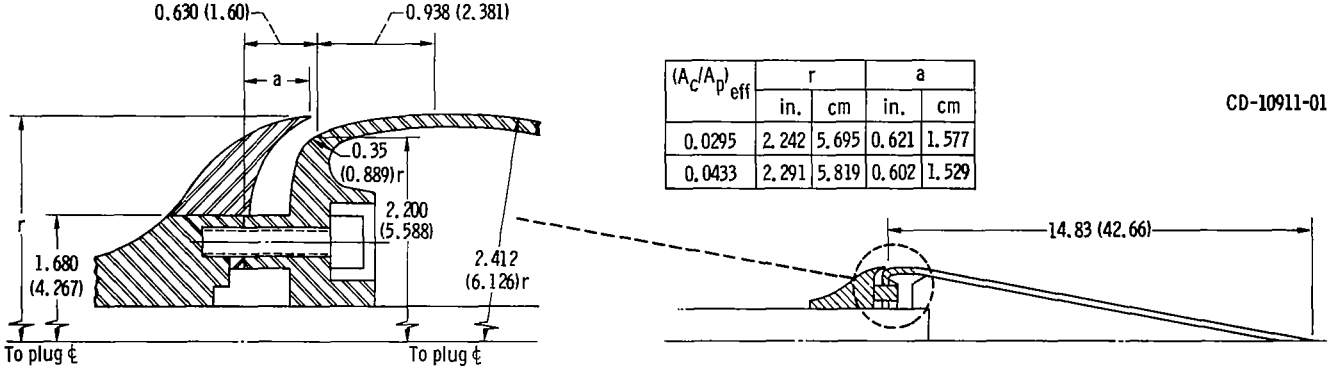

$(A_c/A_p)_{eff}$	r		a	
	in.	cm	in.	cm
0.0295	2.242	5.695	0.621	1.577
0.0433	2.291	5.819	0.602	1.529

CD-10911-01

(c) Full-length plug, coolant slot location at x/L = -0.10.

Figure 4. - Coolant slot configuration details. (All dimensions are in inches (cm).)

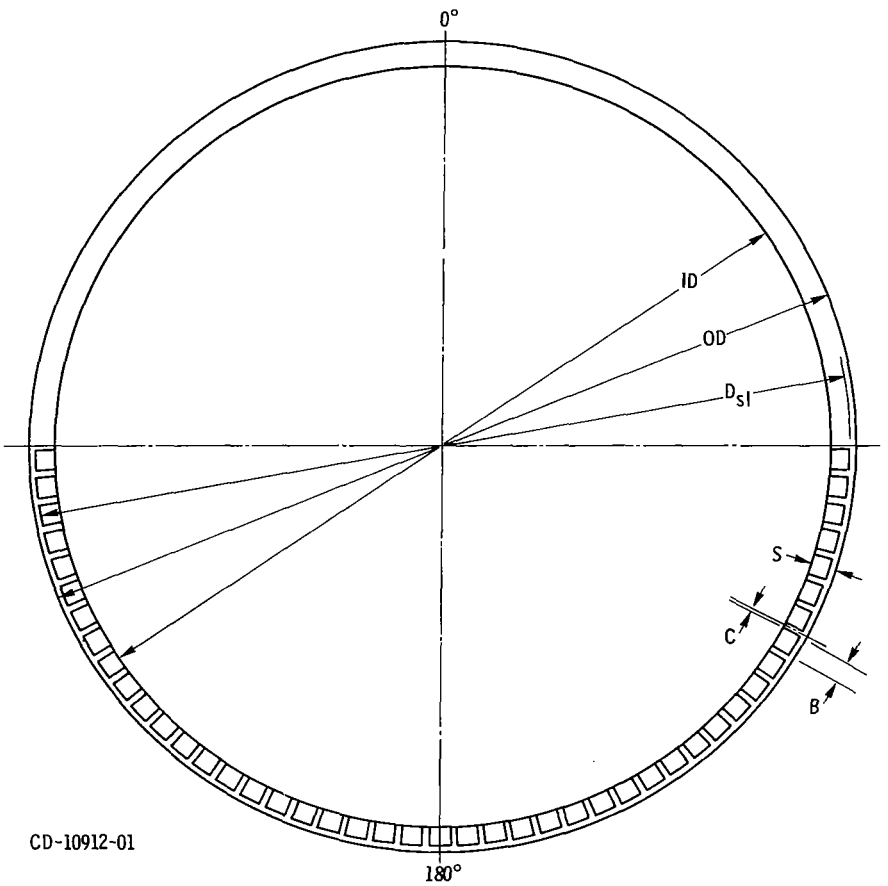

Figure 5. - Coolant slot geometry (see table II).

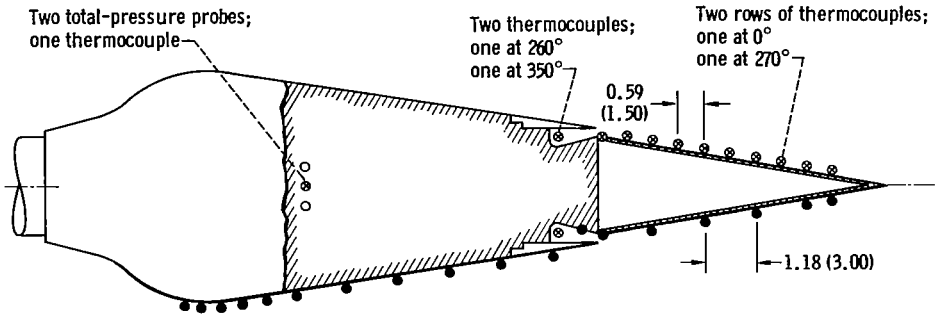

(a) Coolant slot at x/L = 0.50.

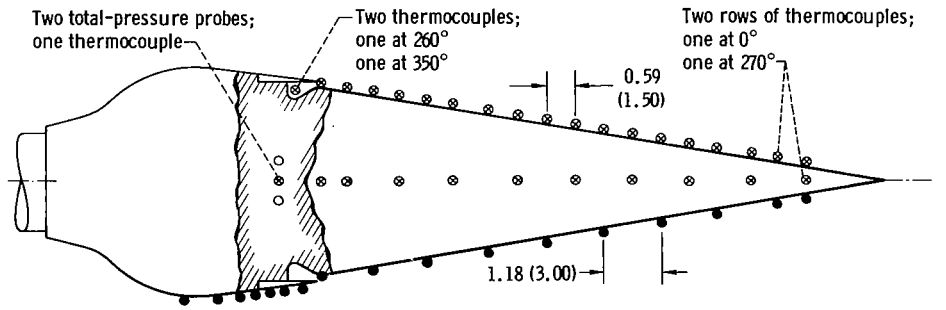

(b) Coolant slot at x/L = 0.10.

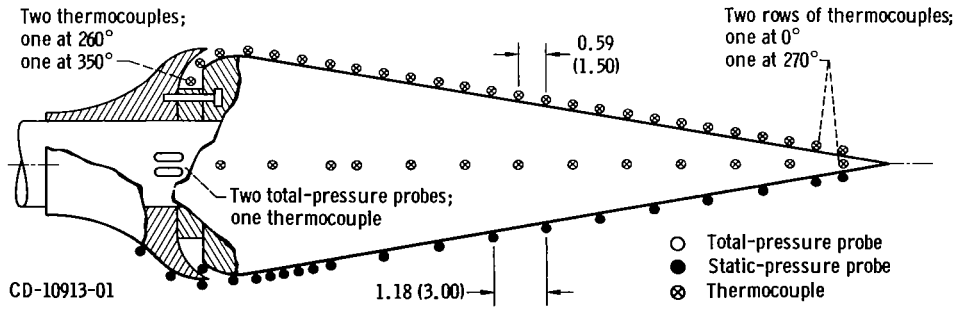

(c) Coolant slot at x/L = -0.10.

Figure 6. - Plug instrumentation. Coolant slots at ratio of axial distance to uncooled plug length, measured from nozzle throat, x/L.

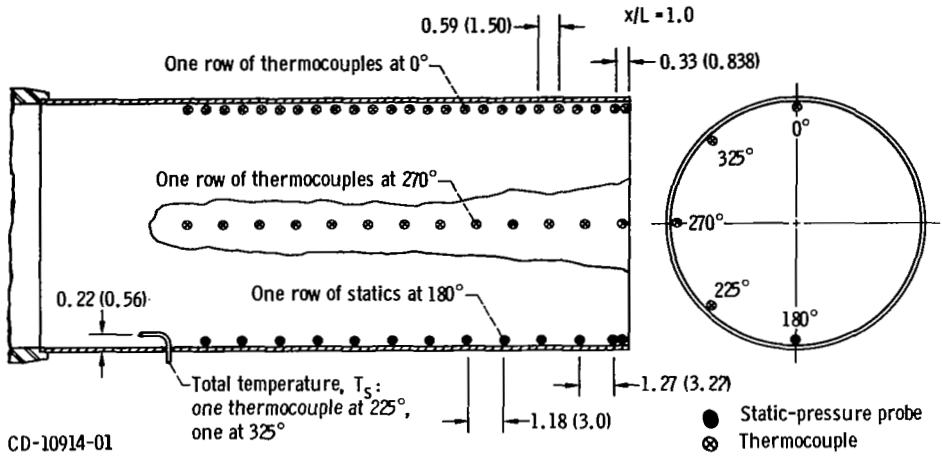

Figure 7. - Heat-transfer shroud instrumentation. (All dimensions are in inches (cm).)

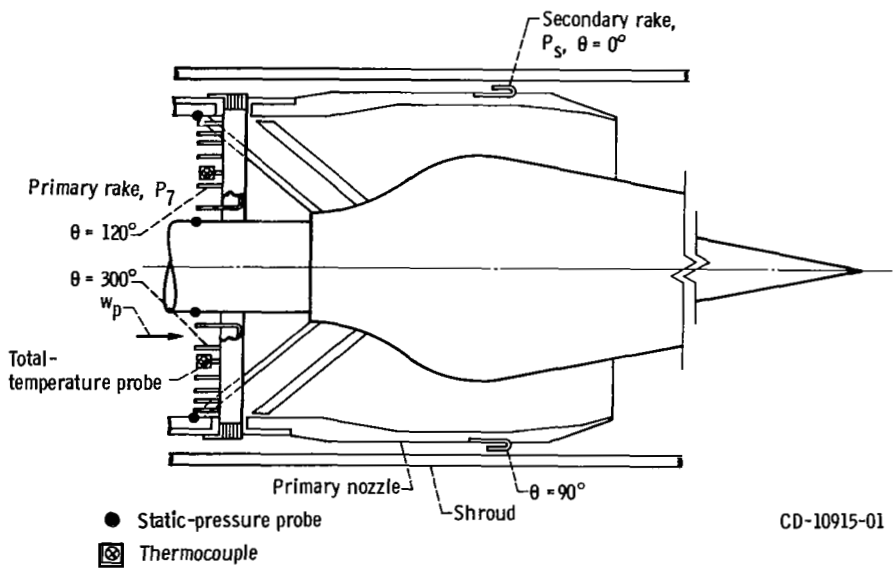

Figure 8. - Model instrumentation.

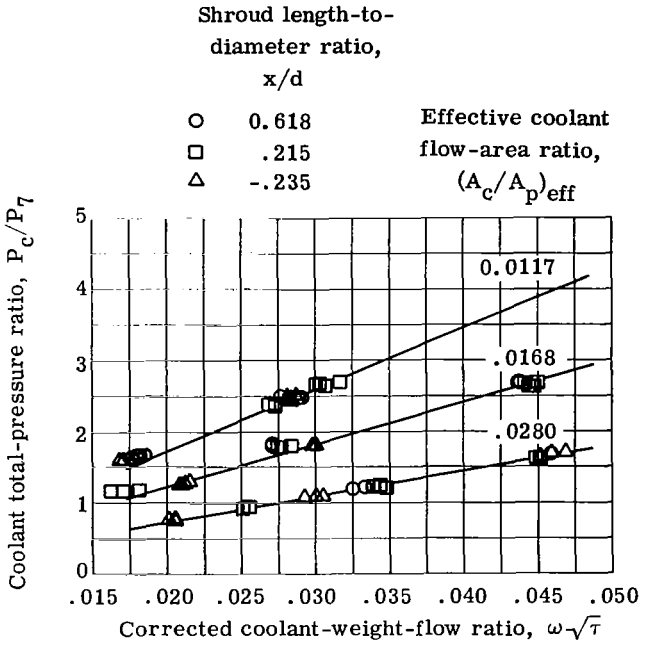

Figure 9. - Pumping characteristics for full-length plug with coolant slot at axial distance from primary nozzle, x/L = 0.50.

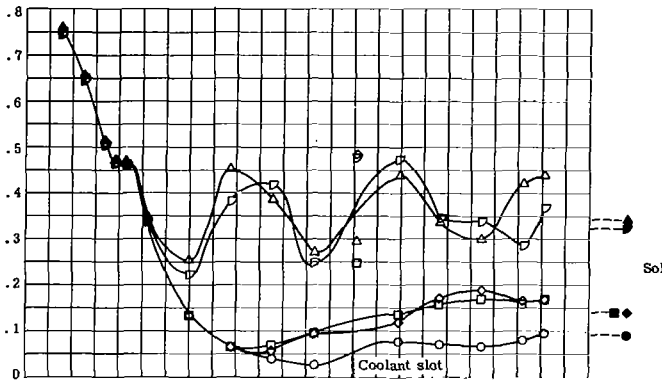

Corrected coolant-weight-flow ratio, $\omega\sqrt{\tau}$	Nozzle pressure ratio, P_7/p_0
○ 0.021	11.0
□ .020	7.3
△ .020	2.9
◇ .039	7.2
▱ .041	3.1

Solid symbols denote p_0/P_7

(a) Shroud length-to-diameter ratio, x/d = -0.235.

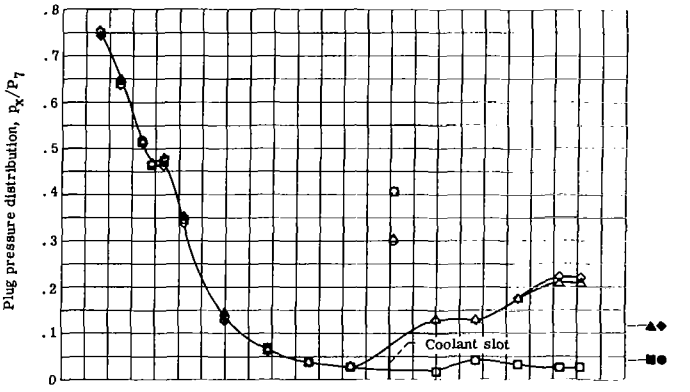

$\omega\sqrt{\tau}$	P_7/p_0
○ 0.025	24.0
□ .034	23.7
△ .026	8.6
◇ .035	8.6

Solid symbols represent p_0/p_7

(b) Shroud length-to-diameter ratio, x/d = 0.215.

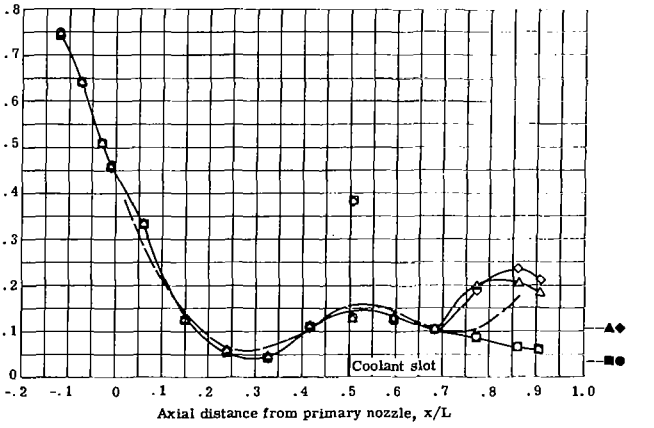

$\omega\sqrt{\tau}$	P_7/p_0
○ 0.011	28.7
□ .033	29.8
△ .012	9.4
◇ .032	9.6
— —	10.0 (ref. 1)

Solid symbols represent p_0/p_7

(c) Shroud length-to-diameter ratio, x/d = 0.618.

Figure 10. - Plug pressure distributions with coolant slot at x/L = 0.50; effective coolant flow-area ratio, $(A_c/A_p)_{eff} = 0.0280$.

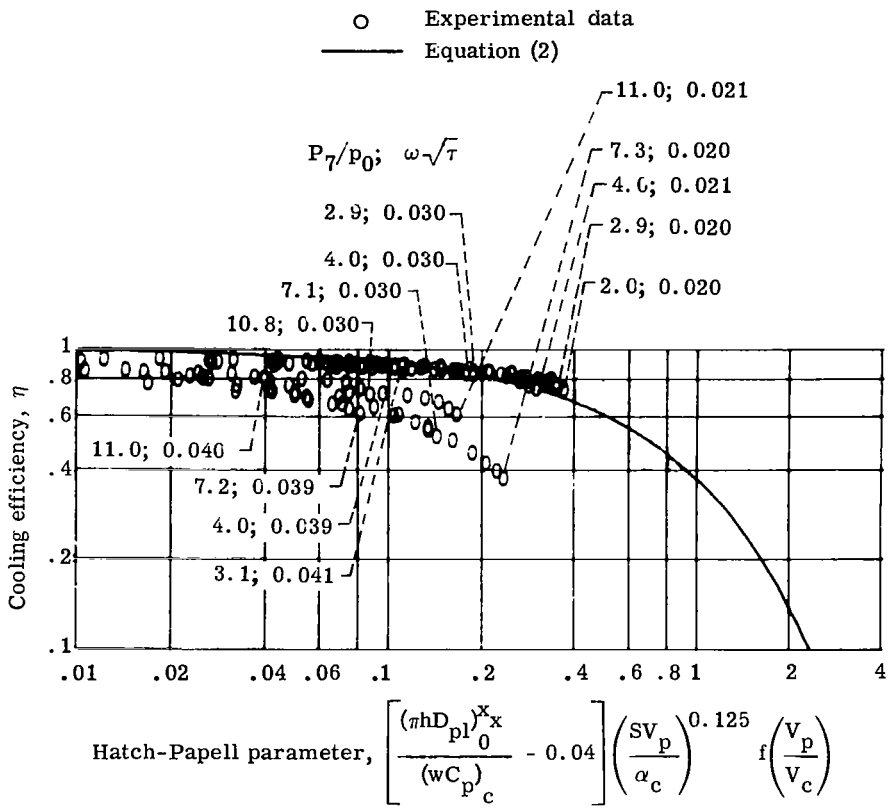

Figure 11. - Comparison of experimental data with Hatch-Papell film-cooling correlation for plug surface with coolant slot at x/L = 0.50. Shroud length-to-diameter ratio, x/d = -0.235; effective coolant flow-area ratio, $(A_c/A_p)_{eff}$ = 0.028; corrected coolant-weight-flow ratio, $0.010 \leq \omega\sqrt{\tau} \leq 0.050$; nozzle pressure ratio, $2 \leq P_7/p_0 \leq 11$.

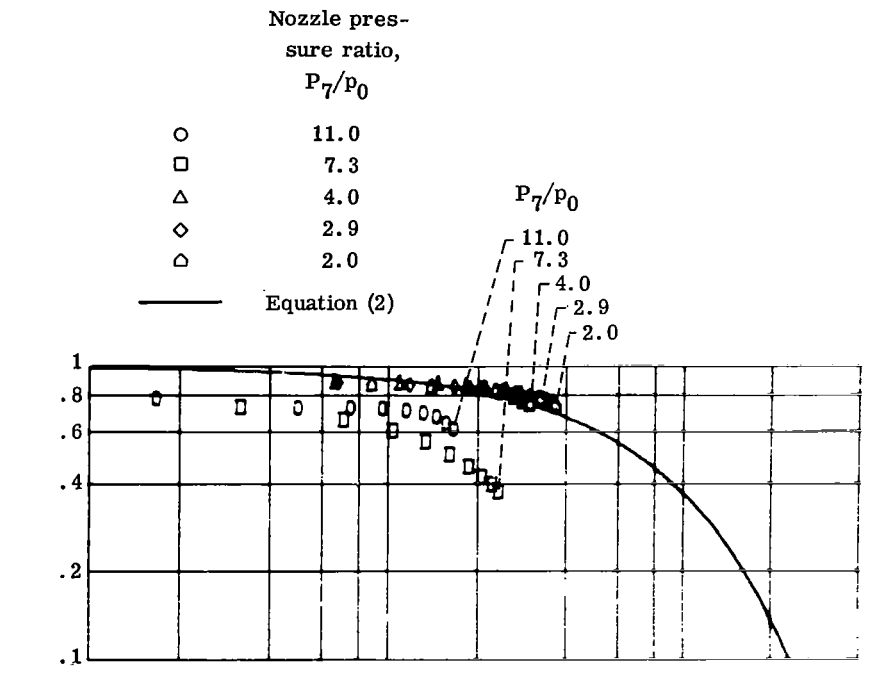

(a) Corrected coolant-weight-flow ratio, $\omega\sqrt{\tau} = 0.02$.

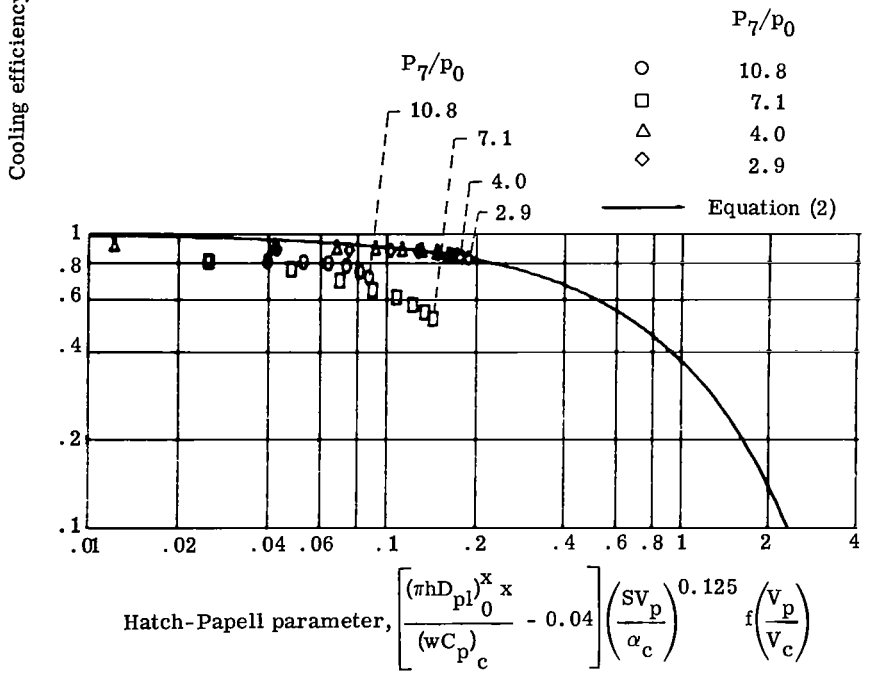

(b) Corrected coolant-weight-flow ratio, $\omega\sqrt{\tau} = 0.03$.

Figure 12. - Effect of nozzle pressure ratio on cooling characteristics of plug surface with coolant slot at x/L = 0.50. Shroud length-to-diameter ratio, x/d = -0.235; effective coolant flow-area ratio, $(A_c/A_p)_{eff} = 0.028$.

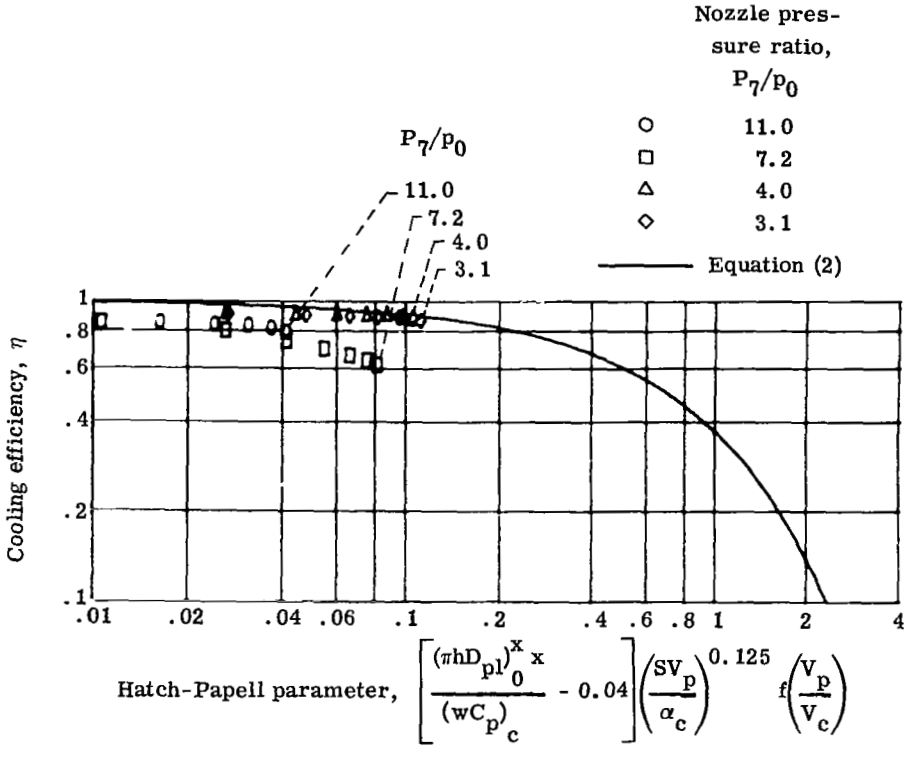

(c) Corrected coolant-weight-flow ratio, $\omega\sqrt{\tau} = 0.04$.

Figure 12. - Concluded.

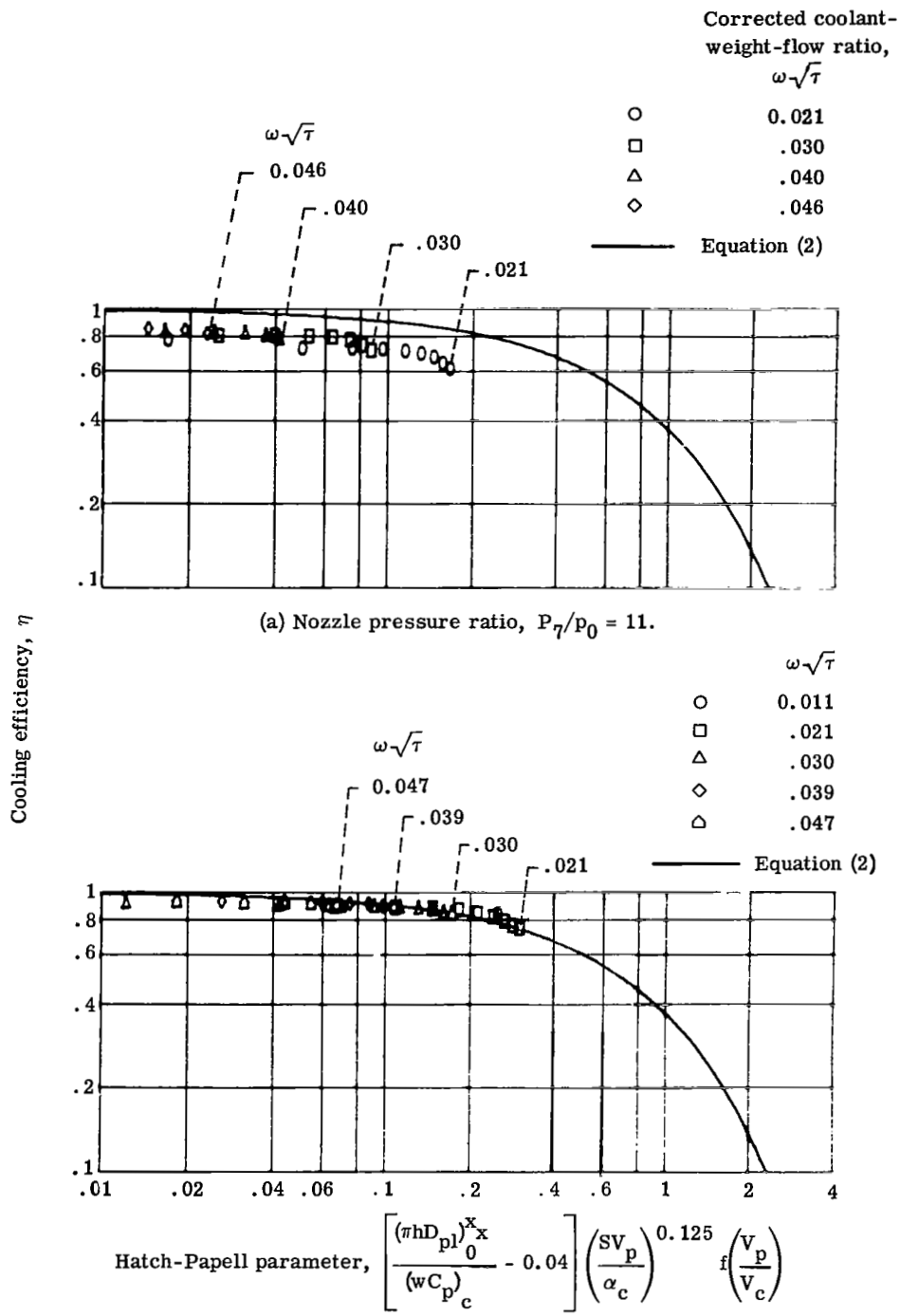

Figure 13. - Effect of corrected coolant flow-area ratio on cooling characteristics of plug surface with coolant slot at $x/L = 0.50$. Shroud length-to-diameter ratio, $x/d = -0.235$; effective coolant flow-area ratio, $(A_c/A_p)_{eff} = 0.028$.

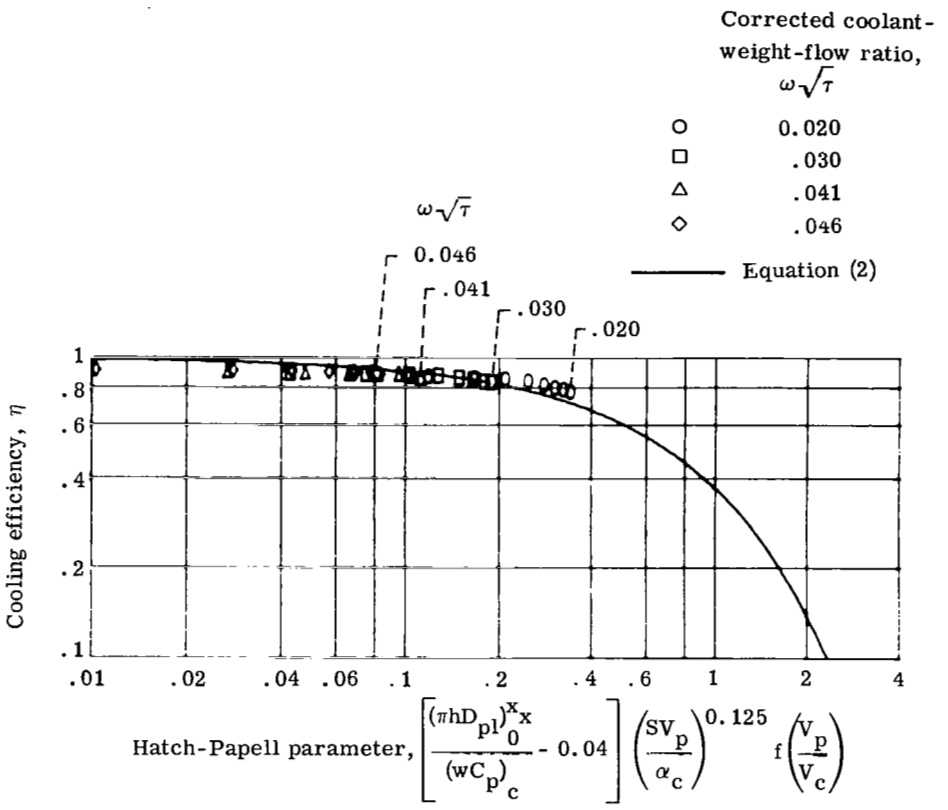

(c) Nozzle pressure ratio, $P_7/p_0 = 3$.

Figure 13. - Concluded.

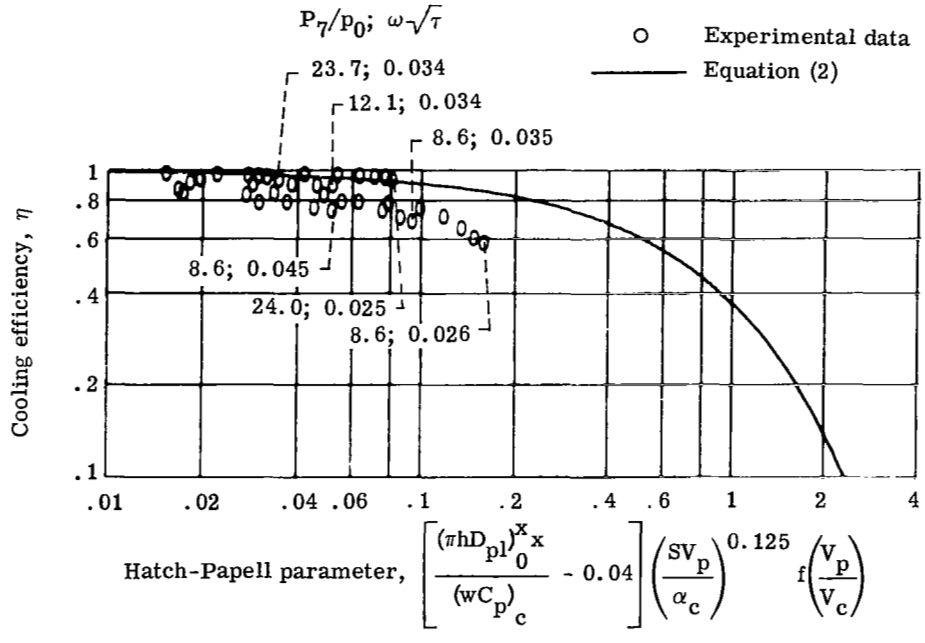

Figure 14. - Comparison of experimental data with Hatch-Papell film-cooling correlation for plug surface with coolant slot at x/L = 0.50. Shroud length-to-diameter ratio, x/d = 0.215; effective coolant flow-area ratio, $(A_c/A_p)_{eff} = 0.028$; corrected coolant-weight-flow ratio, $0.010 \leq \omega\sqrt{\tau} \leq 0.050$; nozzle pressure ratio, $8 \leq P_7/p_0 \leq 24$.

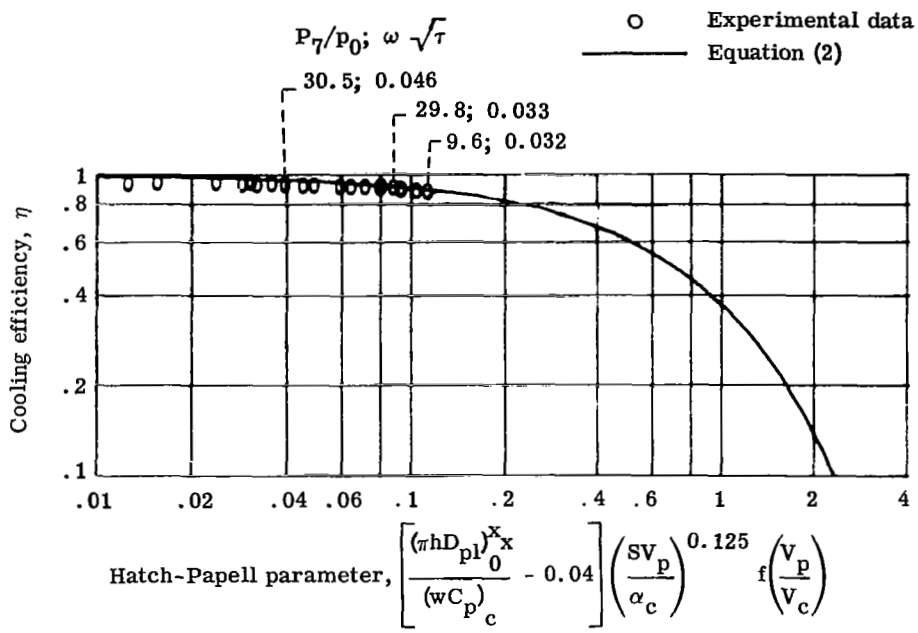

Figure 15. - Comparison of experimental data with Hatch-Papell film-cooling correlation for plug surface with coolant slot at $x/L = 0.50$. Shroud length-to-diameter ratio, $x/d = 0.618$; effective coolant flow-area ratio, $(A_c/A_p)_{eff} = 0.028$; corrected coolant-weight-flow ratio, $0.03 \leq \omega\sqrt{\tau} \leq 0.05$; nozzle pressure ratio, $9 \leq P_7/p_0 \leq 30$.

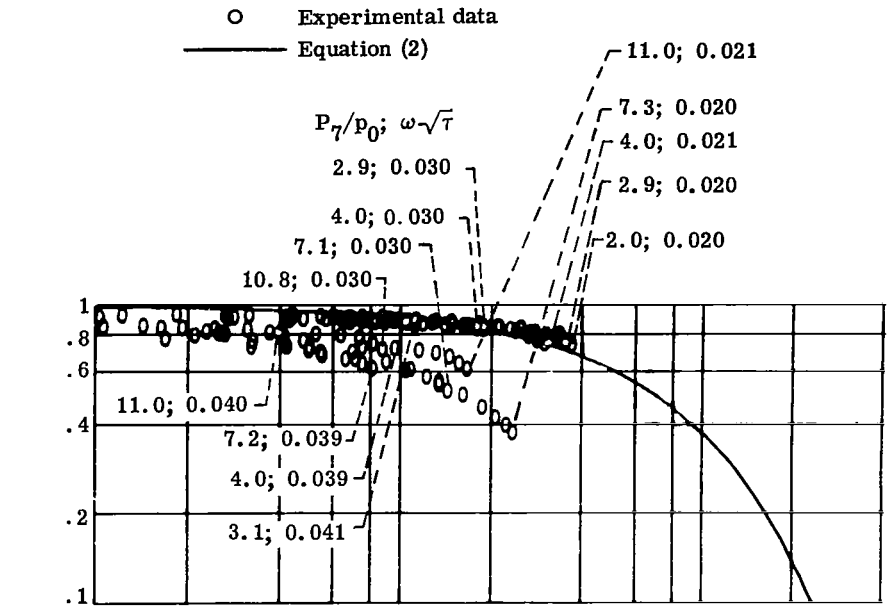

(a) $(A_c/A_p)_{eff} = 0.028$; $0.010 \leq \omega\sqrt{\tau} \leq 0.050$; $2 \leq P_7/p_0 \leq 11$.

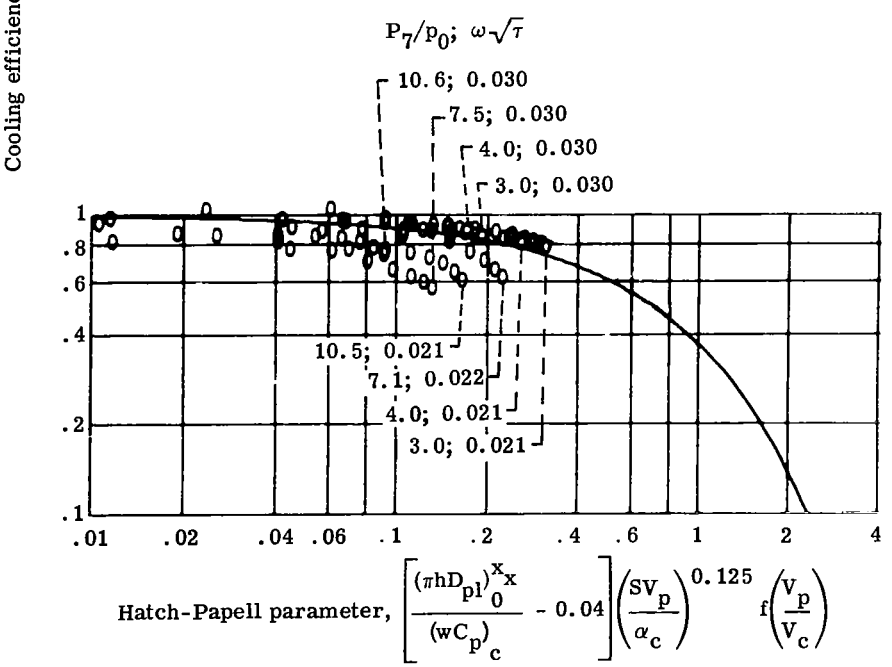

(b) $(A_c/A_p)_{eff} = 0.0168$: $0.010 \leq \omega\sqrt{\tau} \leq 0.030$; $3 \leq P_7/p_0 \leq 11$.

Figure 16. - Effect of coolant slot area on cooling efficiency for plug surface with coolant slot at x/L = 0.50, for various values of effective coolant flow-area ratio, $(A_c/A_p)_{eff}$; corrected coolant-weight-flow ratio, $\omega\sqrt{\tau}$; and nozzle pressure ratio, P_7/p_0. Shroud length-to-diameter ratio, x/d = -0.235.

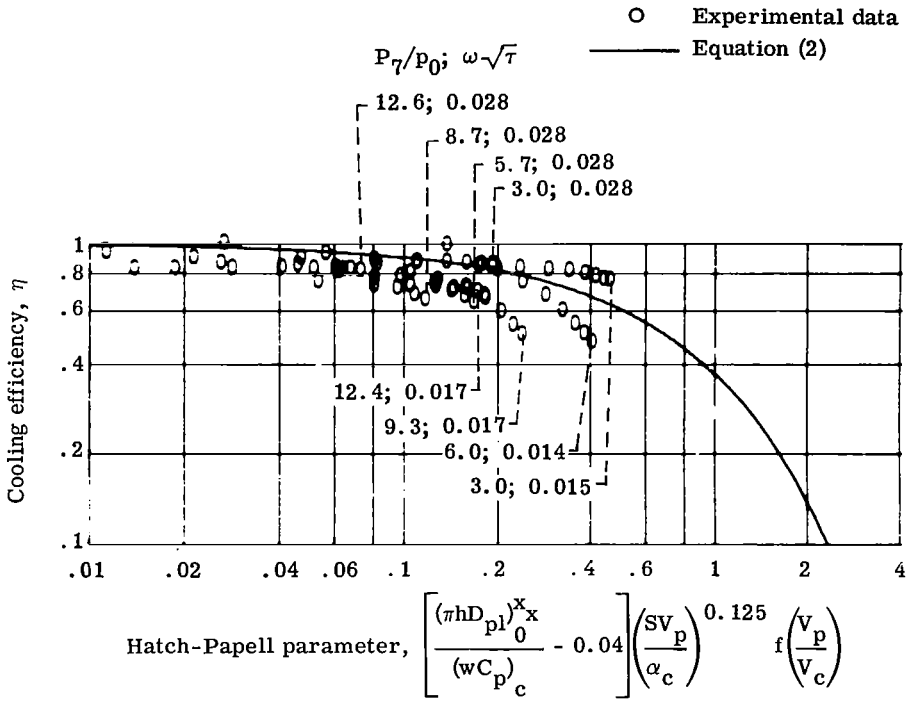

(c) $(A_c/A_p) = 0.0117$; $0.1 \leq \omega\sqrt{\tau} \leq 0.03$; $3 \leq P_7/p_0 \leq 13$.

Figure 16. - Concluded.

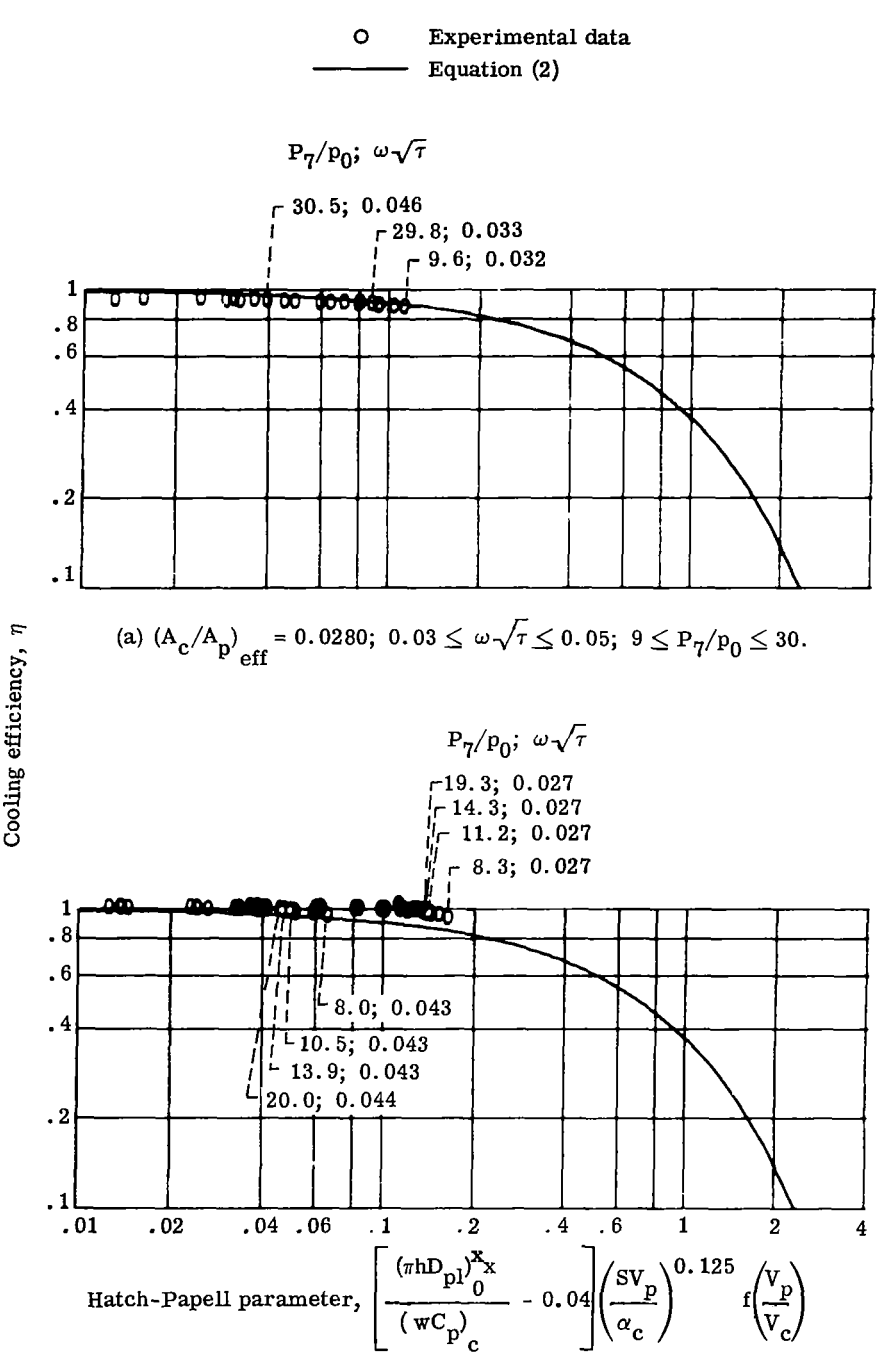

Figure 17. - Effect of coolant slot area on cooling efficiency for plug surface with coolant plot at x/L = 0.50, for various values of effective coolant flow-area ratio, $(A_c/A_p)_{eff}$; corrected coolant-weight-flow ratio, $\omega\sqrt{\tau}$; and nozzle pressure ratio, P_7/p_0. Shroud length-to-diameter ratio, x/d = 0.618.

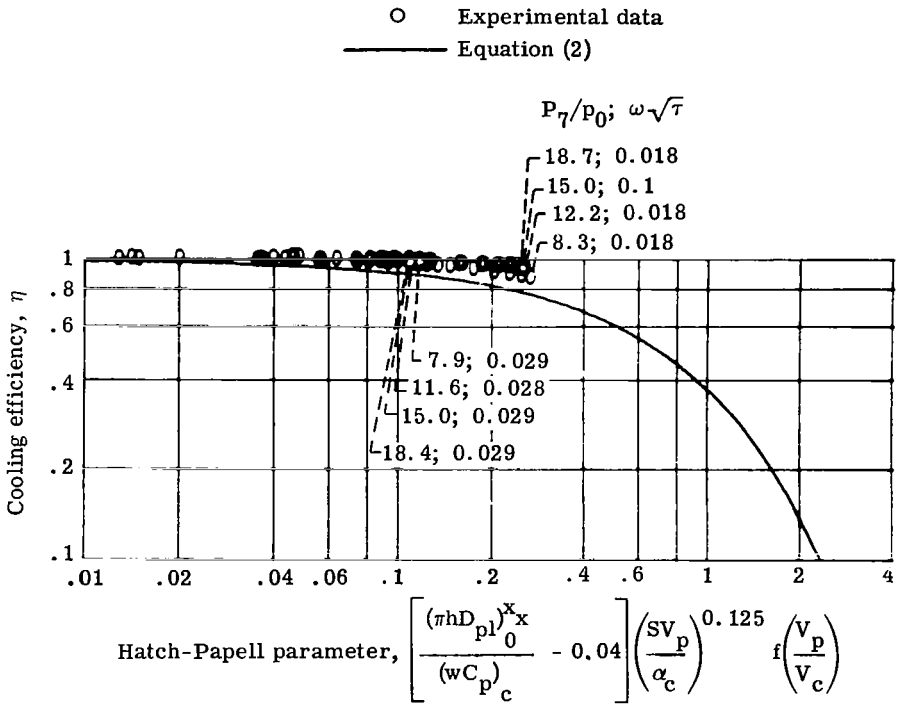

(c) $(A_c/A_p)_{eff} = 0.0117$; $0.010 \leq \omega\sqrt{\tau} \leq 0.030$; $7 \leq P_7/p_0 \leq 19$.

Figure 17. - Concluded.

	Corrected coolant-weight-flow ratio, $\omega\sqrt{\tau}$	Nozzle pressure ratio, P_7/p_0
○	0.011	28.7
□	.033	29.8
△	.012	9.4
◇	.032	9.6

Flagged data measured downstream of plug support strut

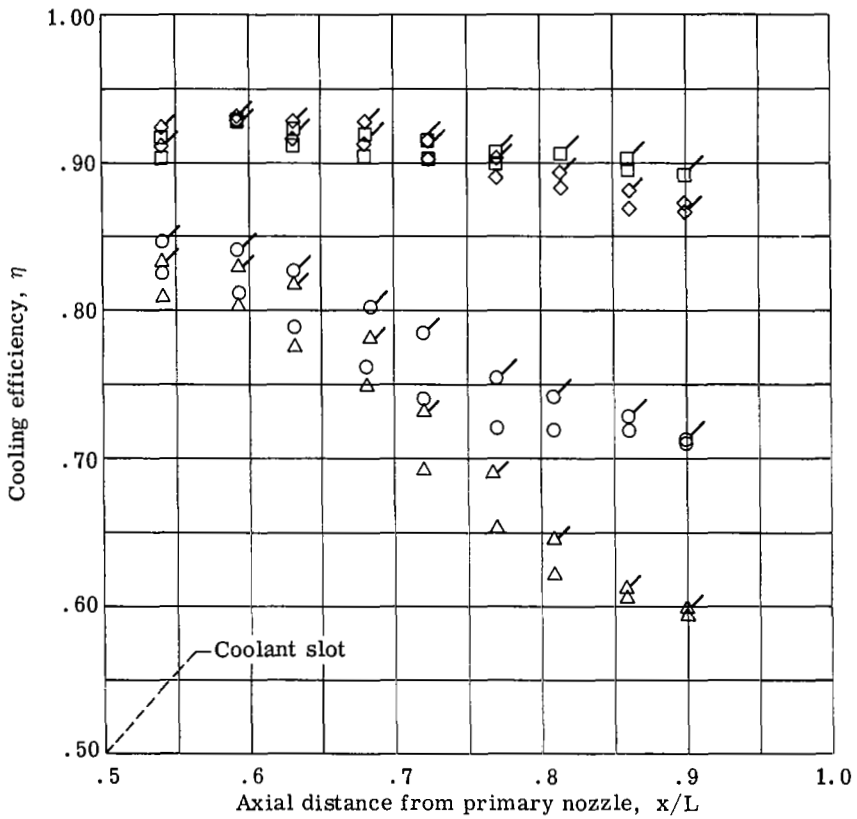

Figure 18. - Effect of plug struts on cooling characteristics of plug nozzle with coolant slot at x/L = 0.50. Shroud length-to-diameter ratio, x/d = 0.618; effective coolant flow-area ratio, $(A_c/A_p)_{eff}$ = 0.028.

	Corrected coolant-weight-flow ratio, $\omega\sqrt{\tau}$	Nozzle pressure ratio, P_7/p_0
○	0.018	18.7
□	.029	18.4
△	.018	8.3
◇	.029	7.9

Flagged data measured downstream of coolant slot tab and plug support strut

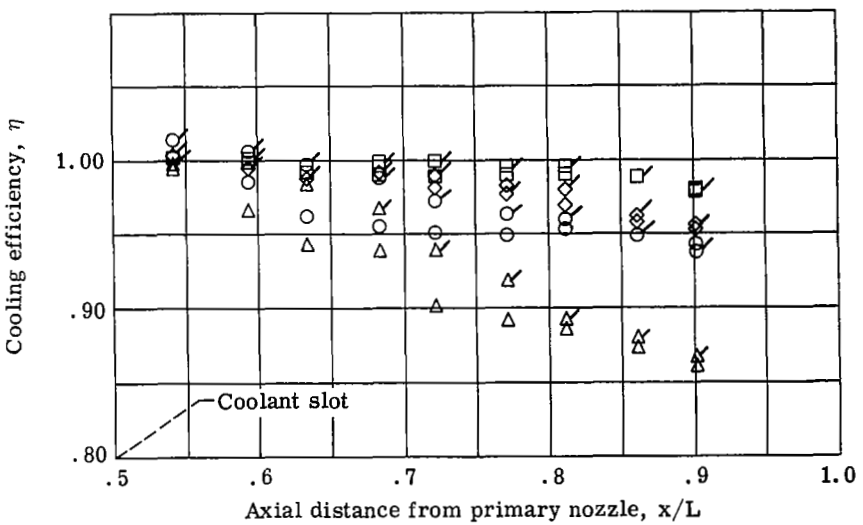

Figure 19. - Effect of coolant slot tabs on cooling characteristics of plug nozzle with coolant slot at x/L = 0.50. Shroud length-to-diameter ratio, x/d = 0.618; effective coolant flow-area ratio, $(A_c/A_p)_{eff}$ = 0.0117.

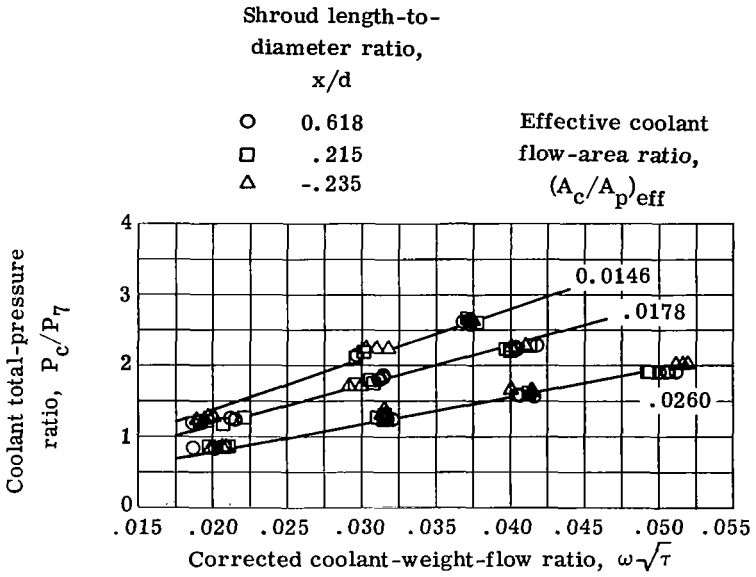

Figure 20. - Pumping characteristics for full-length plug with coolant slot at x/L = 0.10.

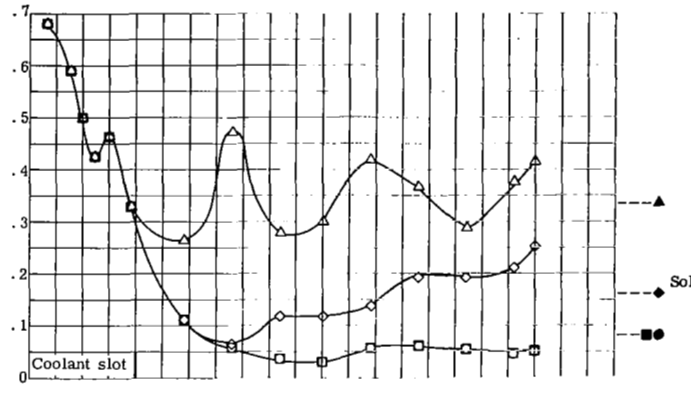

Corrected coolant-weight-flow ratio, $\omega\sqrt{\tau}$	Nozzle pressure ratio, P_7/p_0
○ 0.020	13.0
□ .042	12.7
△ .020	3.0
◇ .019	6.2

Solid symbols denote p_0/P_7

(a) Shroud length-to-diameter ratio, x/d = -0.235.

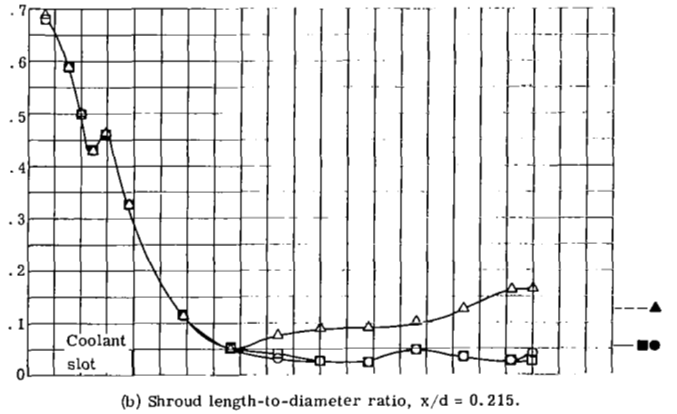

$\omega\sqrt{\tau}$	P_7/p_0
○ 0.021	18.7
□ .041	18.7
△ .020	8.0

Solid symbols denote p_0/P_7

(b) Shroud length-to-diameter ratio, x/d = 0.215.

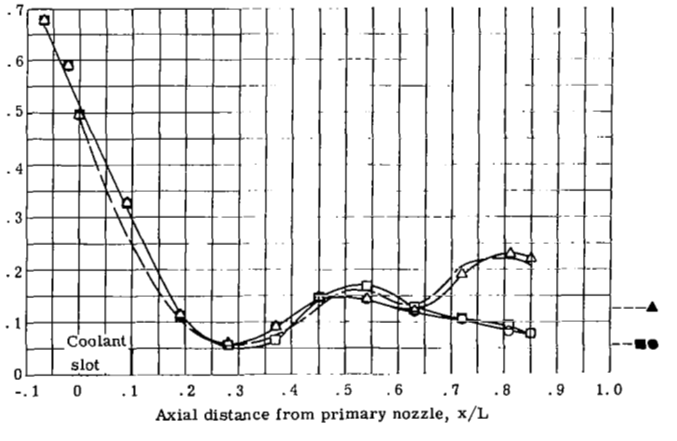

$\omega\sqrt{\tau}$	P_7/p_0
○ 0.019	18.9
□ .040	18.6
△ .020	8.2
— — — -----	7.9 (ref. 1)

Solid symbols denote p_0/P_7

(c) Shroud length-to-diameter ratio, x/d = 0.618.

Figure 21. - Plug pressure distributions with coolant slot at x/L = 0.10. Effective coolant flow-area ratio, $(A_c/A_p)_{eff} = 0.026$.

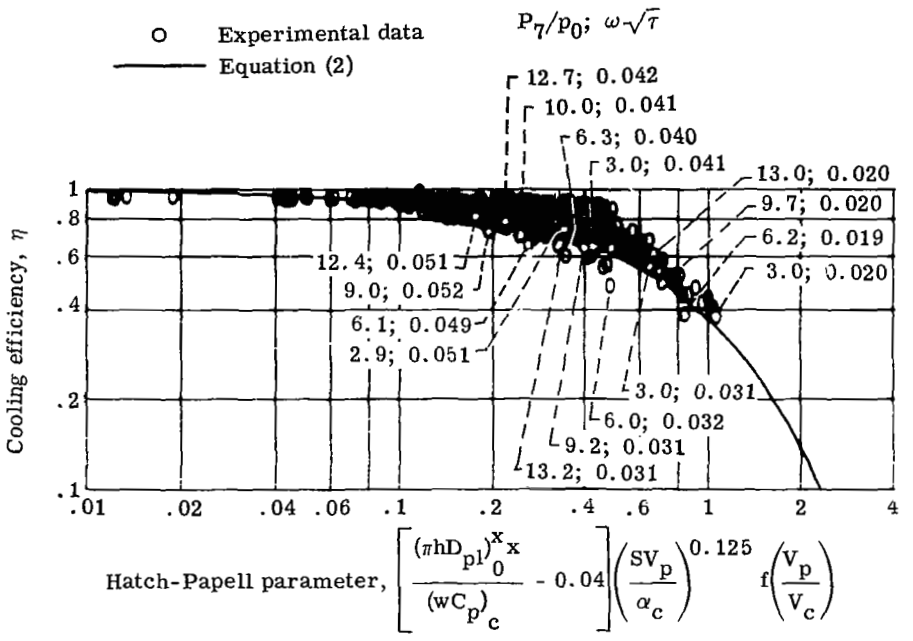

Figure 22. - Comparison of experimental data with Hatch-Papell film-cooling correlation for plug surface with coolant slot at $x/L = 0.10$. Shroud length-to-diameter ratio, $x/d = -0.235$; effective coolant flow-area ratio, $(A_c/A_p)_{eff} = 0.026$; corrected coolant-weight-flow ratio, $0.020 \leq \omega\sqrt{\tau} \leq 0.050$; nozzle pressure ratio, $3 \leq P_7/p_0 \leq 13$.

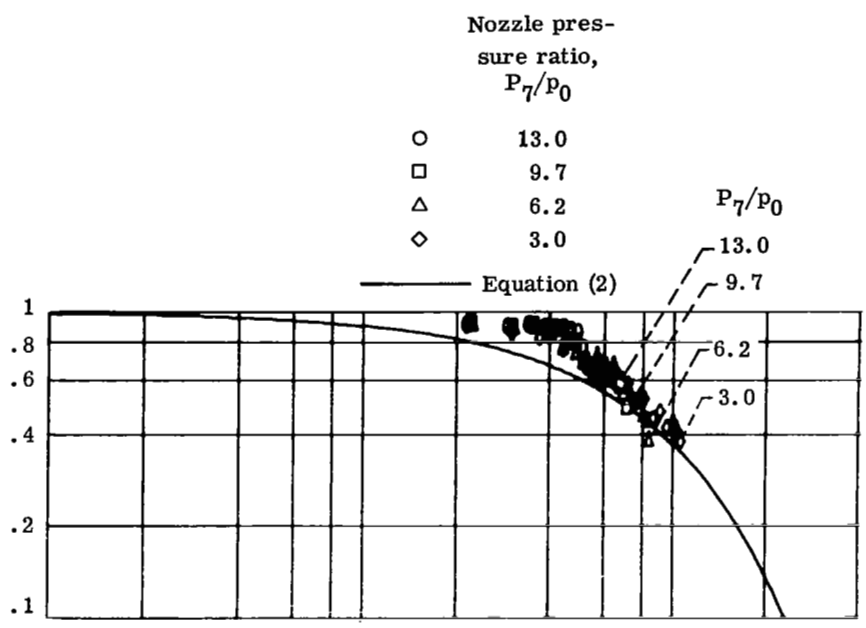

(a) Corrected coolant-weight-flow ratio, $\omega \sqrt{\tau} = 0.02$.

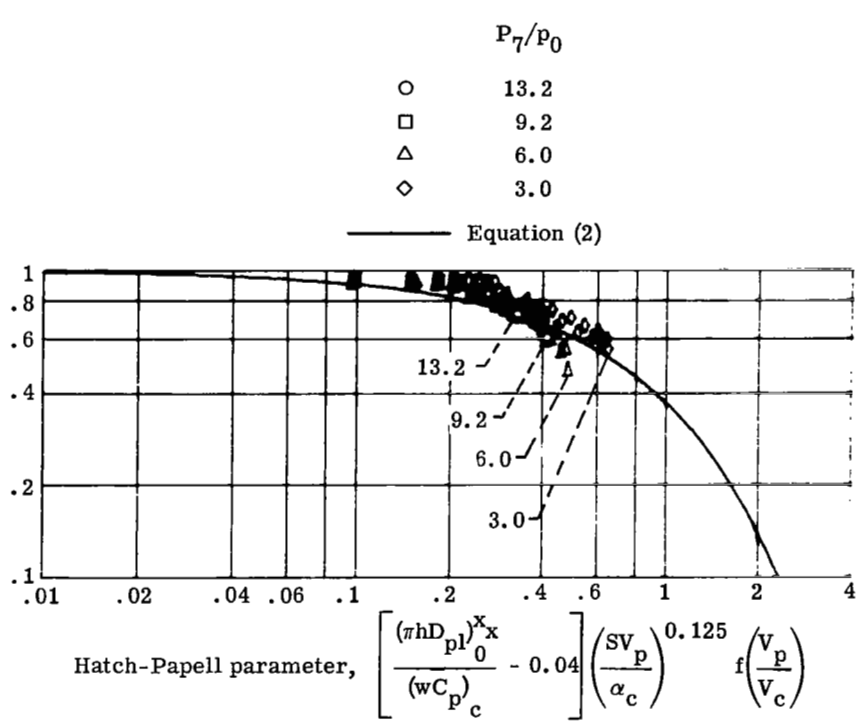

(b) Corrected coolant-weight-flow ratio, $\omega \sqrt{\tau} = 0.031$.

Figure 23. - Effect of nozzle pressure ratio on cooling characteristics of plug surface with coolant slot at $x/L = 0.10$. Shroud length-to-diameter ratio, $x/d = -0.235$; effective coolant flow-area ratio, $(A_c/A_p)_{eff} = 0.026$.

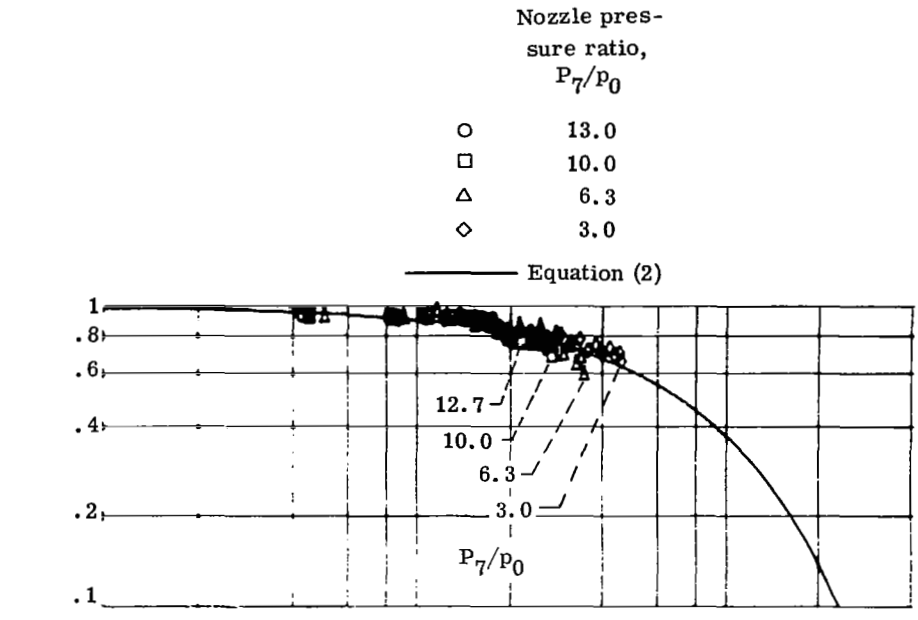

(c) Corrected coolant-weight-flow ratio, $\omega\sqrt{\tau} = 0.041$.

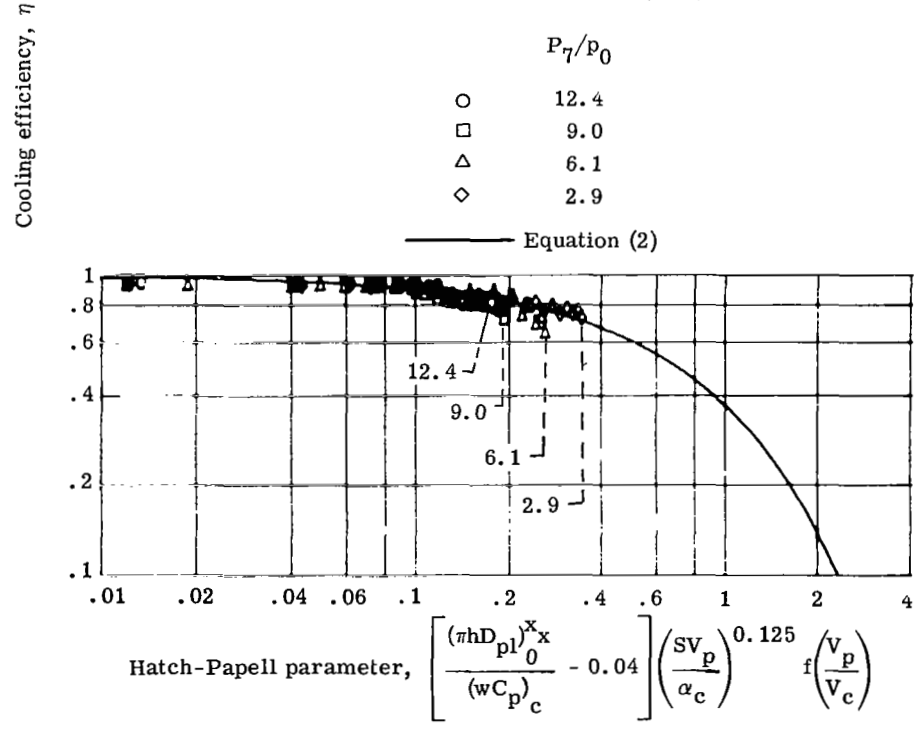

(d) Corrected coolant-weight-flow ratio, $\omega\sqrt{\tau} = 0.051$.

Figure 23. - Concluded.

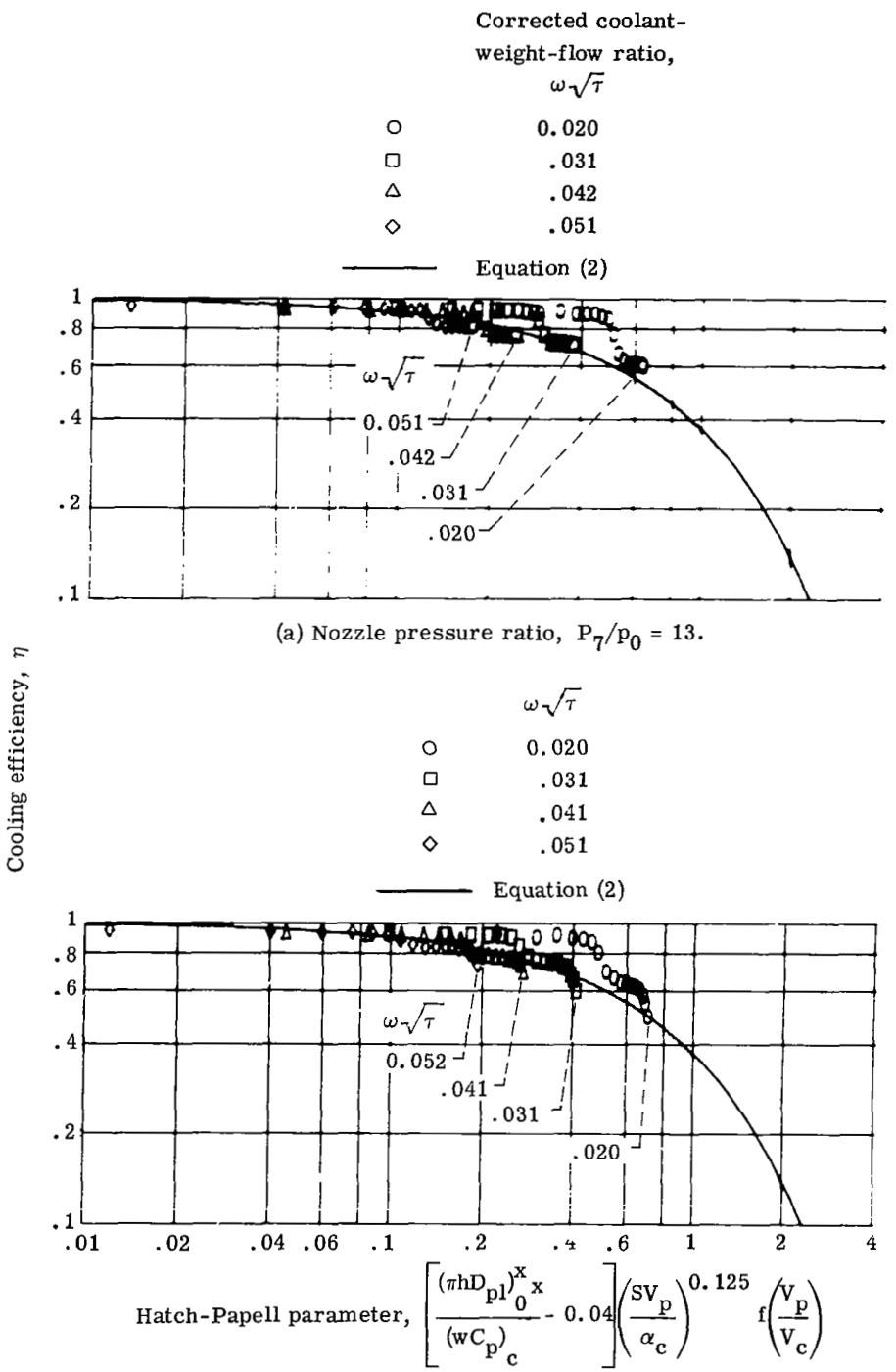

(a) Nozzle pressure ratio, $P_7/p_0 = 13.$

(b) Nozzle pressure ratio, $P_7/p_0 = 9.$

Figure 24. - Effect of corrected coolant-weight-flow ratio on cooling characteristics of plug surface with coolant slot at $x/L = 0.10$. Shroud length-to-diameter ratio, $x/d = -0.235$; effective coolant flow-area ratio, $(A_c/A_p)_{eff} = 0.026$.

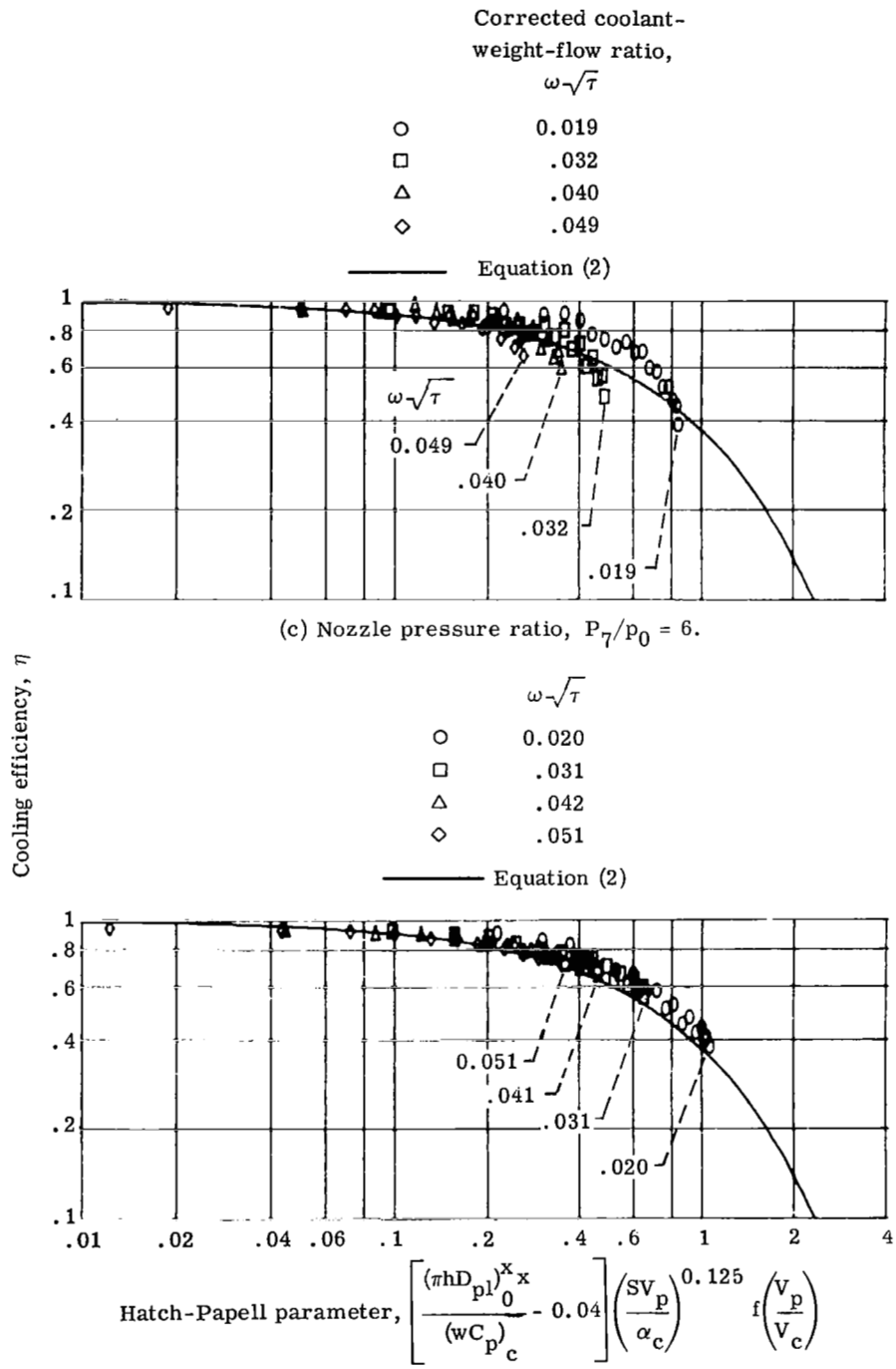

(c) Nozzle pressure ratio, $P_7/p_0 = 6$.

(d) Nozzle pressure ratio, $P_7/p_0 = 3$.

Figure 24. - Concluded.

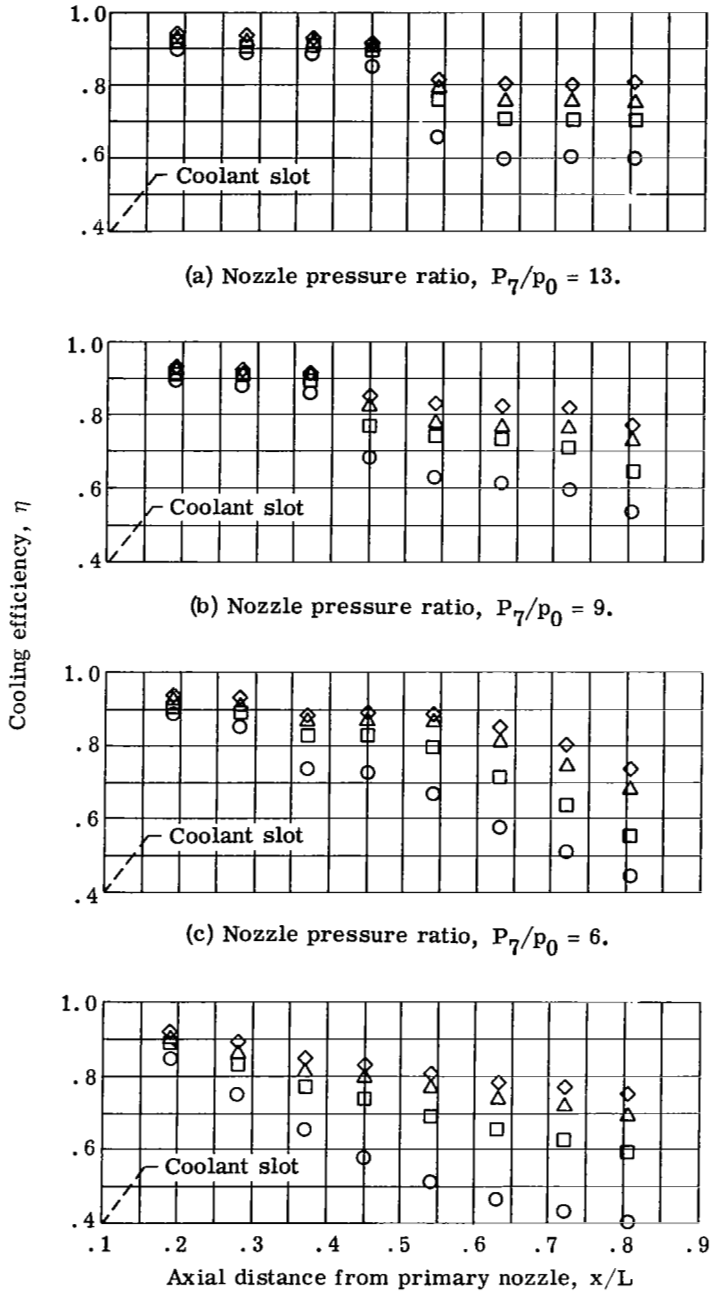

Figure 25. - Cooling efficiency along plug surface with coolant slot at x/L = 0.10. Shroud length-to-diameter ratio, x/d = -0.235; effective coolant flow-area ratio, $(A_c/A_p)_{eff}$ = 0.026.

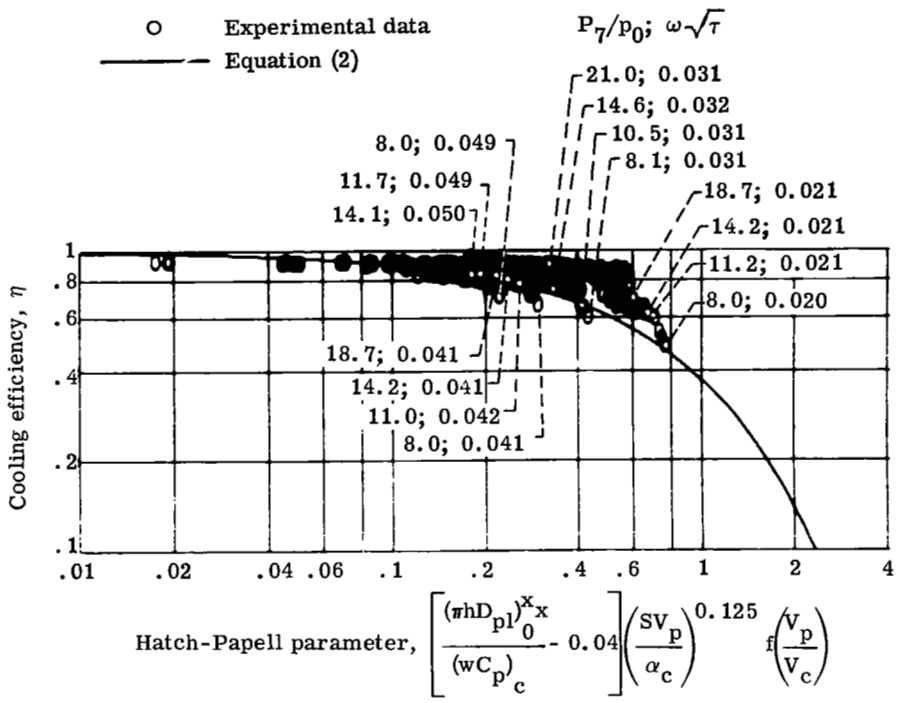

Figure 26. - Comparison of experimental data with Hatch-Papell film-cooling correlation for plug surface with coolant slot at $x/L = 0.10$. Shroud length-to-diameter ratio, $x/d = 0.215$; effective coolant flow-area ratio, $(A_c/A_p)_{eff} = 0.026$; corrected coolant-weight-flow ratio, $0.020 \leq \omega\sqrt{\tau} \leq 0.050$; nozzle pressure ratio, $8 \leq P_7/p_0 \leq 21$.

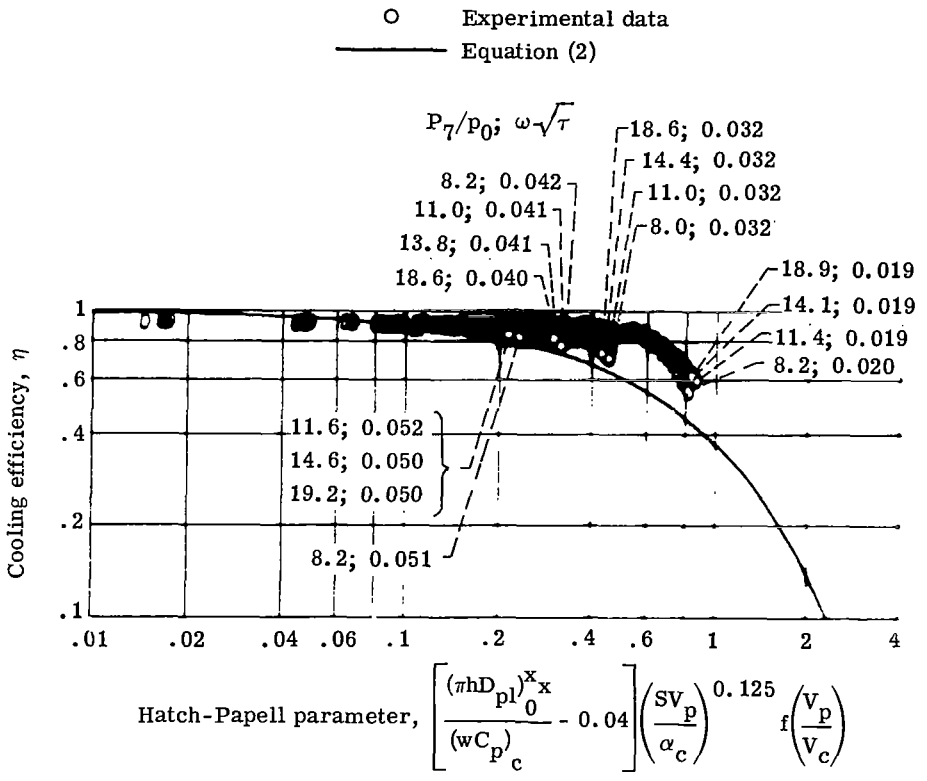

Figure 27. - Comparison of experimental data with Hatch-Papell film-cooling correlation for plug surface with coolant slot at $x/L = 0.10$. Shroud length-to-diameter ratio, $x/d = 0.618$; effective coolant flow-area ratio, $(A_c/A_p)_{eff} = 0.026$; corrected coolant-weight-flow ratio, $0.020 \leq \omega\sqrt{\tau} \leq 0.050$; nozzle pressure ratio, $8 \leq P_7/p_0 \leq 20$.

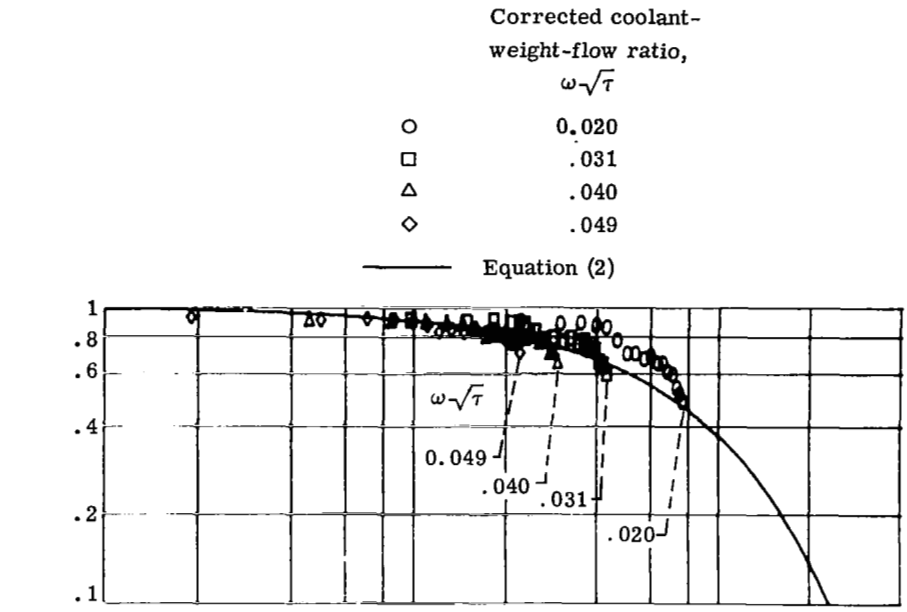

(a) Nozzle pressure ratio, $P_7/p_0 = 8$.

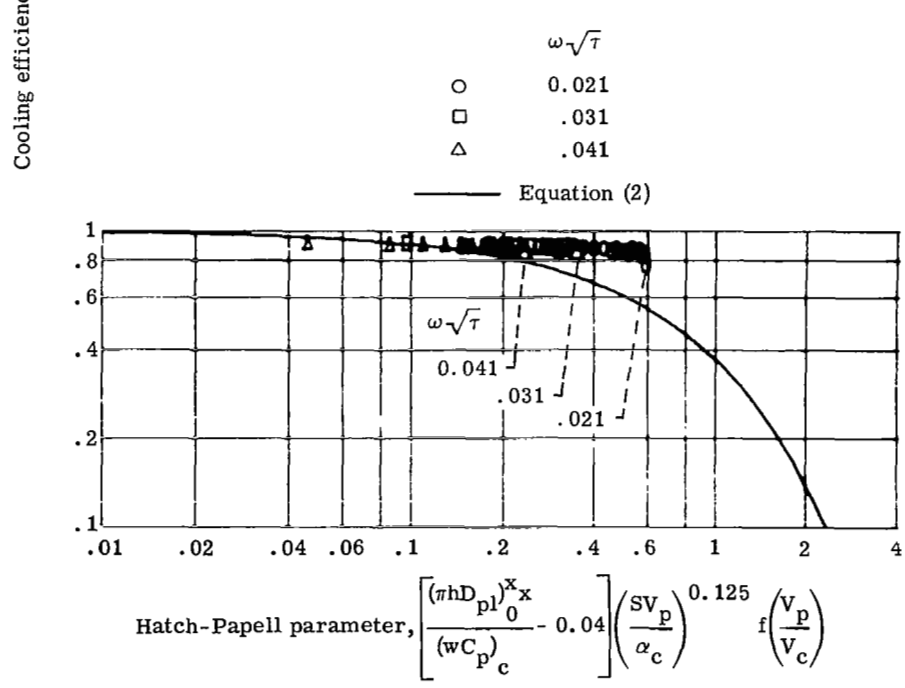

(b) Nozzle pressure ratio, $P_7/p_0 = 19$.

Figure 28. - Effect of corrected coolant-weight-flow ratio on cooling characteristics of plug surface with coolant slot at $x/L = 0.10$. Shroud length-to-diameter ratio, $x/d = 0.215$; effective coolant-flow-area ratio, $(A_c/A_p)_{eff} = 0.026$.

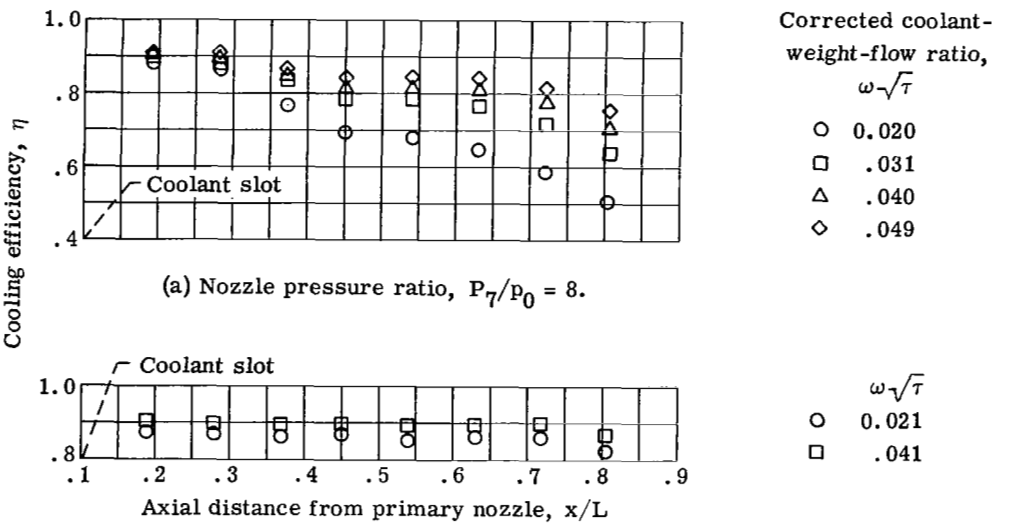

(a) Nozzle pressure ratio, $P_7/p_0 = 8$.

(b) Nozzle pressure ratio, $P_7/p_0 = 19$.

Figure 29. - Cooling efficiency along plug surface with coolant slot at x/L = 0.10. Shroud length-to-diameter ratio, x/d = 0.215; effective coolant flow-area ratio, $(A_c/A_p)_{eff} = 0.026$.

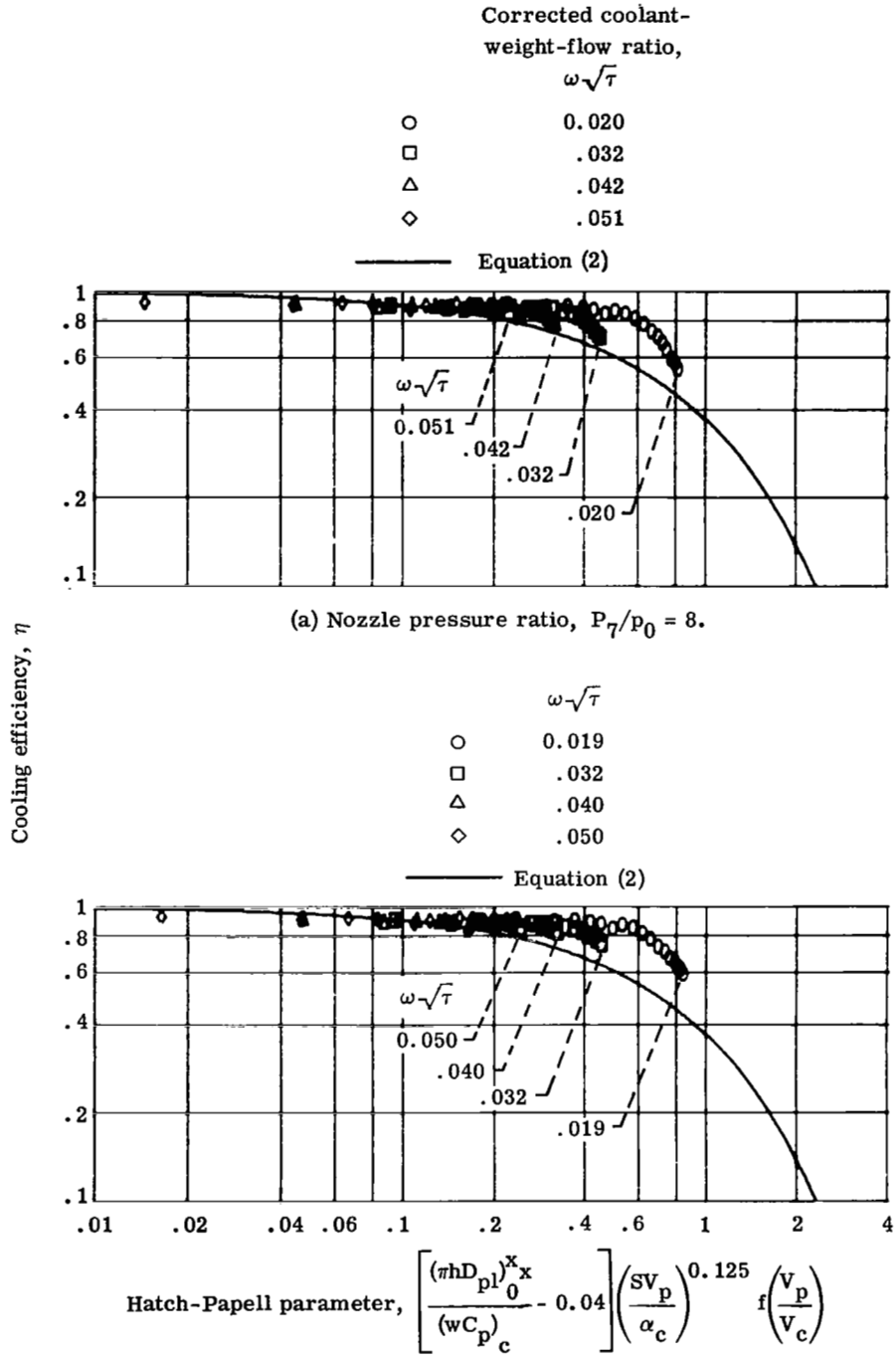

(a) Nozzle pressure ratio, $P_7/p_0 = 8$.

(b) Nozzle pressure ratio, $P_7/p_0 = 19$.

Figure 30. - Effect of corrected coolant-weight-flow ratio on cooling characteristics of plug surface with coolant slot at $x/L = 0.10$. Shroud length-to-diameter ratio, $x/d = 0.618$; effective coolant-flow-area ratio, $(A_c/A_p)_{eff} = 0.026$.

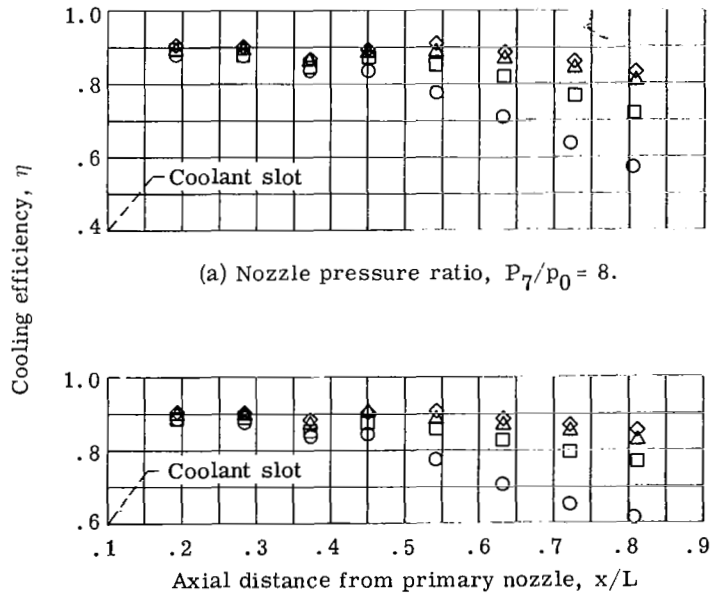

(a) Nozzle pressure ratio, $P_7/p_0 = 8$.

(b) Nozzle pressure ratio, $P_7/p_0 = 19$.

Figure 31. - Cooling efficiency along plug surface with coolant slot at $x/L = 0.10$. Shroud length-to-diameter ratio, $x/d = 0.618$; effective coolant flow-area ratio, $(A_c/A_p)_{eff} = 0.026$.

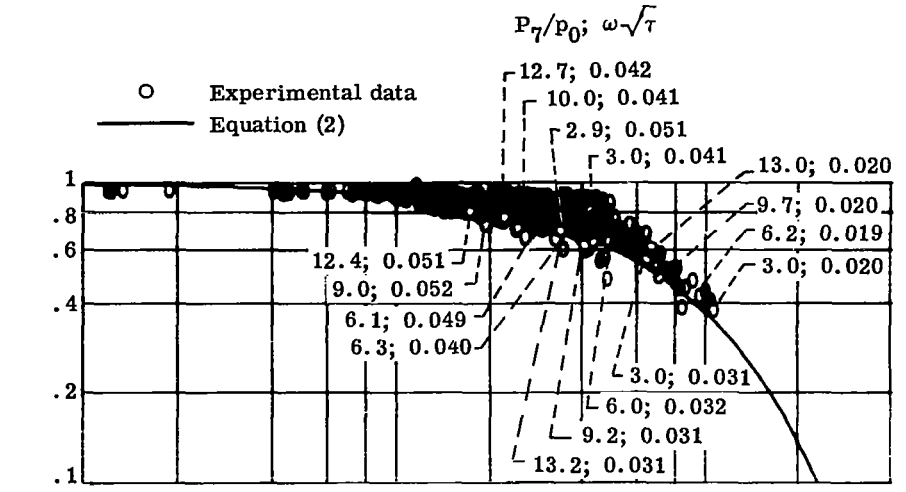

(a) $(A_c/A_p)_{eff} = 0.026;\ 0.020 \leq \omega\sqrt{\tau} \leq 0.050;\ 3 \leq P_7/p_0 \leq 13.$

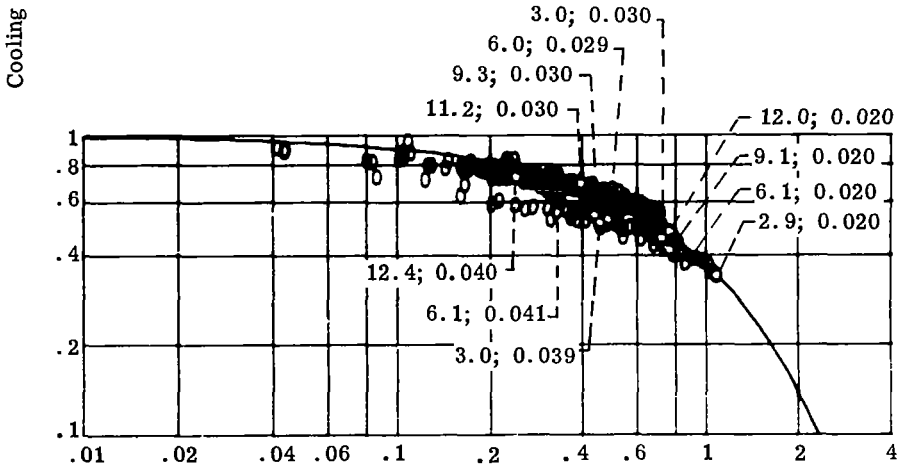

(b) $(A_c/A_p)_{eff} = 0.0178;\ 0.020 \leq \omega\sqrt{\tau} \leq 0.040;\ 3 \leq P_7/p_0 \leq 13.$

Figure 32. - Effect of coolant slot area on cooling efficiency for plug surface with coolant slot at x/L = 0.10, for various values of effective coolant flow-area ratio, $(A_c/A_p)_{eff}$; corrected coolant-weight-flow ratio, $\omega\sqrt{\tau}$; and nozzle pressure ratio, P_7/p_0. Shroud length-to-diameter ratio, x/d = -0.235.

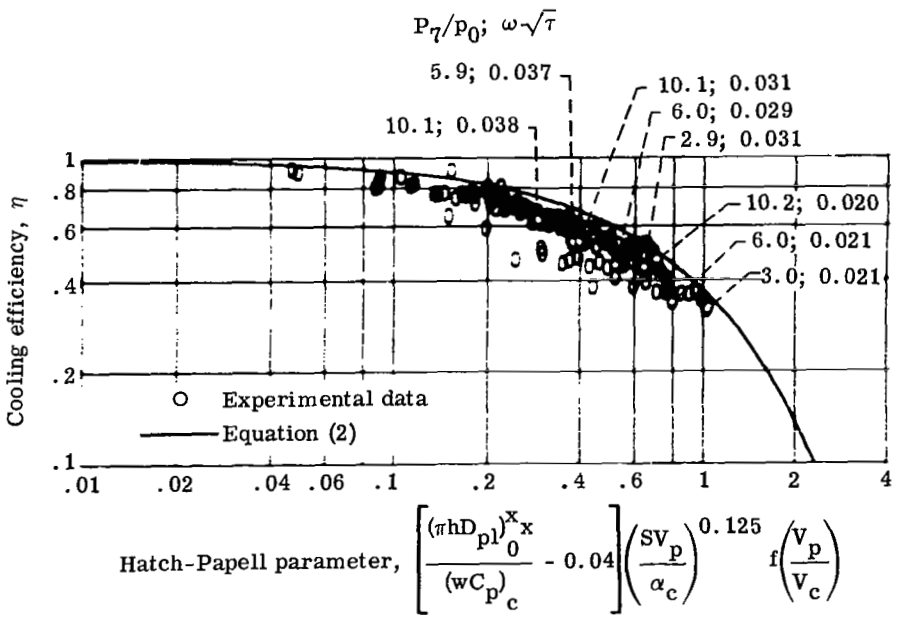

(c) $(A_c/A_p)_{eff} = 0.0146$; $0.020 \leq \omega\sqrt{\tau} \leq 0.040$; $3 \leq P_\eta/p_0 \leq 11$.

Figure 32. - Concluded.

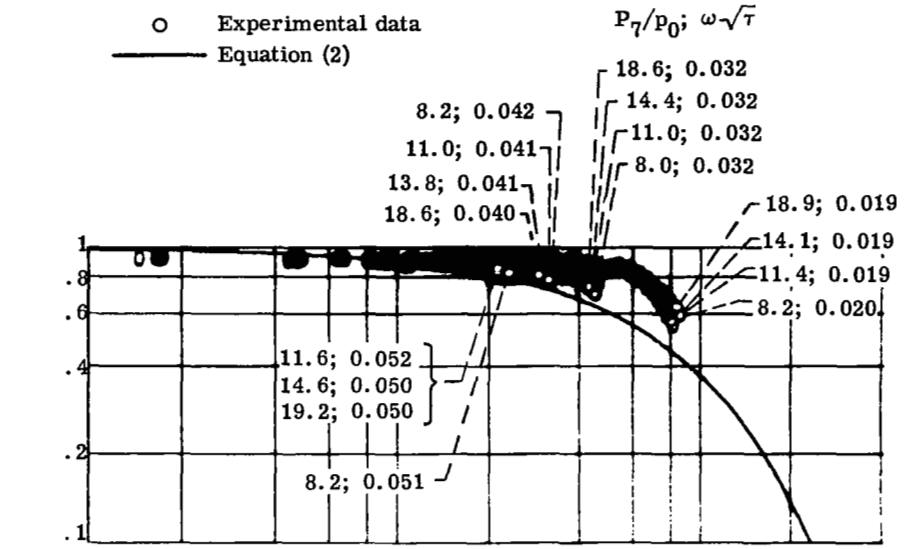

(a) $(A_c/A_p)_{eff} = 0.026$; $0.20 \leq \omega\sqrt{\tau} \leq 0.050$; $8 \leq P_7/p_0 \leq 20$.

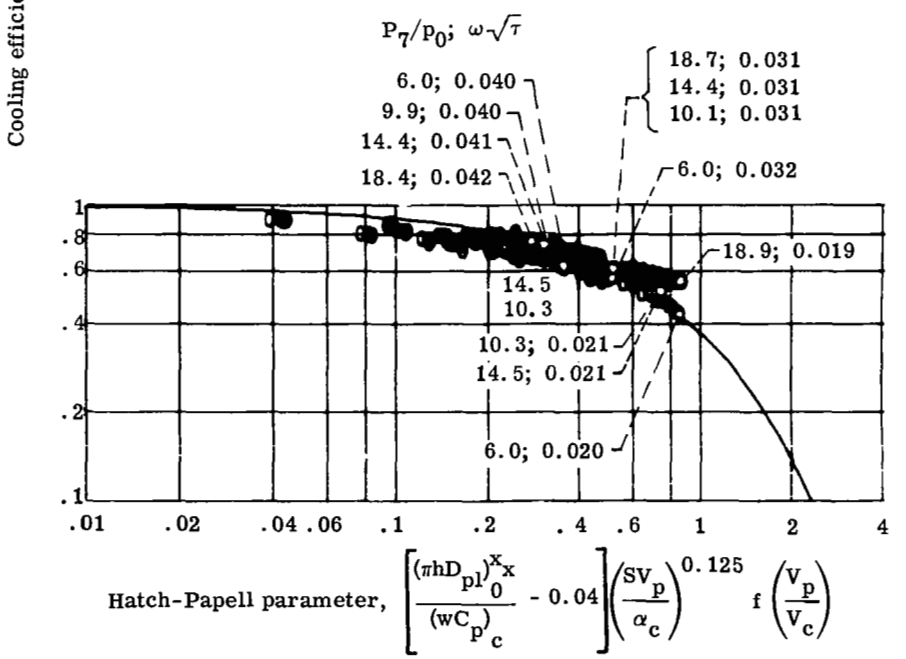

(b) $(A_c/A_p)_{eff} = 0.0178$; $0.020 \leq \omega\sqrt{\tau} \leq 0.040$; $6 \leq P_7/p_0 \leq 19$.

Figure 33. - Effect of coolant slot area on cooling efficiency for plug surface with coolant slot at $x/L = 0.10$, for various values of effective coolant flow-area ratio, $(A_c/A_p)_{eff}$; corrected coolant-weight-flow ratio, $\omega\sqrt{\tau}$; and nozzle pressure ratio, P_7/p_0. Shroud length-to diameter ratio, $x/d = 0.618$.

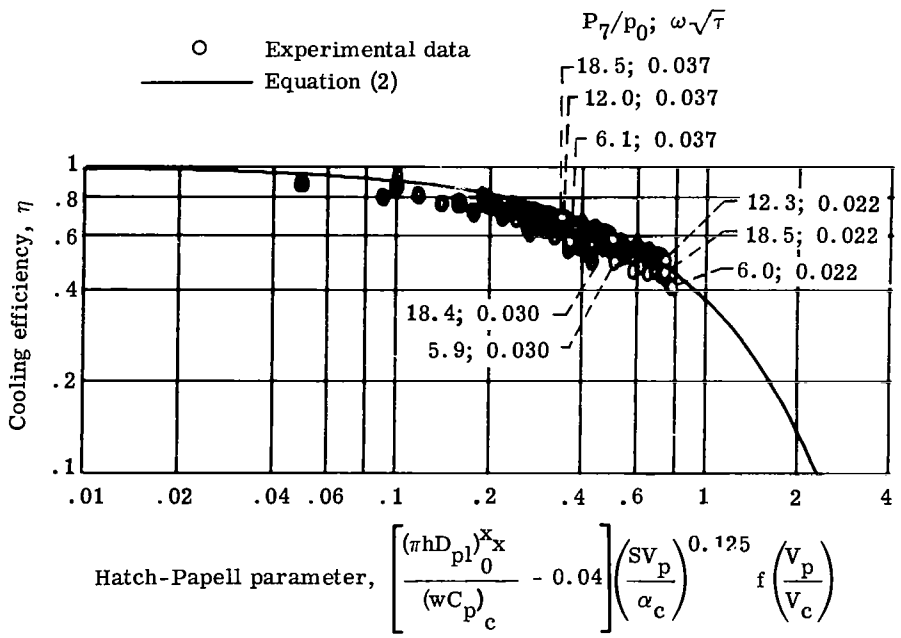

(c) $(A_c/A_p)_{eff} = 0.0146$; $0.020 < \omega\sqrt{\tau} < 0.040$; $6 < P_7/p_0 < 19$.

Figure 33. - Concluded.

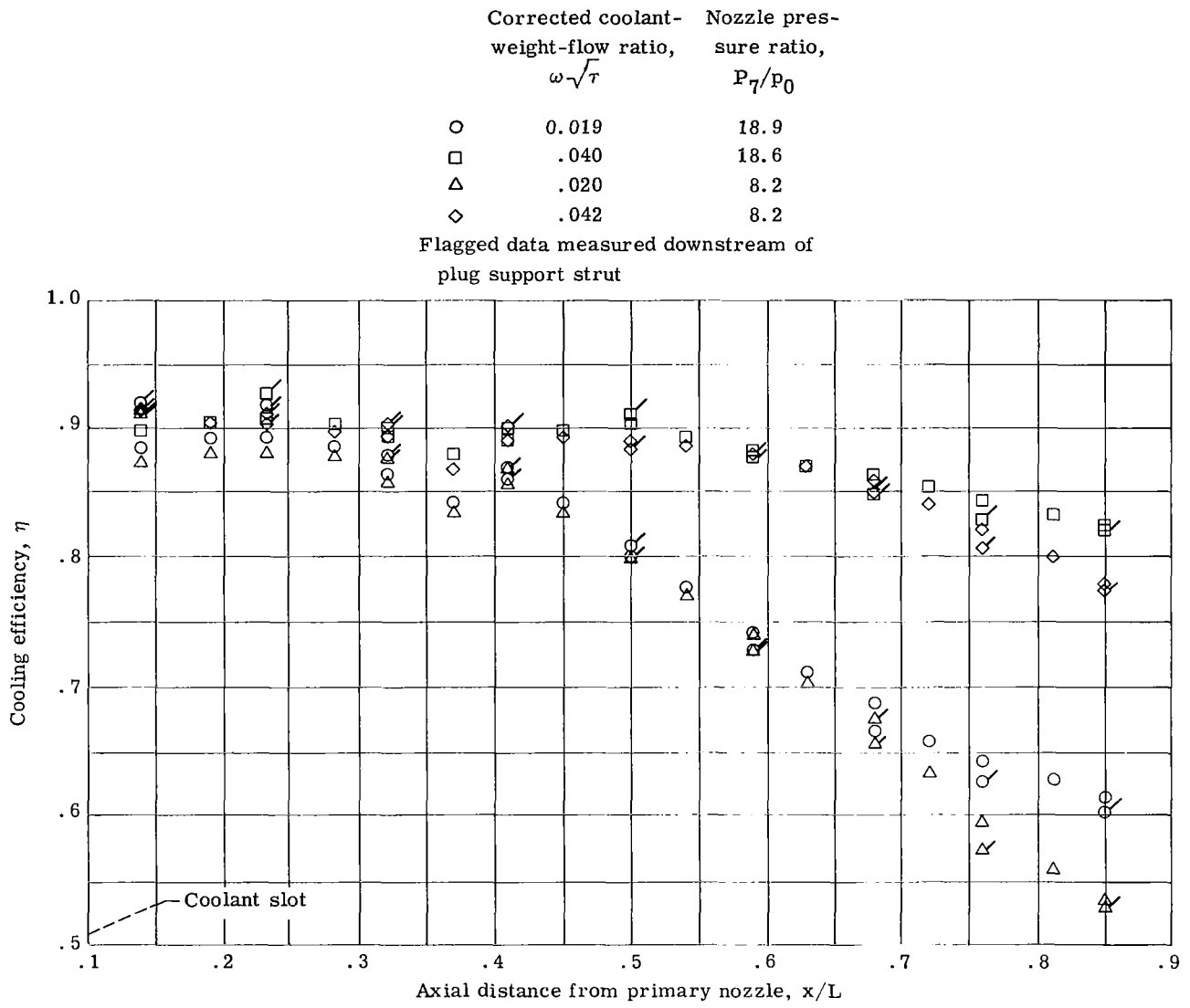

Figure 34. - Effect of plug struts on cooling characteristics of plug surface with coolant slot at x/L = 0.10. Shroud length-to-diameter ratio, x/d = 0.618; effective coolant flow-area ratio, $(A_c/A_p)_{eff} = 0.026$.

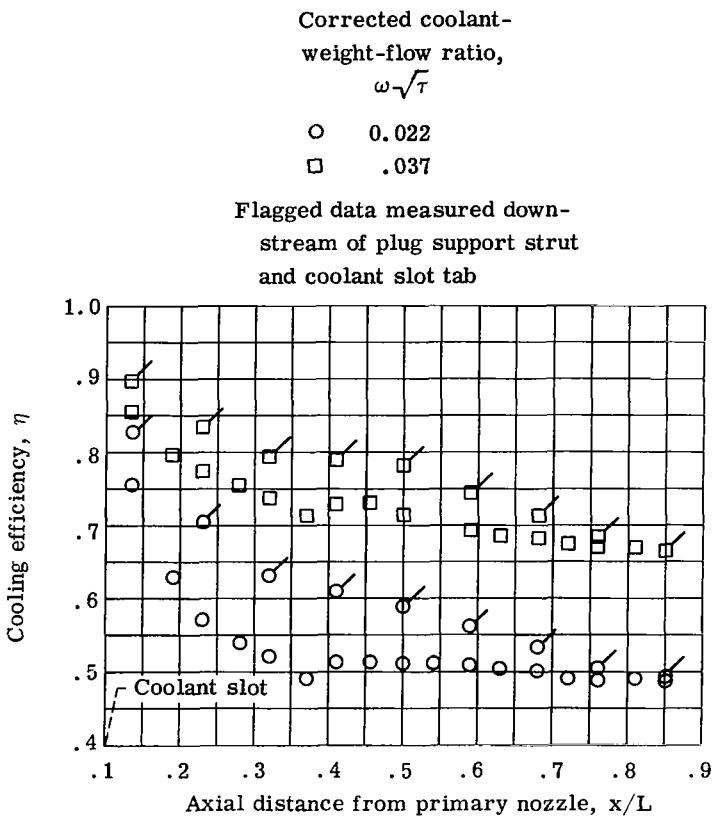

Figure 35. - Effect of coolant slot spacer tabs on cooling characteristics of plug surface with coolant slot at x/L = 0.10. Shroud length-to-diameter ratio, x/d = 0.618; effective coolant flow-area ratio, $(A_c/A_p)_{eff}$ = 0.0146; nozzle pressure ratio, P_7/p_0 = 18.5.

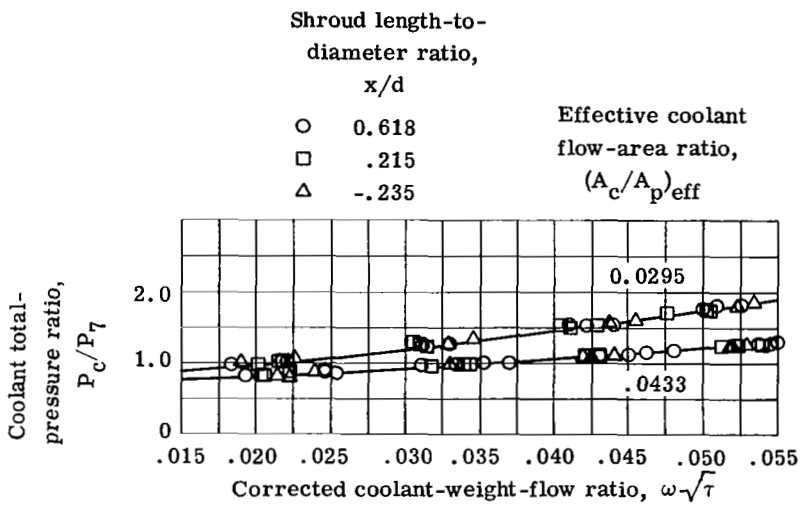

Figure 36. - Pumping characteristics for full-length plug with coolant slot at $x/L = -0.10$.

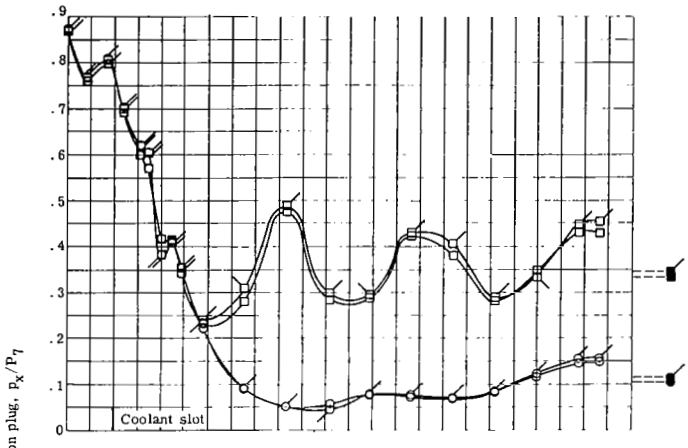

Corrected coolant-weight-flow ratio, $\omega\sqrt{\tau}$	Nozzle pressure ratio, P_7/p_0
○ 0.022	9.2
◌́ .052	8.9
□ .023	3.0
□́ .053	2.9

Solid symbols denote p_0/P_7

(a) Shroud length-to-diameter ratio, x/d = -0.235.

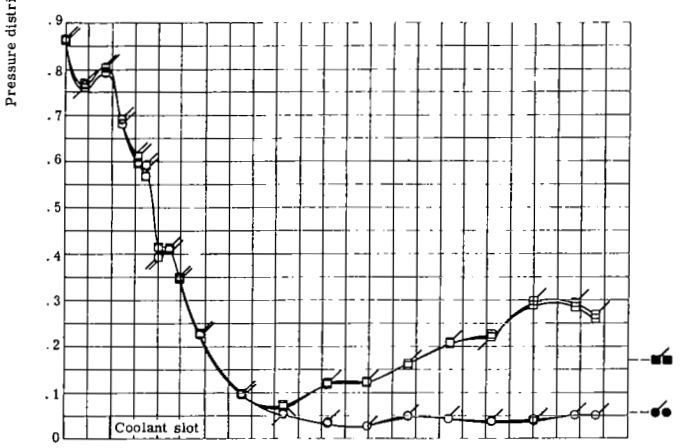

$\omega\sqrt{\tau}$	P_7/p_0
○ 0.022	18.3
◌́ .041	18.3
□ .021	6.0
□́ .041	5.9

Solid symbols denote p_0/P_7

(b) Shroud length-to-diameter ratio, x/d = 0.215.

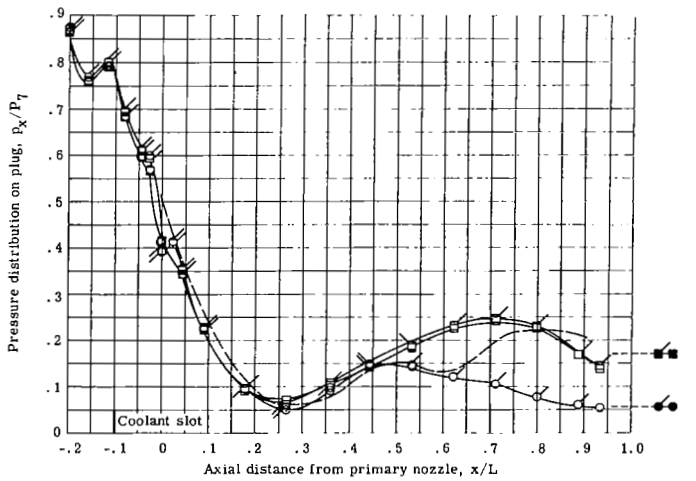

$\omega\sqrt{\tau}$	P_7/p_0
○ 0.022	17.9
◌́ .044	17.9
□ .022	6.0
□́ .042	5.9
– – –	7.9 (ref. 1)

Solid symbols denote p_0/P_7

(c) Shroud length-to-diameter ratio, x/d = 0.618.

Figure 37. - Plug pressure distributions with coolant slot at x/L = -0.10. Effective coolant flow-area ratio, $(A_c/A_p)_{eff} = 0.0295$.

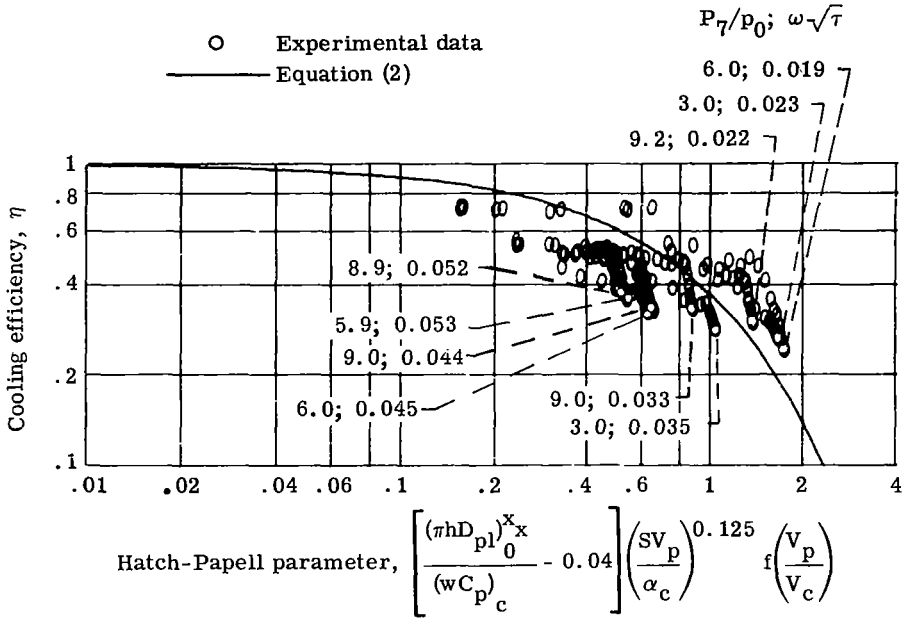

Figure 38. - Comparison of experimental data with Hatch-Papell film-cooling correlation for plug surface with coolant slot at $x/L = -0.10$. Shroud length-to-diameter ratio, $x/d = -0.235$; effective coolant flow-area ratio, $(A_c/A_p)_{eff} = 0.0295$; corrected coolant-weight-flow ratio, $0.02 \leq \omega\sqrt{\tau} \leq 0.06$; nozzle pressure ratio, $3 \leq P_7/p_0 \leq 10$.

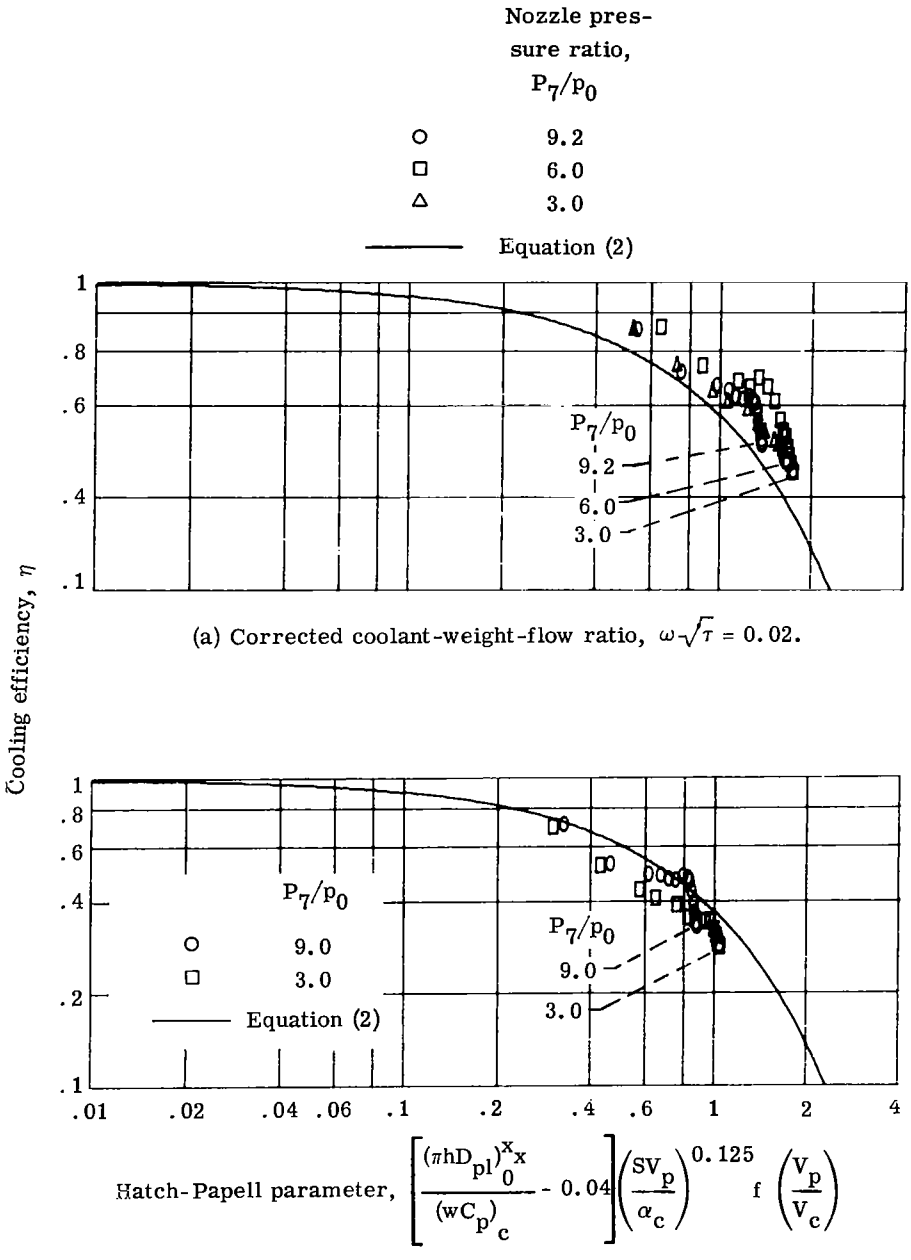

Figure 39. - Effect of nozzle pressure ratio on cooling characteristics of plug surface with coolant slot at x/L = -0.10. Shroud length-to-diameter ratio, x/d = -0.235; effective coolant flow-area ratio, $(A_c/A_p)_{eff} = 0.0295$.

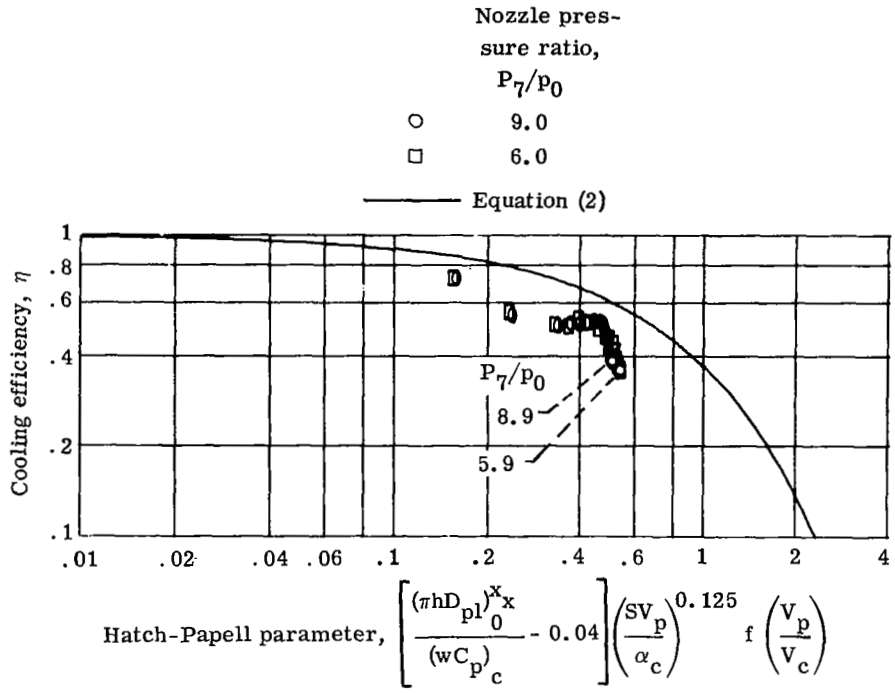

(c) Corrected coolant-weight-flow ratio, $\omega\sqrt{\tau} = 0.05$.

Figure 39. - Concluded.

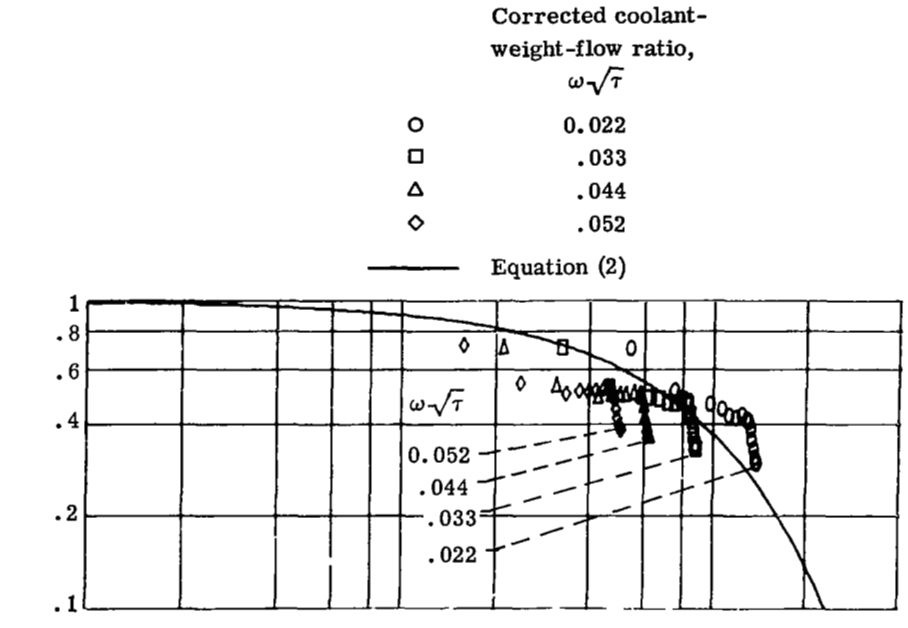

(a) Nozzle pressure ratio, $P_7/p_0 = 9$.

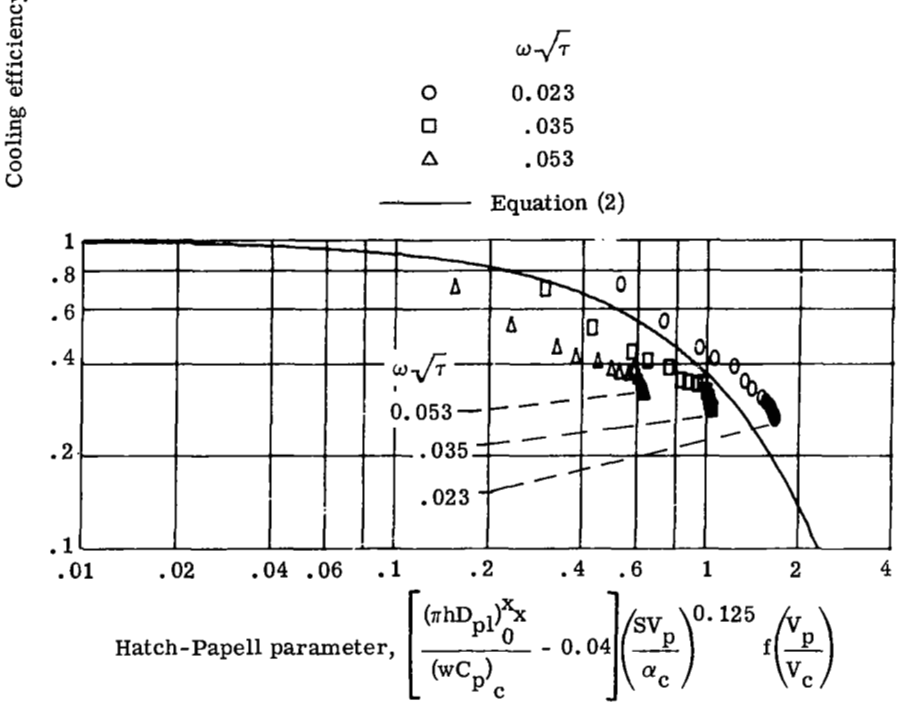

(b) Nozzle pressure ratio, $P_7/p_0 = 3$.

Figure 40. - Effect of corrected coolant-weight-flow ratio on cooling characteristics of plug surface with coolant slot at $x/L = -0.10$. Shroud length-to-diameter ratio, $x/d = -0.235$; effective coolant flow-area ratio, $(A_c/A_p)_{eff} = 0.0295$.

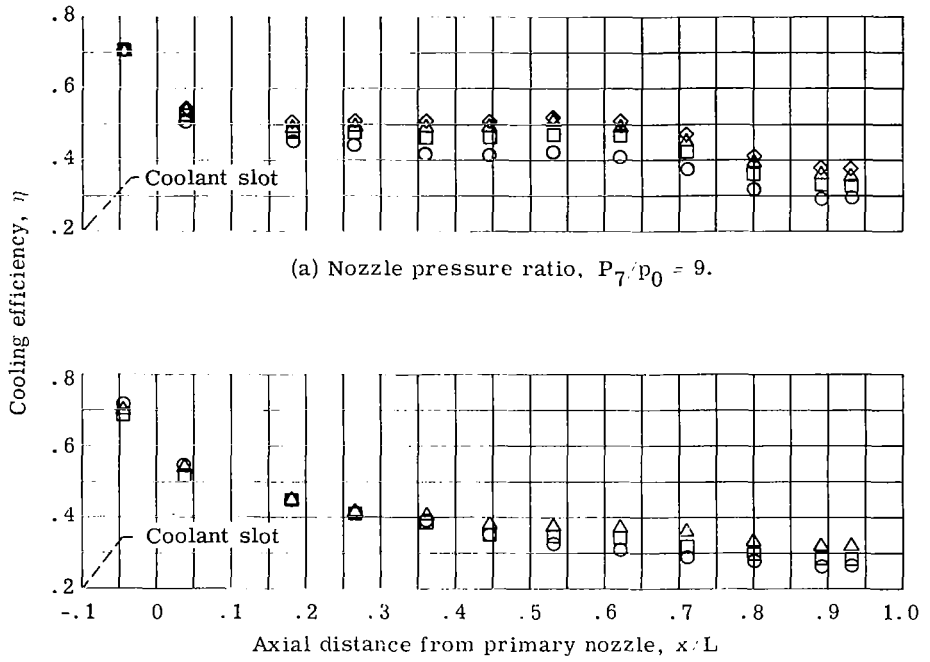

Figure 41. - Cooling efficiency along plug surface with coolant slot at x/L = -0.10. Shroud length-to-diameter ratio, x/d = -0.235; effective coolant flow-area ratio, $(A_c/A_p)_{eff}$ = 0.0295.

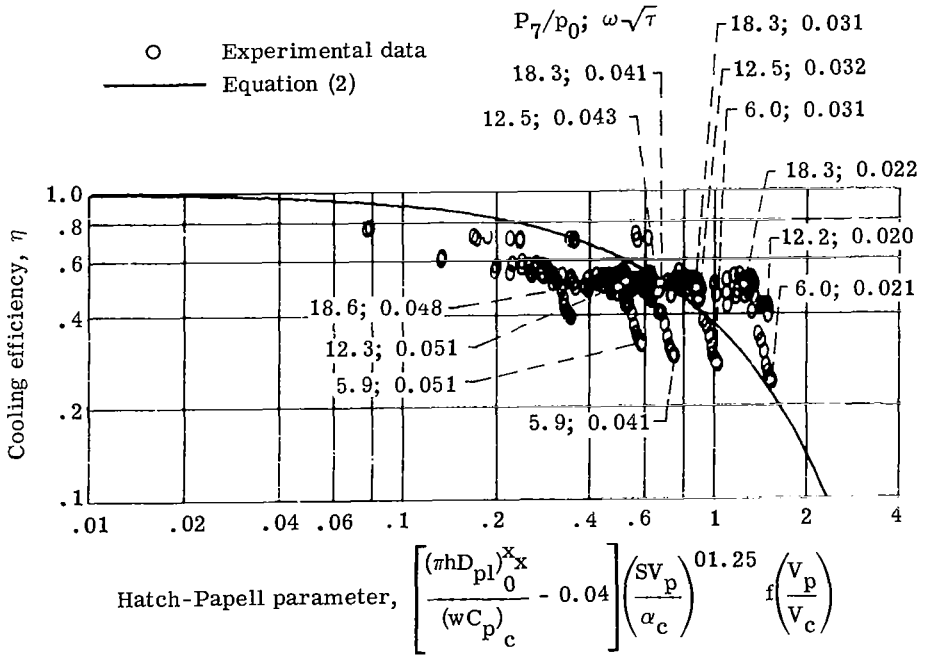

Figure 42. - Comparison of experimental data with Hatch-Papell film-cooling correlation for plug surface with coolant slot at $x/L = -0.10$. Shroud length-to-diameter ratio, $x/d = 0.215$; effective coolant flow-area ratio, $(A_c/A_p)_{eff} = 0.0295$; corrected coolant-weight-flow ratio, $0.02 \leq \omega\sqrt{\tau} \leq 0.060$; nozzle pressure ratio, $5 \leq P_7/p_0 \leq 19$.

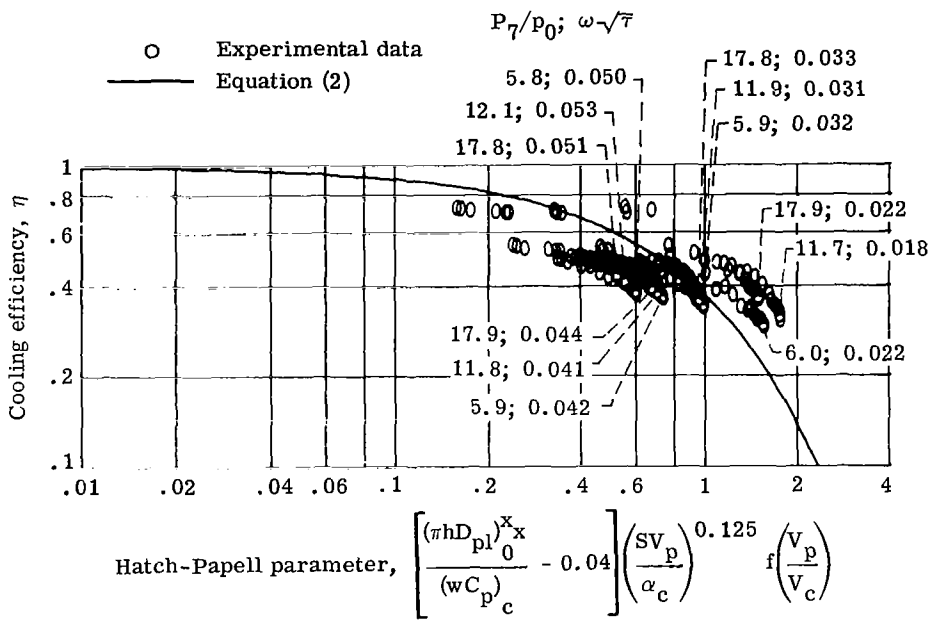

Figure 43. - Comparison of experimental data with Hatch-Papell film-cooling correlation for plug surface with coolant slot at x/L = -0.10. Shroud length-to-diameter ratio, x/d = 0.618; effective coolant-flow-area ratio, $(A_c/A_p)_{eff} = 0.0295$; corrected coolant-weight-flow ratio, $0.02 \leq \omega\sqrt{\tau} \leq 0.06$; nozzle pressure ratio, $5 \leq P_7/p_0 \leq 18$.

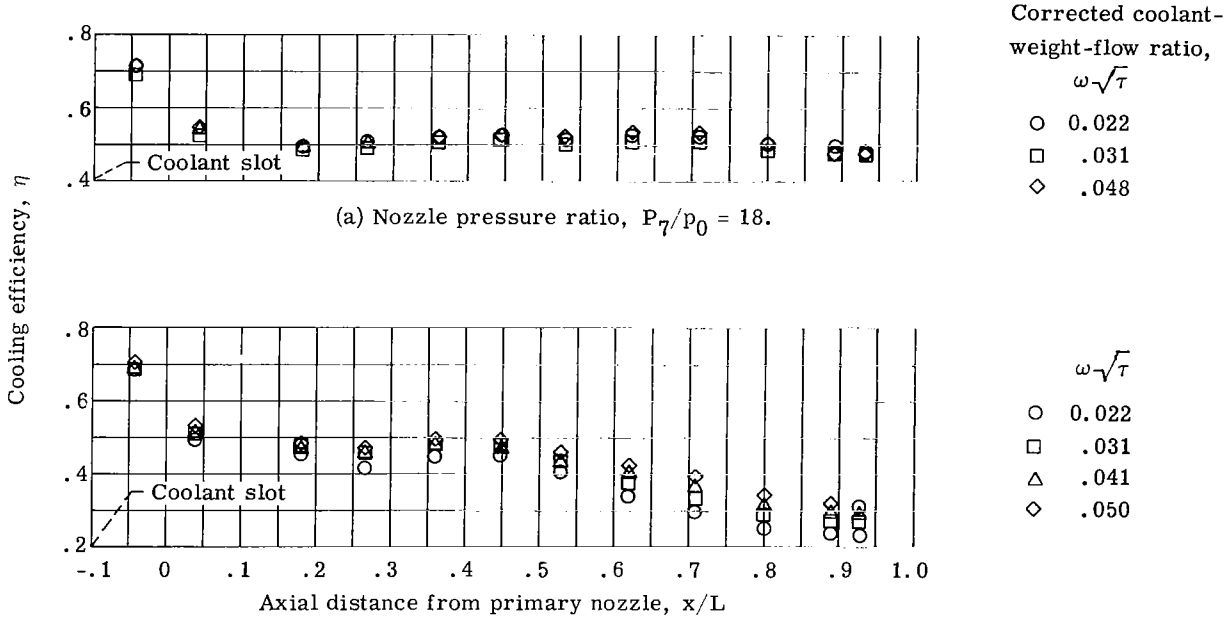

(a) Nozzle pressure ratio, $P_7/p_0 = 18$.

(b) Nozzle pressure ratio, $P_7/p_0 = 6$.

Figure 44. - Cooling efficiency along plug surface with coolant slot at x/L = -0.10. Shroud length-to-diameter ratio, x/d = 0.215; effective coolant flow-area ratio, $(A_c/A_p)_{eff} = 0.0295$.

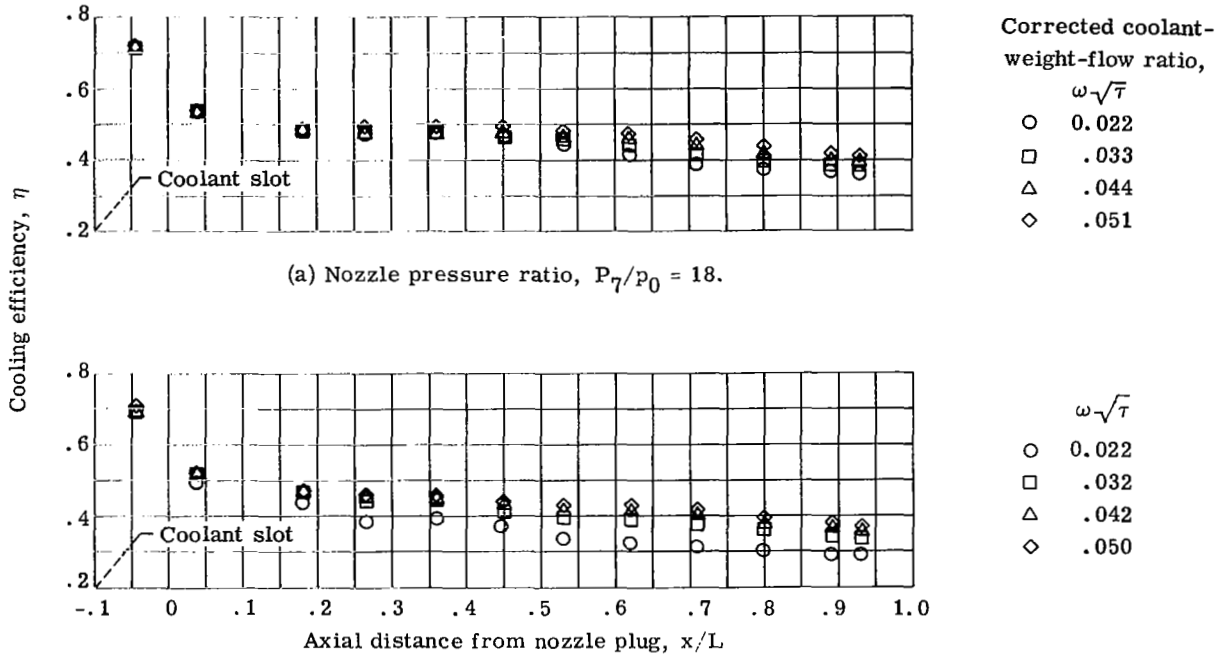

Figure 45. - Cooling efficiency along plug surface with coolant slot at x/L = -0.10. Shroud length-to-diameter ratio, x/d = 0.618; effective coolant flow-area ratio, $(A_c/A_p)_{eff}$ = 0.0295.

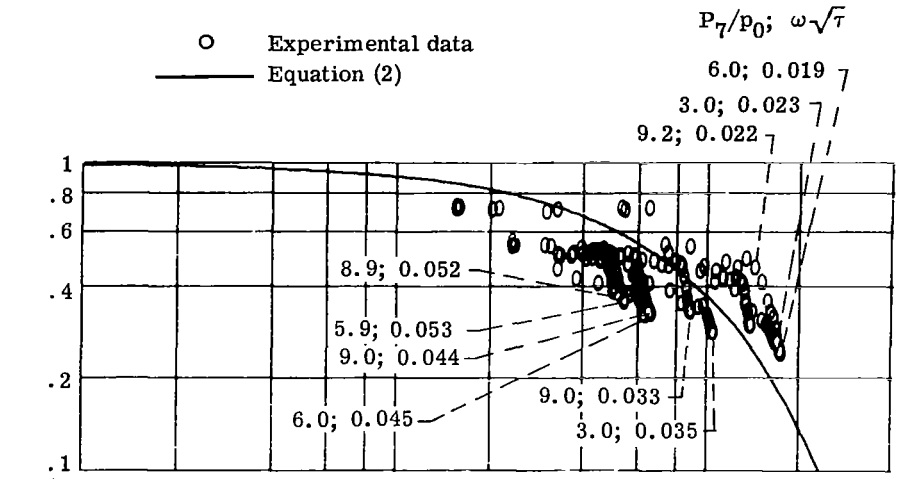

(a) $(A_c/A_p)_{eff} = 0.0295$; $0.02 \leq \omega\sqrt{\tau} \leq 0.06$; $3 \leq P_7/p_0 \leq 10$.

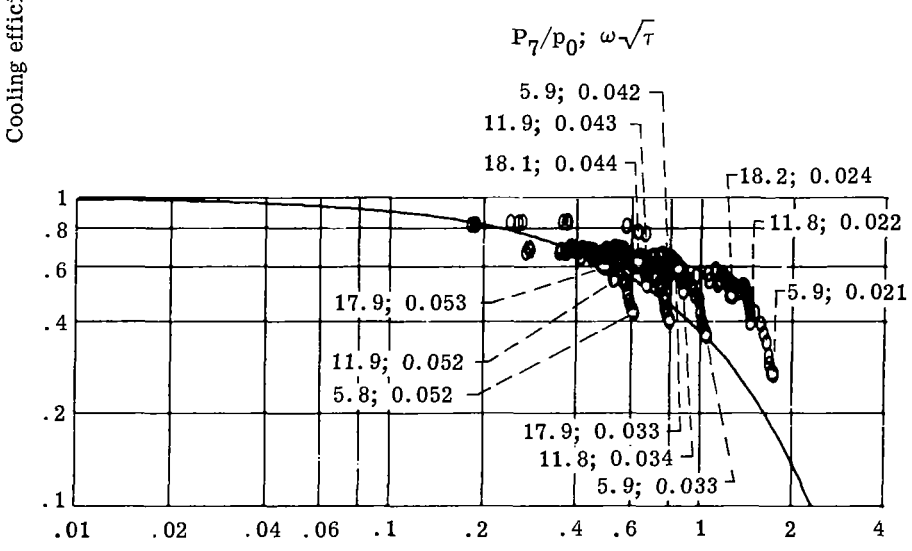

(b) $(A_c/A_p)_{eff} = 0.0433$; $0.02 \leq \omega\sqrt{\tau} \leq 0.06$; $5 \leq P_7/p_0 \leq 19$.

Figure 46. - Effect of coolant slot area on cooling efficiency for plug surface with coolant slot at x/L = -0.10, for various values of effective coolant flow-area ratio, $(A_c/A_p)_{eff}$; corrected coolant-weight-flow ratio, $\omega\sqrt{\tau}$; and nozzle pressure ratio, P_7/p_0. Shroud length-to-diameter ratio, x/d = -0.235.

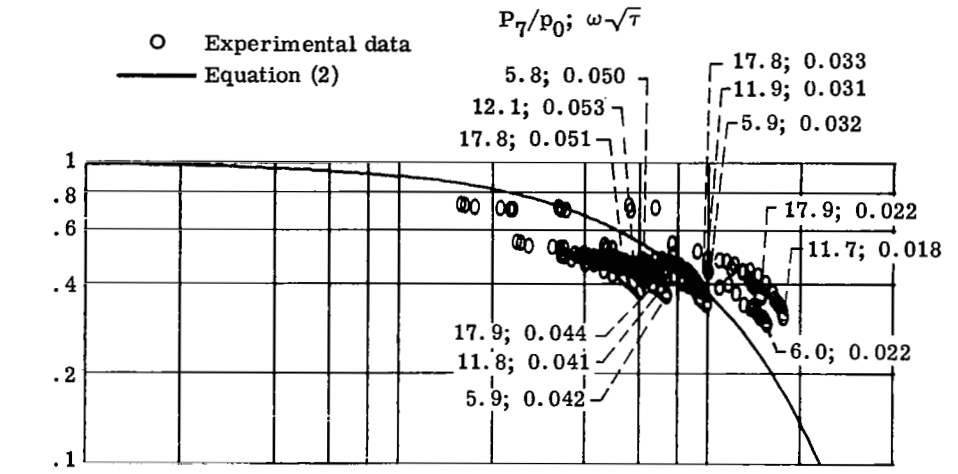

(a) $(A_c/A_p)_{eff} = 0.0295$; $0.02 \leq \omega\sqrt{\tau} \leq 0.06$; $5 \leq P_7/p_0 \leq 18$.

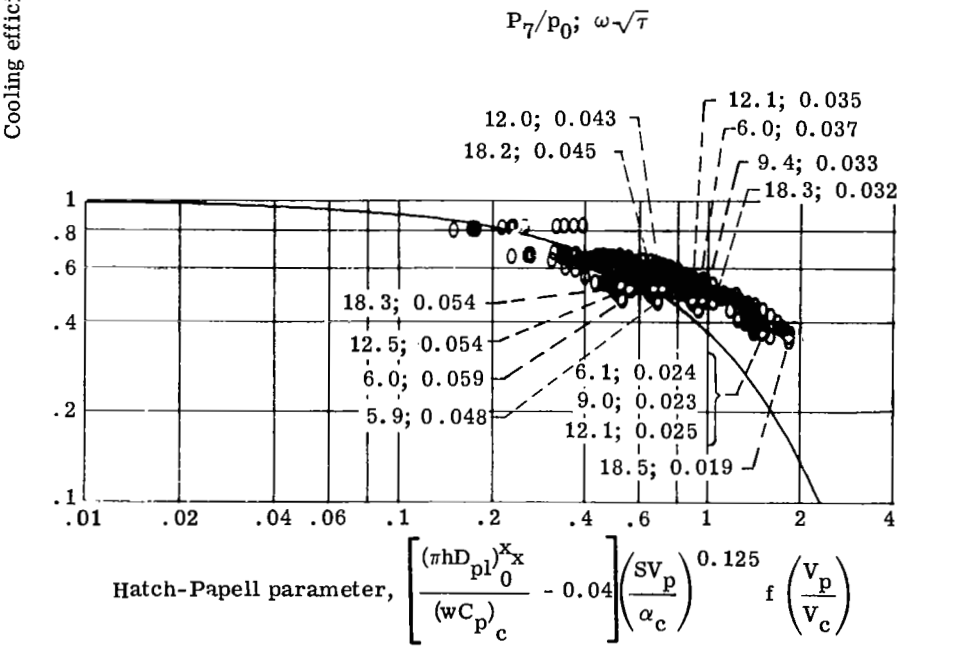

Cooling efficiency, η

Hatch-Papell parameter, $\left[\frac{(\pi h D_{pl})^x_0}{(wC_p)_c} - 0.04\right]\left(\frac{SV_p}{\alpha_c}\right)^{0.125} f\left(\frac{V_p}{V_c}\right)$

(b) $(A_c/A_p)_{eff} = 0.0433$; $0.01 \leq \omega\sqrt{\tau} \leq 0.06$; $5 \leq P_7/p_0 \leq 19$.

Figure 47. - Effect of coolant slot area on cooling efficiency for plug surface with coolant slot at $x/L = -0.10$, for various values of effective coolant flow-area ratio, $(A_c/A_p)_{eff}$; corrected coolant-weight-flow ratio, $\omega\sqrt{\tau}$; and nozzle pressure ratio, P_7/p_0. Shroud length-to-diameter ratio, $x/d = 0.618$.

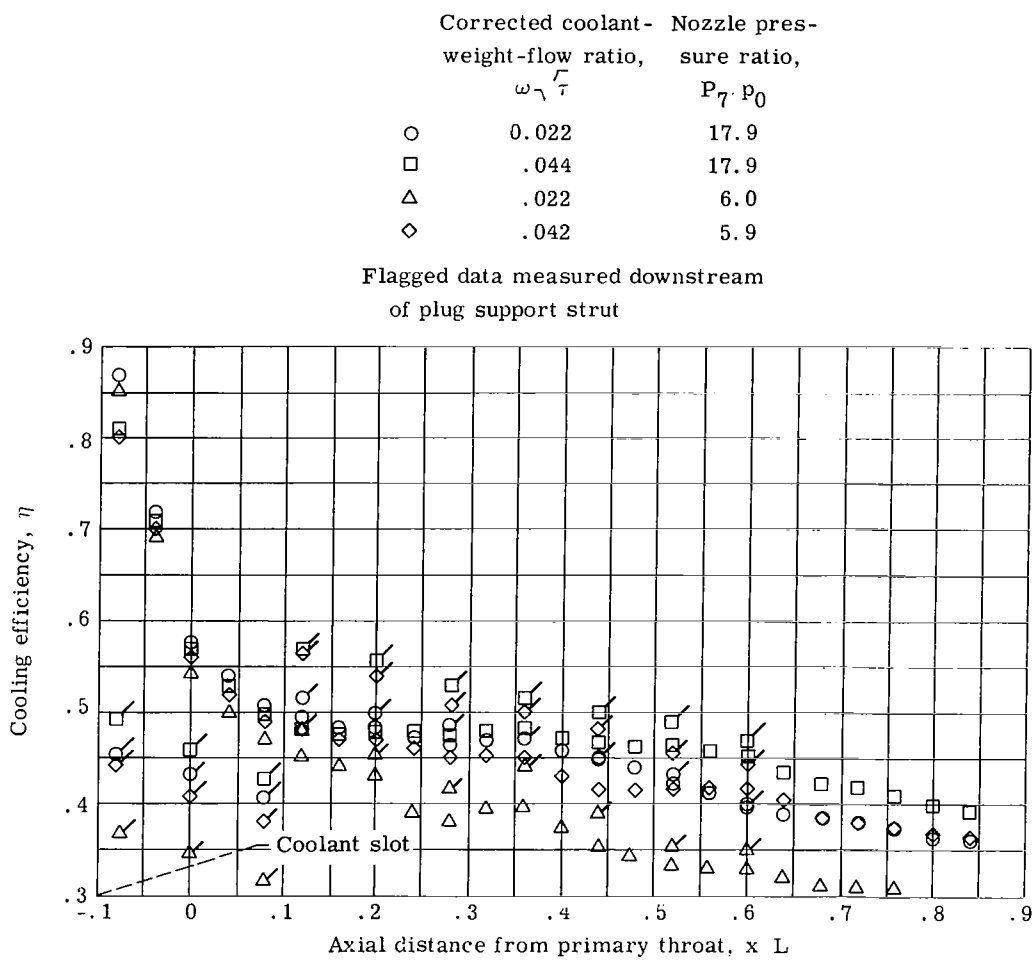

Figure 48. - Effect of plug struts on cooling characteristics of plug surface with coolant slot at x L = -0.10. Shroud length-to-diameter ratio, x α = 0.618; effective coolant flow-area ratio, $(A_c/A_p)_{eff}$ = 0.0295.

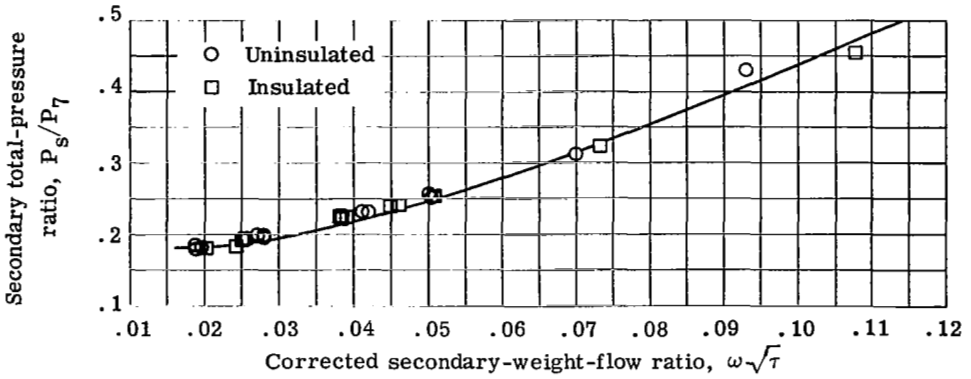

Figure 49. - Pumping characteristics for plug nozzle operating with full-length shroud. Effective secondary-flow-area ratio, $(A_s/A_p)_{eff} = 0.230$.

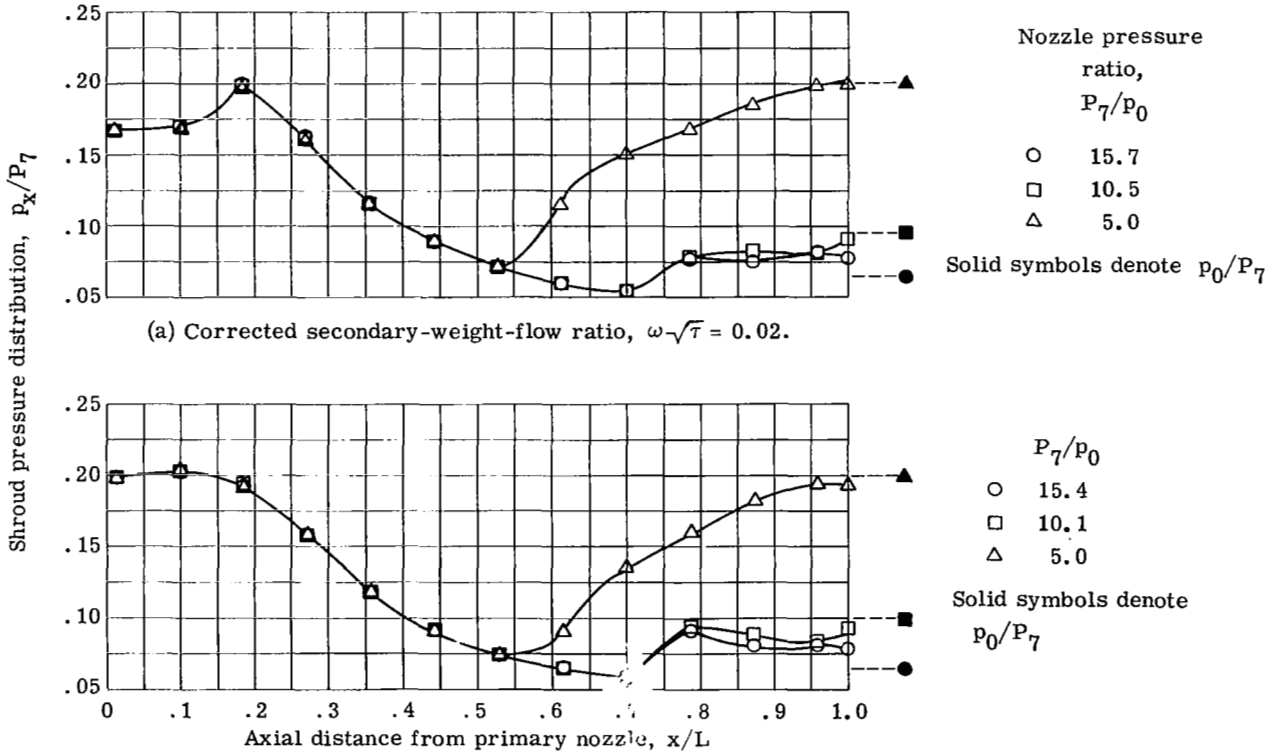

(a) Corrected secondary-weight-flow ratio, $\omega\sqrt{\tau} = 0.02$.

(b) Corrected secondary-weight-flow ratio, $\omega\sqrt{\tau} = 0.05$.

Figure 50. - Pressure distribution with shroud cooling.

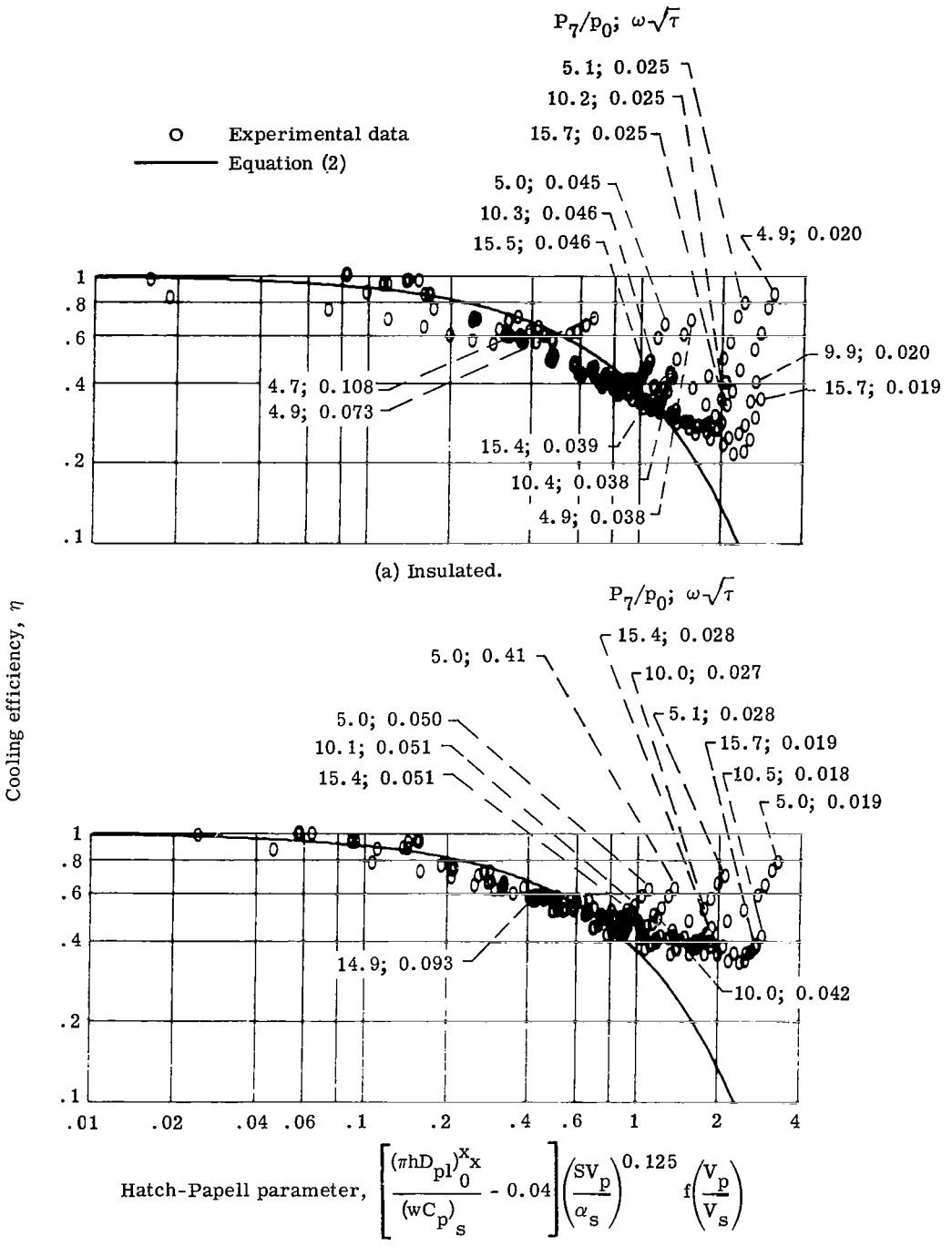

Figure 51. - Comparison of experimental data with Hatch-Papell film-cooling correlation for shroud of a plug nozzle. Effective secondary flow-area ratio, $(A_s/A_p)_{eff} = 0.230$; corrected secondary-weight-flow ratio, $0.02 \leq \omega\sqrt{\tau} \leq 0.10$; nozzle pressure ratio, $5 \leq P_7/p_0 \leq 16$.

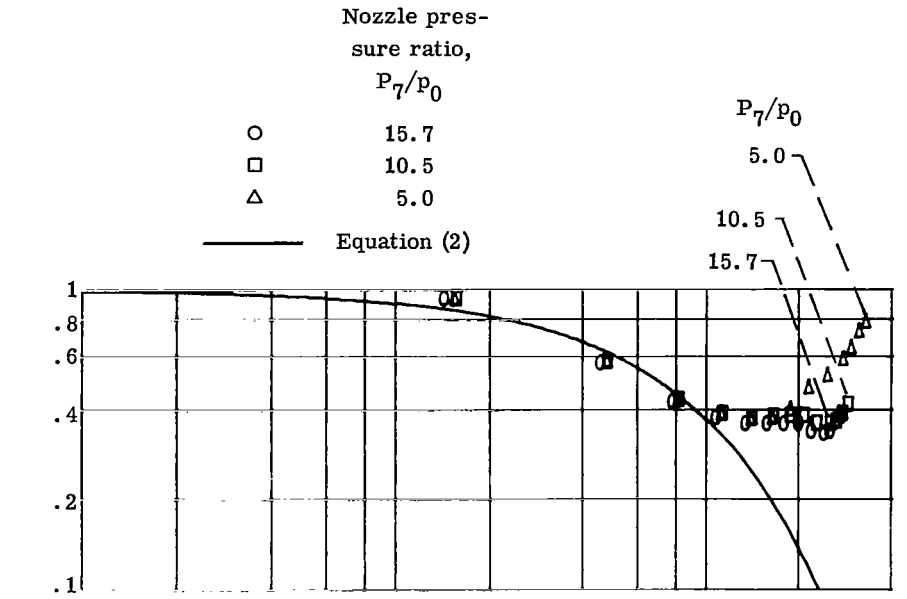

(a) Corrected secondary-weight-flow ratio, $\omega\sqrt{\tau} = 0.02$.

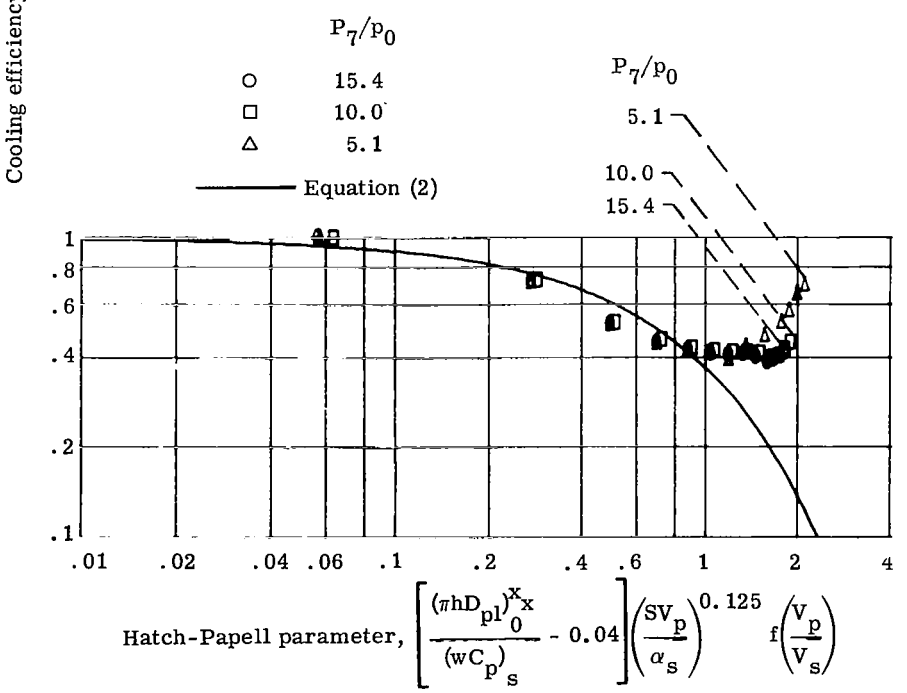

(b) Corrected secondary-weight-flow ratio, $\omega\sqrt{\tau} = 0.03$.

Figure 52. - Effect of nozzle pressure ratio on cooling characteristics of shroud of plug nozzle (uninsulated).

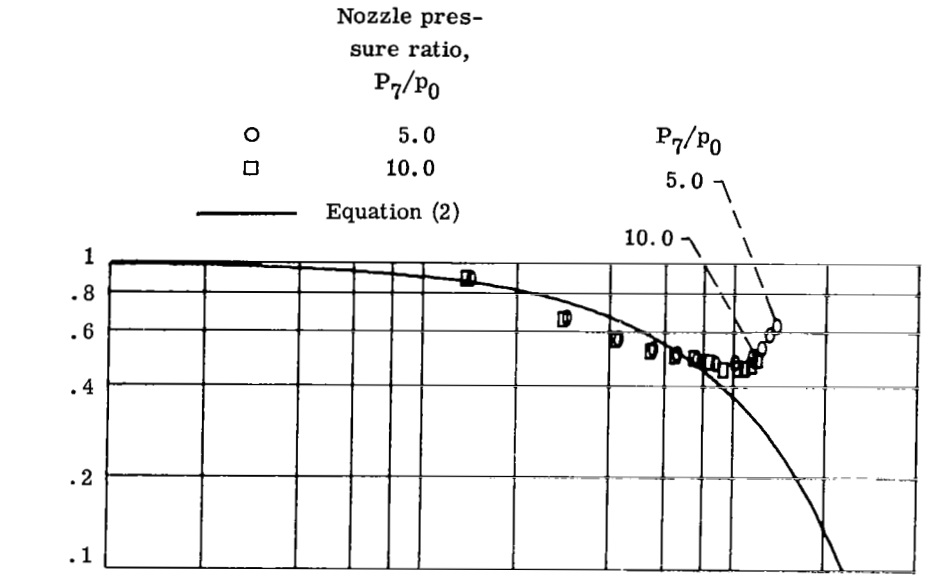

(c) Corrected secondary-weight-flow ratio, $\omega\sqrt{\tau} = 0.04$.

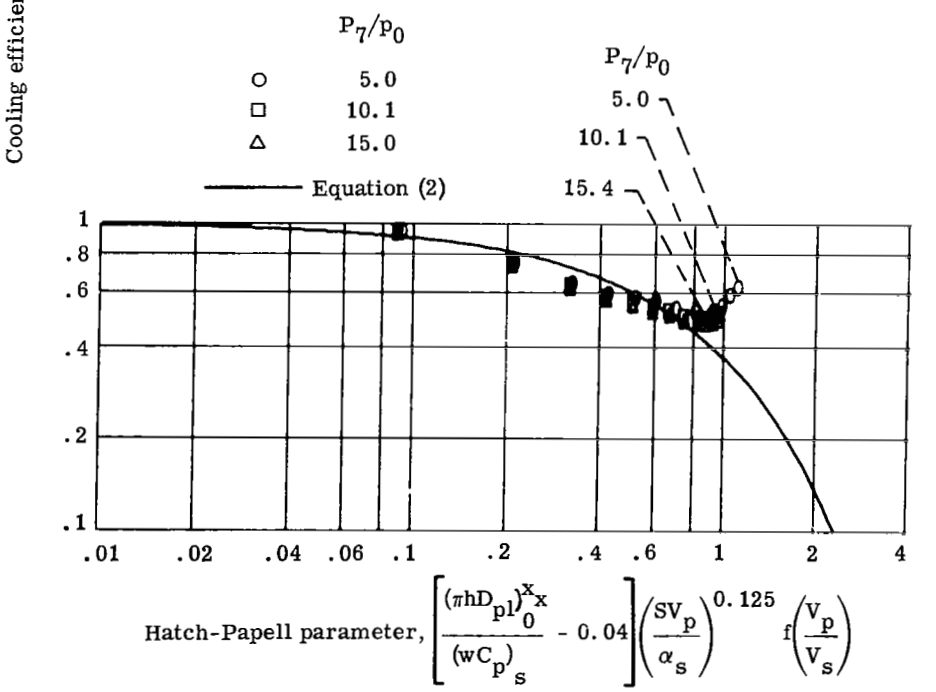

(d) Corrected secondary-weight-flow ratio, $\omega\sqrt{\tau} = 0.05$.

Figure 52. - Concluded.

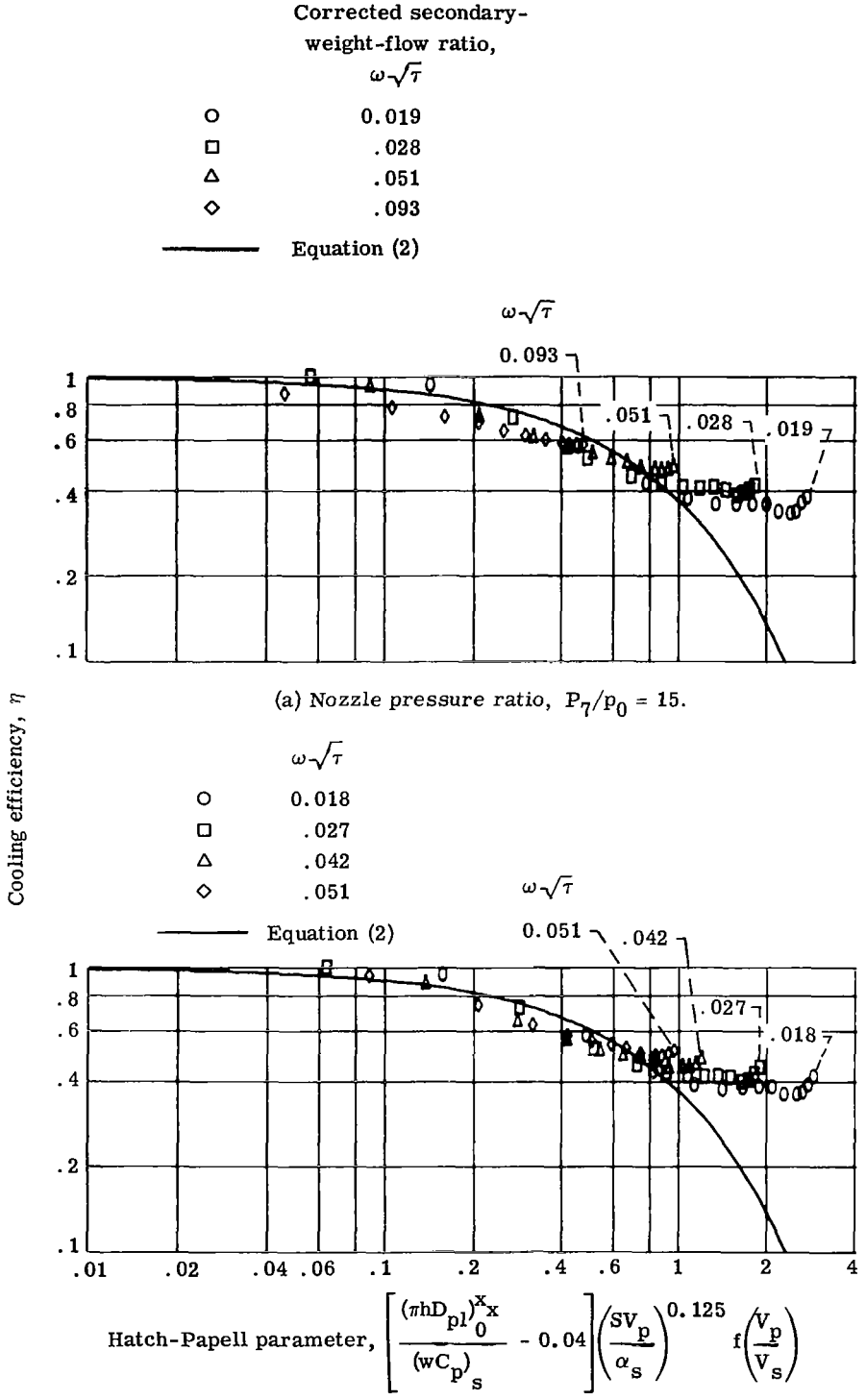

(a) Nozzle pressure ratio, $P_7/p_0 = 15$.

(b) Nozzle pressure ratio, $P_7/p_0 = 10$.

Figure 53. - Effect of corrected secondary-weight-flow ratio on cooling characteristics of shroud of a plug nozzle (uninsulated).

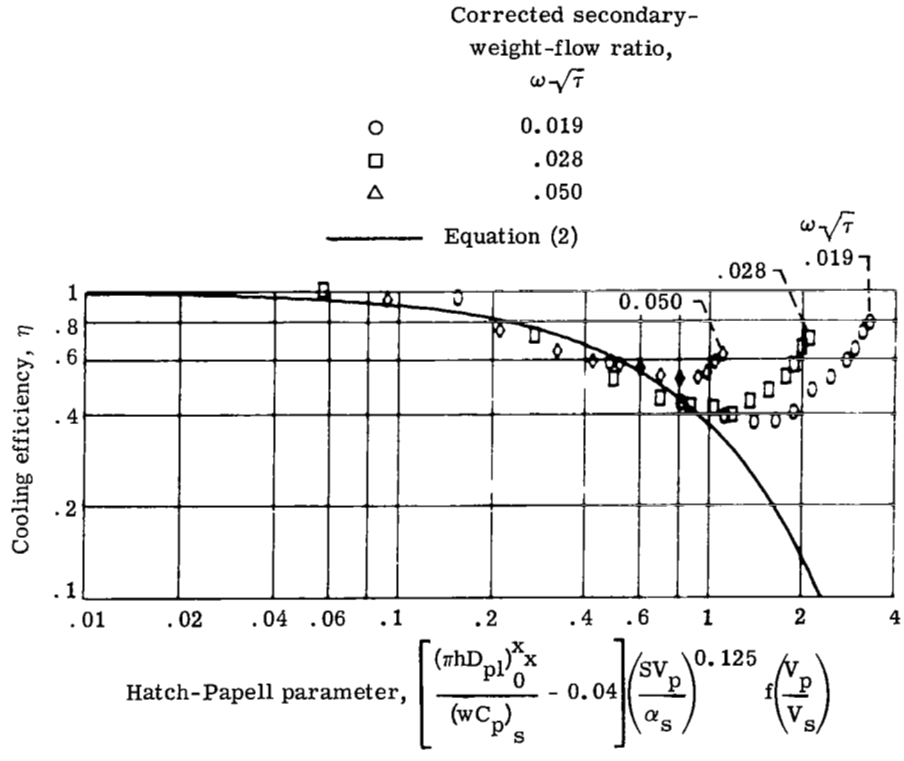

(c) Nozzle pressure ratio, $P_7/p_0 = 5$.

Figure 53. - Concluded.

NASA-Langley, 1971 —— 28 E-5551